Direct Numerical Simulations of Magnetic Helicity Conserving Astrophysical Dynamos

DIRECT NUMERICAL SIMULATIONS OF MAGNETIC HELICITY CONSERVING ASTROPHYSICAL DYNAMOS: A SEARCH FOR THE ELECTROMOTIVE FORCE

By

ALEXANDER J. CRIDLAND, B.SC.

A Thesis Submitted to the School of Graduate Studies in Partial Fulfillment of the Requirements for the Degree Master's of Physics McMaster University

Descriptive Note

MASTER OF PHYSICS (2013) McMaster University (Physics and Astronomy) Hamilton, Ontario

AUTHOR: Alexander J. Cridland, B.Sc. (McMaster University)

SUPERVISOR: Dr. Ethan T. Vishniac

NUMBER OF PAGES: xiv, 85

Abstract

Here we present direct numerical simulations of a shearing box which models the MHD turbulence in astrophysical systems with cylindrical geometries. The purpose of these simulations is to detect the source of the electromotive force - the driver of large scale magnetic field evolution. This electromotive force is responsible for the large scale dynamo action which builds and maintains the magnetic field against dissipation in plasmas. We compare the estimates of the electromotive force from the kinematic approximation of mean field theory - the most prevalent theory for astrophysical dynamos - with a modified version of mean field theory which restricts the electromotive force by the consideration of magnetic helicity conservation. We will show that in general the kinematic approximation overestimates the observed electromotive force for the majority of the simulation, while the term derived from the helicity conservation estimates the electromotive force very well. We will also illustrate the importance of the shear in the fluid to the growth and strength of the resulting large scale magnetic field. Too strong and the small scale dynamo does not grow enough to properly seed a strong large scale dynamo. Too weak, and no large scale magnetic field is observed after the small scale dynamo has saturated. Finally, we will find that in order to maintain the strength of the emerged large scale magnetic dynamo we require a magnetic Prandtl number ($Pr \equiv \nu/\eta$) that is at least an order of magnitude above unity.

Acknowledgments

I would like to thank my supervisor, Dr. Ethan Vishniac for his insight, spirited discussion and endless patience for the code (and its programmer) over our (nearly) two and a half year span of working together. And without whom this thesis would not have had come to fruition. My thanks go out to Dr. Ralph Pudritz and Dr. James Wadsley, who's challenging defense and valuable input helped shape the final form of my thesis. I thank my office mate, Ben Jackel for his forever valuable input and extended conversations surrounding MHD and simulations in general (apparently the CFL condition is a thing).

On a more personal level, I thank my loving girlfriend Brittany (the rock, the hard place) for her support and for always believing in me. I thank my parents and my sister for their love and support, and for encouraging that 10 year old kid to follow his dreams of being an Astronomer - even if it turns out that they wont get that winter home in Hawaii after all. Finally, I thank the Physics and Astronomy softball crew for helping to maintain my sanity - we might not be the best at softball (did I say might?) but we certainly are the best at keeping the Phoenix profitable!

Contents

List of Figures

Chapter 1

Introduction

Since its first use for explaining the origin of cosmic radiation by Fermi (1949), the existence of magnetic fields at large scales in the universe has become a well accepted fact in the astronomy and astrophysical community. Fermi described astrophysical magnetic fields as having '[remarkable] stability because of its large dimension' and electrical conductivity 'so high that one might describe the magnetic lines of force as attached to the matter and partaking in its streaming motion'. This view of a large scale magnetic field that is strongly coupled to the medium where it resides has persisted throughout its study. The hypothesis of galactic scale magnetic fields had early success as Fermi explained: it 'yields naturally an inverse power law for the spectral distribution of the cosmic rays'.

Further evidence for galactic magnetic fields was presented in a letter to nature by Hoyle (1953) which set out to explain the cosmic origin of radio emission assuming that the emission was due to the blackbody radiation of diffuse gas, heated by high speed galactic collisions. He noted that to achieve the proper rate of emission seen in observation, one had to assume a charge separation that could easily be accomplished with a large scale magnetic field. In a later paper, Hoyle (1959) expanded on a theory proposed by Ginzburg and Shklovsky that suggested that the non-thermal, non-stellar radio emission is due to the synchrotron radiation of electrons moving in the presence of a magnetic field.

More recently, radio polarization studies have allowed for the mapping of the magnetic field structure in nearby spiral galaxies. M51 is one of the most studied galaxies in this field, as it is nearly completely face-on. Since the early 70s (Berkhuijsen, 1997) linear polarization studies

of radio emission have been conducted, and magnetic field structure deduced. Berkhuijsen (1997) constructed a general method of analyzing radio polarization by parameterizing the deduced magnetic field data in terms of the Fourier expansion of the field along the azimuthal angle (for cylindrical polar coordinates).

$$\mathbf{B} = \sum_m \mathbf{B}_m e^{im\phi}$$

Their main conclusions were that over a large portion of the galaxy, the magnetic field could be globally represented by a superposition of the two lowest azimuthal ($m = 0, m = 1$) Fourier modes. Additionally, Berkhuijsen (1997) showed a strong correlation between the dynamical history of the disk and the structure of the magnetic field and that the inner part of the disk showed evidence of a strong coherent magnetic field. Meanwhile the outer disk, which is known to have had an encounter with a companion, showed an incoherent field of weak strength.

The property of astrophysical magnetic fields mimicking the structure of their host environment is not isolated to M51. Beck et al. (1996) collected all of the available polarization data (32 galaxies reported) of nearby galaxies which showed large scale, structured magnetic fields. The global structure of the sample varied greatly between galaxies: in the spiral structure of galaxies, the global magnetic field was generally dominated by an axisymmetric, bisymmetric or mixed spiral structure field. In general the fields were dominated by the $m = 0$ amplitude superimposed with mixed amplitudes of higher order azimuthal modes. These higher order amplitudes tended to carry along the particular symmetries seen in the fields.

So we require a theoretical framework to explain the creation and persistence of large scale magnetic fields. An obvious starting point is to assume that the magnetic field has primordial origins; that it existed before the galaxy and was captured by the ionized gas as the galaxy was forming. During the collapse, the field would be magnified as the gas is compressed; a result that can be attributed to flux conservation of the field (Parker, 1969a). For a statistically isotropic universe, one would expect that the primordial field would be similarly isotropic. However as the gas compresses, the magnetic field would be re-oriented and further amplified by the differential rotation of the forming galaxy resulting in a structure much like what we see today (Parker, 1969a). The trouble with this construct is that for one, the amplification of the field is only linear in time (as we will see later). And second, the field quickly diffuses away due to the resistivity (inverse of the conductivity) in the interstellar medium.

While the above approach ultimately is not expected to produce a large scale magnetic field of strengths observed today, it does bring up a critical component of dynamo theory that is worth discussing. For all dynamo theories, a common element is the need for a seed field to begin the amplification. Such a seed field could have been produced at the beginning of the Big Bang; in the framework of a Friedmannian cosmology. Zeldovich noted that a weak uniform magnetic field can be given as an initial condition at the Big Bang (Beck et al., 1996). One can constrain the strength of such a field, as it would create anisotropies in the spin-flip of neutrinos in the early universe. Doing so constrains the strength to a few $10^{-13}G$ or lower. This framework, however is unsatisfactory as the incorporation of an initial magnetic field to the early universe does not fit with the current understanding of homogeneous and isotropic cosmology (Beck et al., 1996). Alternatively, small-scale magnetic fields could be generated by quantum effects in the early universe (see Beck et al. (1996) and references there in). The resulting magnetic field would have scales less than the scale of protogalaxies (even after cosmological expansion) and a magnitude at most a few $10^{-23}G$ (Beck et al., 1996). Finally, at later times seed fields can be created through mechanisms such as the Biermann Battery mechanism. Through such a mechanism, magnetic fields can be created from an electron pressure term that is found in the generalized Ohm's law. This term will cause an initially zero magnetic field to grow linearly until the dynamo term takes over (Kulsrud, 1999), seeding the dynamo with field on the order of a few $10^{-20}G$ and up to $10^{-19}G$ (see Kulsrud (1999) and Pudritz & Silk (1989)) in protogalaxies.

The linear rate of growth of the magnetic field approach above also assumes that the fluid in the galaxy is a laminar flow. This kind of flow is not what is believed to be dominating the gas in the galactic disk, turbulent motion tends to dominate flow and further complicates the picture of magnetic field growth. In the limit of weak field strength, the dynamics of the velocity field of the plasma will be mostly dominated by turbulent motions rather than forces exerted by the magnetic field. In this limit, if you consider a closed bundle of magnetic field lines, a field of toroidal shape, work will be done against the magnetic stresses and kinetic energy will be converted to magnetic energy (Biermann, 1953). This process is expected to continue until the magnetic energy density is comparable to the kinetic energy density, at which point the dynamics of the turbulence becomes comparable by the magnetic force lines.

Considering the same limit, Bachelor found that the induction equation is identical to the equation of motion of the vorticity (Kraichnan & Nagarajan, 1967). This suggests a similarity between the

dynamics of the vorticity and the dynamics of the magnetic field. Kraichnan & Nagarajan (1967) showed that if you follow this assumption to its conclusion, the magnetic field should ultimately decay to zero. The reason for this comes from the conservation of fluid helicity, as a creation of vorticity at one scale results in the destruction of it in another, and similarly for the magnetic field. So the decay of magnetic energy at small scale due to Ohmic dissipation could only be counteracted by withdrawing magnetic energy from larger scales (Kraichnan & Nagarajan, 1967). Such a process is known as an 'anti-dynamo' where the large scale magnetic field is destroyed through a direct cascade of energy from the largest scales to the smallest. In the Kraichnan & Nagarajan (1967) paper, the magnetohydrodynamics equations were closely analyzed and terms representing both creation and annihilation of magnetic fields were found for all scales. It was argued that because the terms are of the same order, a simple physical argument is insufficient for explaining the existence (or nonexistence) of dynamo action. The claim is that a full, quantitative analysis is required to understand whether a turbulent velocity field would cause the growth or decay of magnetic fields.

This quantitative analysis was worked out by Parker (1969b) and applied to galaxies by Parker (1969a). The work showed that in the weak field limit, the magnetic field would grow quickly at all scales. Parker (1969a) estimated that the timescale for the growth would be on the order of a few hundred million years, growing up to a field strength on the order of a few micro gauss. At this magnitude, it is expected that the magnetic field would then become important in the fluid dynamics, and so the weak field analysis could say no more past this point. Parker points out that at this point, the differential rotation would further stretch out the field, increasing the magnetic energy density in a fashion similar to the process described by Biermann (1953).

The work done by Parker, and followed up by many other authors, soon became known as the kinematic limit of mean field dynamo theory. The kinematic limit assumes that the magnetic field is weak enough that it does not effect the dynamics of the plasma, so one chooses a known velocity field to input into the induction equation. Mean field dynamo theory is a method of determining the dynamics of the large scale magnetic field by averaging the induction equation and only analyzing the average (large scale) field while ignoring fluctuating quantities. As in Parker (1969b), the kinematic limit is believed to apply up to the point when the magnetic and kinematic energies are comparable (known as equipartition). Mean field dynamo theory benefits from its simplicity and physical clarity but completely overlooks the effect of small scale fluctuations in the magnetic field (Zeldovich et al., 1983). Frisch et al. (1975) showed that when the small scale fluctuations of the magnetic field

are considered, the dynamics of the magnetic helicity becomes an important factor in the growth of magnetic energy.

The kinematic picture of mean field dynamo theory has fallen under scrutiny recently due to further analysis which has shown that the kinematic limit might not last as long as previously expected. Cattaneo & Vainshtein (1991) showed that the magnetic field can have nonlinear effects while appearing to be in the kinematic limit, when the magnetic energy is factor of the magnetic Reynolds number ($Rm = UL/\eta$) below equipartition. This could pose a serious issue in an astrophysical setting, due to the wide range of magnetic Reynolds number ($Rm \approx 10^7$ in stellar convection zones and $\approx 10^{14}$ in the galaxy, see Cattaneo & Vainshtein (1991)). Kulsrud & Anderson (1992) argued that the kinematic limit was in fact invalid since the turbulence becomes modified by the magnetic field well before the dynamo starts. Gruzinov & Diamond (1994) and Gruzinov & Diamond (1996) showed this last fact explicitly by computing a suppression of the standard mean field theory α-parameter numerically.

In the following chapter the kinematic limit of mean field dynamo theory will be elaborated in more detail. The numeric and theoretical issues of the kinematic approximation will then be introduced as a way of motivating a different source for dynamo action. This new source, constrained by the conservation of magnetic helicity, will be derived and its repercussions will be discussed. In chapter 3 the numerical method that was implemented to test the predictions of this new source of dynamo action will be introduced and its mathematical consistency will be verified. Finally in chapter 4 the results of the four runs of the code are introduced and their implications are discussed. In general we will find that the new source does a better job of estimating the electromotive force than the kinematic approximation.

Chapter 2

Dynamo Theory

The collective knowledge regarding magnetic field growth in astrophysical systems is contained within Dynamo Theory. Astrophysical systems often contain many levels of complications over different length scales; so several assumptions and simplifications must be made if we wish to study the underlying physical processes that drive the dynamo. To that end, we will often reference galaxies as a testing ground for dynamo theory. This choice is partially a historical one, since the galactic magnetic field was a main driver for magnetic dynamo research and partially due to the simplicity of the geometry in galactic disks. The latter stems from the assumption of a two dimensional shearing field, with little large scale motion in the third direction. Conversely if one considers a system with spherical geometry (the Earth and Sun for example), one must contend with differential rotation as well as convection (if appropriate) which results in large scale motions in all three dimensions.

So we will make reference to galaxies only as far as they give us a strong motivation for selecting the particular geometry that is used in our numerical simulations. We will also make appropriate assumptions, like incompressibility and a lack of self-gravity that will allow for the study of the underlying physics involved in dynamo action while ignoring much of the complicated structure that is present.

2.1 Definitions

As mentioned in the last chapter, compressing the primordial field during the initial collapse of the galaxy and realigning it with differential rotation is insignificant to explain the current magnitude

and orientation of galactic magnetic fields. So the question became, how is it that magnetic fields can be amplified over many orders of magnitude? And how can the field be sustained against diffusion over such a long time span? It is generally accepted that the answer to these questions is a dynamo process. A dynamo amplifies initially weak magnetic fields by converting the kinetic energy of the fluid into magnetic energy. The exact method of this conversion and amplification remains debatable, however the presence of a dynamo process to explain the persistence of magnetic fields is required.

Because of the presence of turbulence, the importance of different scales to the dynamo will become apparent. The dynamo process can be split into two parts: the small scale and large scale dynamo. For this work, small scale denotes features of size comparable to or smaller than the eddy scale (the typical size of the turbulent motion), while large scale structure has a size on the same order as the whole system. A small scale dynamo would produce and sustain small scale magnetic fields which tend to be highly turbulent and close to equipartition as they are highly controlled by turbulent motion. Large scale dynamos are believed to produce larger, more ordered magnetic fields such as the fields found around the Earth (Busse, 1978), the Sun (Parker, 1977) and as mentioned earlier the Milky Way and other galaxies.

Large and small scale dynamos tend to result from different mechanisms, so their existence has different requirements and they require different initial conditions. Small scale dynamos require only small (on the order of eddy scales), incoherent magnetic fields, while the large scale dynamo generally requires a large, coherent magnetic field, often being created by the small scale dynamos. This last fact does not imply the co-existence of small scale and large scale dynamos, as magnetic fields can be saturated in the small scale dynamo phase long before the emergence of a large scale dynamo.

2.2 Turbulence

The topic of turbulence has come up a number of times, so some discussion is required. Turbulence is characterized by generally chaotic motions in fluids and is generally accepted to be a dominant state of the interstellar fluid (see the reviews Elmegreen & Scalo (2004) and Scalo & Elmegreen (2004)). A primary property of turbulence is its ability to transfer energy through scales. This transfer is often called a cascade and has two directions: direct and inverse. In direct cascades, power is transferred from the largest scales to the smallest scales, while in an inverse cascade the power is transferred from the smallest scales to the largest.

There are two important scales to consider when (direct) cascade is involved. The first is known as the inertial scale, where energy is injected into the system. The second is the dissipation scale, where energy can be dissipated faster than the eddy turnover time - the characteristic time it takes energy to be passed between scales. Since the final state for a system in inverse cascade is a build up at large scales, the dissipation scale is not typically considered as dissipation is inefficient at large scales. There is an eventual equilibrium that can be reached in the case of a direct cascade with constant energy input. The equilibrium is set once the rate at which energy is dissipated equal to the rate of input. Andrey Kolmogorov was the first to consider the effect of the cascade in this equilibrium system mathematically. Kolmogorov's work will be summarized here (taken from (Biskamp, 2003, p. 96-97)): take the largest scale of the system and split it into a discrete number of N scales $l_n = 1/k_n$ where the largest scale l_0 is close to the inertial scale and the smallest l_N is the dissipative scale. A typical turbulent eddy of size l_n in an incompressible fluid is defined by the average difference in velocity δv_{l_n} or δv_n between the edges of l or by the Fourier component v_k where $k = 1/l$ (whose equality is taken for simplicity), the eddy turnover time is then

$$\tau_n \sim l_n/\delta v_n$$

so the constant energy flux in an equilibrium state would be given by

$$E_n/\tau_n \sim \delta v_n^3/l_n \sim \epsilon$$

and so the velocity differences would be given by

$$\delta v_n \sim \epsilon^{1/3} l_n^{1/3}$$

We wish to write the energy in terms of Fourier component k_n so assuming that $E_k \simeq v_k^2$ is the spectral energy density

$$\begin{aligned} \int_{k_n}^{k_{n+1}} E_k dk \simeq E_k k &\approx E_n \sim \delta v_n^2 \\ E_k &= C_K \epsilon^{2/3} k^{-5/3} \end{aligned} \tag{2.1}$$

which of course is the well-known Kolmogorov spectrum. The Kolmogorov constant C_K has been

shown to be invariant to small statistical scatter, and has a value that varies between $1.6 - 1.7$ (Biskamp, 2003, p. 97) over a broad range of Reynolds number ($30 \leq R_e \leq 3 \times 10^4$). The Reynolds number is a common dimensionless parameter defined by $Re = UL/\nu$ and is used to describe the type of flow. High Reynolds number implies less viscous, 'faster' motion and small Reynolds number implies more viscous, 'slower' motion. The idea of analyzing turbulent systems in terms of their power spectrum is an important part of turbulent theory, and so we will revisit this idea in later sections.

2.3 Magnetohydrodynamics (MHD) Equations

For all considerations above we have implicitly assumed that the galaxy can be approximated by a fluid. A fluid approximation requires that the mean free path of the particles is smaller than the gradients in the system. When the particles in the fluid are charged, an additional requirement is that the magnetic fields are considered on scales larger than the internal scales of the plasma. An example is the Larmor radius, which takes on the role of the mean free path when the motion is perpendicular to the magnetic fields. Most astrophysical systems follow the fluid approximation apart from systems of weakly interacting particles, when the mean free path becomes large. Under the fluid approximations, one can model the dynamics of a magnetized plasma by the Navier-Stokes (momentum) equation and Faraday's law (Induction equation). As most astrophysical systems are rotating systems, the MHD equations are often written in a rotating reference frame (combing equations 2.7,2.15 and 2.26 from Biskamp (Biskamp, 2003, p.12-16)):

$$\partial_t \mathbf{V} + (\mathbf{V} \cdot \nabla)\, \mathbf{V} = -\frac{1}{\rho}\nabla P + \frac{1}{c\rho}\mathbf{J} \times \mathbf{B} + 2\mathbf{V} \times \mathbf{\Omega} + \mathbf{f} + \nu \left(\nabla^2 \mathbf{V} + \frac{1}{3}\nabla\nabla \cdot \mathbf{V} \right) \tag{2.2}$$

$$\partial_t \mathbf{B} = \nabla \times (\mathbf{V} \times \mathbf{B}) + \eta \nabla^2 \mathbf{B}, \qquad \nabla \cdot \mathbf{B} = 0 \tag{2.3}$$

Boldfaced values denote vectors. The above equations contain the velocity field $\mathbf{V}$, magnetic field $\mathbf{B}$, electric current density $\mathbf{J} = 1/4\pi\nabla \times \mathbf{B}$, fluid density ρ and pressure P, viscosity ν and magnetic diffusivity η (also known as resistivity). All external mass forces per unit volume are denoted by $\mathbf{f}$ except for the Lorentz force $\mathbf{J}/\rho \times \mathbf{B}/c$ which describes the effect that the magnetic field has on the fluid and is included explicitly. The Coriolis force $\mathbf{V} \times \mathbf{\Omega}$ arises from the rotating reference frame and is included, while the Centrifugal force is not. This fact will be discussed below.

In most theoretical work, incompressibility of the fluid is assumed. This simplifies the above equations since for an incompressible fluid $\nabla \cdot \mathbf{V} = 0$ and one may assume that $\rho = \rho_0 = const.$ For a fluid to be incompressible, any fluid motion $\mathbf{v}$ must be slower than the fastest compressible wave in the direction of $\mathbf{v}$. Additionally, the frequency of the fluid motion must be small compared to the compressible wave, or equivalently the change in the velocity field must be slow compared to its advection. For a weak magnetic field, or motion parallel to a strong magnetic field the size of the divergence is

$$\nabla \cdot \mathbf{V} \sim (V/V_S)^2 \frac{V}{L}$$

where V_S is the sound speed and L is a typical gradient scale. When the magnetic field is strong, motions perpendicular to the field are distinguished from a parallel motion. In the perpendicular case, Faraday's law gives the relation for the divergence of $\mathbf{V}$, resulting in

$$\nabla \cdot \mathbf{V} \sim (V/V_A)^2 \frac{V}{L}$$

where $V_A = B/\sqrt{4\pi\rho_0}$ is the Alfvén speed. So for incompressible motion we require that $V \ll V_S$ or for motions perpendicular to the magnetic field $V \ll V_A$. In general the latter is usually true, particularly in laboratory plasmas where the fluid is incompressible for motions perpendicular to a strong magnetic field. Meanwhile, the former is typically not incompressible and compressible motions become important to the dynamics.

In astrophysical systems, compressibility is clearly an important feature of fluid motion. Shock fronts in the interstellar medium and density waves in galactic disks are two examples of the effects of compressibility in astrophysics. Regardless, the effects of compressibility are often ignored, and incompressibility is assumed. In general, slow processes are not effected by compressibility. Dynamo action and MHD turbulence falls under this category, as it is often observed and simulated in an incompressible plasma.

So we will make the assumption of a fluid of constant density $\rho(\mathbf{r}, t) = \rho_0$ which forces incompressibility ($\nabla \cdot \mathbf{V}$). Additionally, since we will become interested in the evolution of different scales of the magnetic field the fields in eqs. 2.2 and 2.3 are generalized by the 'total' fields $U_T = U + u$ and $B_T = B + b$, denoted by a subscript T. The total field is composed of the large scale field (denoted by a capital letter) and a small scale field (denoted by a lower case letter). And so, using a standard

vector identity we get:

$$\partial_t \mathbf{U}_T + (\mathbf{\Omega}_T \times \mathbf{U}_T) = -\nabla P' + \mathbf{J}_T \times \mathbf{B}_T + 2\mathbf{U}_T \times \mathbf{\Omega}_{cor} + \nu\nabla^2 \mathbf{U}_T + \mathbf{f} \tag{2.4}$$

$$\partial_t \mathbf{B}_T = \nabla \times (\mathbf{U}_T \times \mathbf{B}_T) + \eta\nabla^2 \mathbf{B}_T \tag{2.5}$$

together with $\nabla \cdot \mathbf{U}_T = 0$ from the assumption of incompressibility and $\nabla \cdot \mathbf{B}_T = 0$ from Maxwell's equations give the equations of motion for the system. The modified pressure $P' = P/\rho_0 + U_T^2/2$ replaces the original pressure, and is calculated using the projection method to force incompressibility in the fluid. In an incompressible fluid, any force term that comes in as the gradient of a scalar potential can be incorporated into the modified pressure and effectively ignored. So the centrifugal force and an external gravitational potential may be ignored without loss in generality. Self gravity and vertical gravity are ignored as it would tend to create over densities which would break our requirement of a constant density. In the context of the galactic disk, such an assumption does not miss any important physics. Parker (1966) showed that: 1) the force of attraction from hydromagnetic forces was about five times the strength of the gravitational force and 2) that the interstellar medium should tend to drain downward towards the midplane of the disk (where vertical gravity is minimized) along the magnetic field lines. These results from Parker (1966) motivate our ignoring of the effects of gravity in our analysis. The magnetic field is written in units of $1/\sqrt{4\pi\rho_0}$, which implies that we are involving the Alfvén velocity. The total vorticity $\mathbf{\Omega}_T = \nabla \times \mathbf{U}_T$ and the rotation vector responsible for the coriolis force $\mathbf{\Omega}_{cor}$ are differentiated by their subscript. The remaining forcing term $\mathbf{f}$ will be discussed later.

2.4 Helicity

A concept that will become important in our discussion is the idea of helicity. Helicity is a topological property of a field, that describes the twists and folds of the field. In the simplest system, two enclosed tubes of the field (also known as flux tubes), the helicity of the field is related to the linking number of the tubes. The linking number is a measure of the number of times two flux tubes are wrapped around each other, weighted by the strength of the flux and the relative direction of the two flux tubes. The total helicity of field $\mathbf{C}$ is defined by the volume integral of the dot product of the field

and its curl:

$$H_C = \int_V \mathbf{C} \cdot \nabla \times \mathbf{C} \, dV$$

In MHD turbulence there are three important helicities for our consideration:

$$\begin{aligned} \text{Kinetic helicity} : h^k &= \mathbf{u} \cdot \nabla \times \mathbf{u} = \mathbf{u} \cdot \omega \\ \text{Current helicity} : h^{cur} &= \mathbf{b} \cdot \nabla \times \mathbf{b} = \mathbf{b} \cdot \mathbf{j} \\ \text{Magnetic helicity} : h^m &= \mathbf{a} \cdot \nabla \times \mathbf{a} = \mathbf{a} \cdot \mathbf{b} \end{aligned}$$

Kinetic and current helicity are physical quantities and represent the twist and fold of the velocity and magnetic fields respectively. Meanwhile, the magnetic helicity represents the twist and fold of the magnetic *vector potential* and lacks a direct physical meaning due to its gauge dependence. It is however conserved in MHD systems so is a valuable property to study in the context of dynamo action. These properties and more will be elaborated on in a later section.

2.5 STF Dynamo

As a first effort in understanding dynamo action we consider the stretch-twist-fold (STF) dynamo (Vainshtein & Zeldovich, 1972) within a laminar flow. Though simple, such a dynamo relies on some key aspects that are revisited in more complicated dynamo theories. That is, the conservation of magnetic flux $\Psi = \int_S \mathbf{B} \cdot d\mathbf{S}$ through a surface for highly conductive ($\eta \to 0$) fluids, also known as the 'freezing-in' condition. To see this, we start by taking the time derivative of the magnetic flux:

$$\frac{\partial \Psi}{\partial t} = \int_S \frac{\partial \mathbf{B}}{\partial t} \cdot d\mathbf{S} + \int_S \mathbf{B} \cdot \frac{\partial}{\partial t} d\mathbf{S}$$

The first term represents the change of the magnetic field within the surface, and the second term is the flux of the magnetic field through the boundary C of the surface S as the surface itself changes due to fluid motions. As the surface changes, a small element $d\mathbf{l}$ on C will sweep out an area of $\mathbf{V} \times d\mathbf{l}$. With this, along with eq. 2.3 we have

$$\frac{\partial \Psi}{\partial t} = \int_S \left(\nabla \times (\mathbf{V} \times \mathbf{B}) + \eta \nabla^2 \mathbf{B} \right) \cdot d\mathbf{S} + \int_C \mathbf{B} \cdot \mathbf{V} \times d\mathbf{l}$$

The second term can be rewritten as $\int_C \mathbf{B} \times \mathbf{V} \cdot d\mathbf{l} = \int_S \nabla \times (\mathbf{B} \times \mathbf{V}) \cdot d\mathbf{S} = -\int_S \nabla \times (\mathbf{V} \times \mathbf{B}) \cdot d\mathbf{S}$ by Green's theorem. The result is that the time derivative becomes:

$$\frac{\partial \Psi}{\partial t} = \int_S \eta \nabla^2 \mathbf{B} \cdot d\mathbf{S} \to 0, \quad \text{as} \quad \eta \to 0$$

The freezing-in condition is often expressed as the magnetic field being 'stuck' to the ions in the plasma. Flow transverse to the field lines tends to sweep the field lines along, while flow along the field lines does little to the field orientation.

The effect of such a condition can be modeled by the STF dynamo. Consider a closed flux tube within a laminar, incompressible, highly conductive fluid flow. If the length of the loop is doubled, the incompressibility of the fluid requires that the cross-section of the loop is halved to conserve the volume of the loop. Through flux conservation, the magnitude of the field is also doubled. To complete the dynamo, the loop is twisted, forming a figure-eight and folded at the crossing point. Next it is required that at least some diffusion is allowed in order for the two folded loops to diffuse together, re-forming the original configuration of the magnetic field but with twice the magnitude. In principle the process may be repeated indefinitely, doubling the magnitude with every iteration. This stretch, twist and fold dynamo is an important feature of any dynamo theory as it captures the need for the shear to convert kinetic energy to magnetic energy through stretching, and for a process (possibly turbulence) to twist and fold the stretched flux tube back to an organized orientation. It is important to note that the direction of the flux, twist or fold was not mentioned nor does it change the above picture, and as a result such a dynamo does not require turbulence of net helicity.

2.6 Small Scale Dynamo

Small scale dynamos are expected to amplify magnetic fields on the scale of the largest turbulent eddy and below, down to the dissipative scale where energy is most efficiently lost. Turbulence is typically modeled by a process called Richardson diffusion: a random process which causes particles that were initially close together to drift apart. As the particles move apart the frozen-in magnetic field is stretched and the magnitude is amplified through the same mechanisms as in the stretching phase of the STF dynamo. As the field is stretched, the scale of the field perpendicular to the stretching is decreased and the effect of dissipation strengthens, eventually reaching an equilibrium.

Such a system will quickly build a strong (close to equipartition) magnetic field that is spatially chaotic. In non-ideal MHD (even in the limit of vanishing resisitivity), finite diffusion limits the efficiency of such a mechanism as diffusion allows for the magnetic field lines to drift with respect to the ions.

Some theoretical success has come in studying such a chaotic dynamo by Kazantsev (1968), and more recently by Chertkov et al. (1999). The formalism assumes that the turbulence undergoes a homogeneous, isotropic strain and is Gaussian white noise (West et al., 2003). The growth rate of the even modes of the magnetic field energy density was worked out by Chertkov et al. (1999) (the lowest order being worked out by Kazantsev (1968)). The modes tended to grow exponentially, and form a structure similar to an elongated strip. Numerical simulations by West et al. (2003) showed good agreement between the theoretical predictions and the numerical results. A result of the theoretical and numerical work is that the small scale dynamo requires the magnetic Reynolds number $Rm = VL/\eta$ to be larger than some critical value: $R_{m,c} \sim 60$ (Subramanian, 1997). This one requirement appears to be the only required property in the turbulence for the small scale dynamo to exist.

The interaction between the small scale and the large scale dynamo is not completely clear. It has been shown in numerical simulations that the small scale dynamo can act as seed to the large scale dynamo (see for example Poezd et al. (1993)), while other work has shown that the two mechanisms can be completely independent. An interaction that will become important to our discussion comes from the fact that the Richardson diffusion mechanism does not conserve magnetic helicity. The importance of such a statement will become more clear in a later section (2.7.4); for now, it suffices to say that it is expected that turbulent motions can act as a source of magnetic helicity at eddy scales. Its production, and subsequent inverse cascade to larger scales does suggest an important connection between the small and large scale dynamos; which is considered in later sections.

2.7 Large Scale Dynamo

While the small scale dynamos can efficiently create and sustain magnetic fields on the scale of the largest eddies, they typically result in random, isotropic fields. As seen in astrophysical settings, magnetic fields tend to be large scale, on the order of the whole system (often orders of magnitude larger than the largest eddy) and strongly ordered. The magnetic field of our Earth, Sun and external

galaxies are excellent examples of this. So there must be a separate mechanism for the generation and organization of large scale magnetic fields.

2.7.1 Kinematic Approximation

Solving the MHD equations has long been a challenge for theorists, as they are a set of nonlinear, and coupled differential equations. Analytically, no solution exists for these equations, while numerically the set of equations are computationally expensive to solve and resources for high magnetic Reynolds number ($Rm \gg 1$) MHD turbulence simulations still do not exist. Most analytical work is done using the kinematic approximation. In such an approximation, it is assumed that the magnetic field is sufficiently weak that the Lorentz force in the Navier-Stokes equation does not contribute to the dynamics of the velocity field. In such an approximation, one takes a prescribed velocity field $V(\mathbf{r}, t)$ (either laminar or turbulent flow) and solves the Induction equation to achieve the dynamics of the magnetic field. The approximation was believed to be valid up until the magnetic energy density is comparable to the kinetic energy density (equipartition), at which point the Lorentz force then becomes dominant and the velocity field would change in response to the new force. The issues with the kinematic approximation were not fully understood until numerical simulations of MHD turbulence were performed. It was found that nonlinearities in the MHD equations (eg. Lorentz force) became important before when the system was still on the order of the magnetic Reynolds number below equipartition (Cattaneo & Vainshtein, 1991). Because astrophysical systems are nonlinear, we will require a more complicated view than the kinematic approximation.

2.7.2 Mean Field Dynamo Theory

The nature of the problem suggests a way of solving the complicated set of MHD equations. Because we are interested in solving the dynamics of the largest scale component of the magnetic field, we focus on evolving only the average magnetic field, ignoring the fluctuating quantities that are difficult to observe. This method of understanding the large scale dynamo is known as the Mean Field Dynamo Theory (MFT, see Moffat (1978) and Parker (1979)). To derive the evolution of the average magnetic fields, we apply a low-pass filter to the Induction equation in eq. 2.5. This low-pass filter is denoted by angle brackets and returns the large scale component of the filed. By definition, for any field $A_T = A + a$ the large scale (observable) component is defined as $A = \langle A_T \rangle$

and the small scale (turbulent) component $a = A_T - A$. Obviously, the low-pass filter of a large scale field returns the same field, so $\langle a \rangle = 0$. Any product of a large scale and small scale quantity will have a negligible large scale component. So it is assumed that double products $\langle Aa \rangle \approx 0$ and triple products $\langle AAa \rangle \approx 0$ are assumed negligible at large scales. This leads to a convenient form of any multiplication operator '$\circ$': $\langle A_T \circ B_T \rangle \equiv \langle A \rangle \circ \langle B \rangle + \langle a \circ b \rangle$, the effects of which can be seen in eq. 2.6. The filter operator and the derivative operator commute, hence $\langle \mathbf{J}_T \rangle = \langle \nabla \times \mathbf{B}_T \rangle = \nabla \times \langle \mathbf{B}_T \rangle$.

So we apply the filter to the induction equation which results in:

$$\begin{aligned} \partial_t \langle \mathbf{B}_T \rangle &= \nabla \times \langle \mathbf{U}_T \times \mathbf{B}_T \rangle + \eta \nabla^2 \langle \mathbf{B}_T \rangle \\ \partial_t \mathbf{B} &= \nabla \times (\mathbf{U} \times \mathbf{B} + \langle \mathbf{u} \times \mathbf{b} \rangle) + \eta \nabla^2 \mathbf{B} \end{aligned} \tag{2.6}$$

where $\langle \cdot \rangle$ denotes a filtered quantity. Recall that the total field is broken into two components, the large scale (average) field and the small scale (turbulent) field so that $\langle \mathbf{B}_T \rangle = \mathbf{B}$. Applying such a filter requires a sufficiently well defined separation of scales, meaning that the power in the largest scales and the power in eddy scales are well separated in spectral space. Since the size of astrophysical systems can vary over many orders of magnitude, the form of eq. 2.6 is beneficial as it greatly narrows the scales that must be analyzed. In general, the large scale interaction between the magnetic and velocity fields ($\mathbf{U} \times \mathbf{B}$) do not produce a sufficient dynamo action to sustain a large scale magnetic field. This is mainly due to the large scale component of the fields being strongly aligned in typical systems, so that their cross product is small. Because of its size, this term is generally ignored in mean field dynamo calculations. This simplifies the goal for MFT: to calculate the electromotive force $\mathcal{E} = \langle \mathbf{u} \times \mathbf{b} \rangle$ - the driver of large scale dynamo action.

From the definition of the small scale fields above, the evolution of the fluctuating magnetic field can be calculated:

$$\partial_t \mathbf{b} = \nabla \times (\mathbf{U} \times \mathbf{b} + \mathbf{u} \times \mathbf{B}) + \nabla \times \mathbf{G} + \eta \nabla^2 \mathbf{b} \tag{2.7}$$

where $\mathbf{G} = \mathbf{u} \times \mathbf{b} - \langle \mathbf{u} \times \mathbf{b} \rangle$.

To calculate the evolution of the average field, we wish to estimate $\mathcal{E}$. In the kinematic limit, when $\mathbf{V}$ and $\mathbf{B}$ are independent eq. 2.7 implies that $\mathbf{b}$ and $\mathcal{E}$ are linear in $\mathbf{B}$ and its derivatives (see

Yoshizawa (1990) or (Biskamp, 2003, p. 69)):

$$\mathcal{E}_i = \alpha_{ij} B_j + \beta_{ijk} \partial_k B_j + \dots \tag{2.8}$$

where α_{ij} and β_{ijk} are tensors that generally depend on the velocity field and the viscosity. For non-zero α the underlying velocity field should be mirror asymmetric. The simplest way this can occur is if the fluid possesses non-zero kinetic helicity. This condition is in general not mandatory, as a fluctuating (but zero average) kinetic helicity can produce a non-zero α.

For a homogeneous, isotropic turbulence the coefficients in eq. 2.8 can be written as $\alpha_{ij} = \alpha\delta_{ij}$ and $\beta_{ijk} = \beta\varepsilon_{ijk}$ so

$$\mathcal{E} = \alpha\mathbf{B} - \beta\mathbf{J} \tag{2.9}$$

So we find that the evolution of the large scale magnetic field depends on the magnitude of the 'induction' α and turbulent diffusivity β in the plasma. The first term in eq. 2.9 is the familiar 'α-effect': $\partial_t\mathbf{B} = \nabla\times(\alpha\mathbf{B})$ and lends itself to a convenient starting point for a dynamo mechanism. The α-effect will tend to twist the magnetic field into the orientation of the current field. For example, a poloidal field (toroidal current) embedded in a flow of non-zero kinetic helicity will twist into a toroidal field under the influence of the α-effect. The α-effect plays an important role in the $\alpha\Omega$ dynamo that is believed to be acting in the Sun. For an initially poloidal field, differential rotation stretches the field into a toroidal field (Ω-effect). Then through the α-effect, the toroidal field is twisted, re-producing a component in the poloidal field.

Mean Field Dynamo Theory quickly gained acclaim in the astrophysical community as it greatly simplified the calculation of the large scale dynamo action. The challenge then came down to calculating the turbulent transport coefficients. Often, the coefficients α and β are calculated using eq. 2.7 and assuming that the turbulent fluctuations in the term $\mathbf{u}\times\mathbf{b}$ is negligible, meaning that $\mathbf{G} = 0$. This assumption is known as the first order smoothing approximation (FOSA) and requires that the fluctuation of the magnetic field is small: $\mathbf{b} \ll \mathbf{B}$. Furthermore, for small fluctuations the time derivative of $\mathbf{b}$ is small and can be ignored. With that, and solving eq. 2.7 with a known velocity field one gets (Biskamp, 2003, p. 123-125)

$$\alpha = -\tau h^k/3 \quad \text{and} \quad \beta = \tau|\left\langle \mathbf{u}^2 \right\rangle|/3 \tag{2.10}$$

where τ is the correlation time of the turbulence (eddy turnover time). In general, FOSA is only applicable in the low Reynolds number limit, however as long as the correlation time is small FOSA can be made applicable in the limit of high Reynolds number. In this limit, eq. 2.7 can still be solved, and the values α and β do not change significantly.

2.7.3 Problems with MFT

There have been several objections, both theoretical and numerical to the kinematic approximate mean field dynamo (see Cattaneo & Hughes (1996) and Gruzinov & Diamond (1994) and (1996)). Most objections surround the assumption that the magnetic field does not effect the dynamics of the velocity field. It was shown in numerical simulations by Cattaneo & Vainshtein (1991) that the critical magnetic energy density for the saturation of the dynamo was on the order of Rm times lower than equipartition. This is a problem for astrophysical dynamos since Rm can vary between 10^7 for solar convective zones, and 10^{14} for galaxies (Cattaneo & Vainshtein, 1991). So we would expect strong suppression of the dynamo for weak magnetic fields. Further theoretical work by Vainshtein & Cattaneo (1992) and later by Gruzinov & Diamond (1994) showed that the suppression could be modelled by a modification to the α parameter by the large scale magnetic field. The new α parameter is

$$\alpha = \frac{\alpha_0}{1 + R^2} \tag{2.11}$$

where $\mathbf{R} = Rm^{1/2}\mathbf{B}/\left(\rho V^2\right)^{1/2}$ is the root of the magnetic energy density, in units of the equipartition energy and the Reynolds number Rm, and it is assumed that α_0 is the original MFT α parameter. Note that as large scale magnetic energy increases, the α parameter decays and the dynamo is quenched. Known as the α-quenching problem, it begs the question of whether MFT is able to accurately model the nonlinear interactions involved in astrophysical systems, and whether the α-effect is responsible for dynamo growth at large scale.

The validity of FOSA is also largely debated. This is mainly due to the fact that as we have seen, the small scale dynamo tends to be an efficient way of growing the fluctuating component of the magnetic field (for $Rm > Rm_{crit} \sim 60$). This exponential growth breaks the requirement of a weak fluctuating field that was made in section 2.7.2.

Additionally, the MFT has no construct to explain scale propagation. While the α-effect can

amplify a seed field, the scale remains the same. Alternatively, a small scale dynamo may only increase the scale of a magnetic field up to the size of the largest turbulent eddy. So if we wish to seed a large scale dynamo by a small scale dynamo, we require a mechanism not covered in MFT to cascade energy to larger scales. As we will see, there is evidence that such a mechanism could be linked to the inverse cascade of magnetic helicity.

There is also an issue surrounding the usage of kinematic helicity as a driver for dynamo growth, as a net kinetic helicity can effect the energy cascade of the fluid. Kinetic helicity $H^k = \mathbf{V} \cdot \mathbf{\Omega}$ is associated with an explicit sign, denoting the alignment between the velocity field (V), and its associated vorticity (Ω). A positive kinetic helicity implies a more aligned velocity and vorticity, meaning that the nonlinear term in the Navier-Stokes equation: $\mathbf{V} \times \mathbf{\Omega}$ is small. In this case, the resulting cascade would be slower, reducing the effective dissipation in the turbulence. Additionally, it was shown by Teitelbaum & Mininni (2008) that in the presence of rotation, such an effect was amplified and the decay rate of kinetic energy was drastically altered. Like kinetic energy, kinetic helicity undergoes a direct cascade, and so builds up at the smallest scales. This can be seen with a simple dimensional analysis by seeing that $\mathbf{V} \cdot \mathbf{\Omega} \sim V \cdot kV \sim E/L$ is similar to an energy divided by a length scale. Obviously, E/L is largest at the smallest scale due to the inverse cascade of kinetic energy. While kinetic helicity is perfectly conserved in ideal hydrodynamics, in MHD and non-ideal hydrodynamics it is not. The evolution of the total kinetic helicity changes drastically when finite viscosity is added. One can calculate an approximate evolution from scaling arguments

$$\frac{d}{dt}\left|\int_V (\mathbf{V} \cdot \mathbf{\Omega})\, dV\right| \sim \nu^{-1/2} \to \infty \quad \text{as} \quad \nu \to 0 \tag{2.12}$$

so the conservation diverges very badly even for infinitesimal viscosity. Such a conclusion was backed by direct numerical simulations by Chen et al. (2003) who showed that in the limit of $\nu \to 0$ the small scale helicity of different sign diverge, even when the net helicity is constant and finite.

As we have seen in eq. 2.11, the α parameter is modified by the large scale magnetic field, even during the linear regime. Additionally, further nonlinear modifications can come from a build up of current helicity ($\mathbf{j} \cdot \mathbf{b}$). Yoshizawa (1990) derived the effect of the current helicity on the electromotive force, it was found that its derivative evolved as:

$$\frac{\partial \mathcal{E}}{\partial t} = \langle \dot{\mathbf{u}} \times \mathbf{b} \rangle + \left\langle \mathbf{u} \times \dot{\mathbf{b}} \right\rangle = -\frac{1}{3}\left(\langle \mathbf{u} \cdot \omega \rangle - \langle \mathbf{j} \cdot \mathbf{b} \rangle\right) \mathbf{B} - \frac{1}{3}\left(\left\langle \mathbf{u}^2 \right\rangle\right) \mathbf{J} + \ldots \tag{2.13}$$

The included terms are quadratic in the small scale fields, and all higher order terms are ignored. This then suggests a new form of the α and β terms from before:

$$\alpha' = -\frac{1}{3}\left(h^k - h^{cur}\right) \quad \text{and} \quad \beta' = -\frac{1}{3}\left\langle u^2 \right\rangle \tag{2.14}$$

Note that the correlation time τ is dropped here, because eq. 2.13 represents the derivative of $\mathcal{E}$ rather than the function itself. In the presence of a large scale magnetic field, both terms will pick up a prefactor as in eq. 2.11. In general the $\mathcal{E}$ from eq. 2.14 is difficult to compute, as there does not exist an equation to connect the current helicity to mean values. However, it can be said that there exists a magnetic back-reaction in the current helicity that can lead to a suppression in the dynamo when the fluctuating magnetic field is strong. So we are finding that the build up of kinetic helicity alone can not sustain a large scale dynamo for a long time, as the small scale dynamo can quickly build up a back-reacting field that can either saturate or reverse the dynamo.

2.7.4 Magnetic Helicity

A quantity that can not be ignored in the context of MHD turbulence and dynamo action is the conserved quantity: magnetic helicity. Like the kinetic and current helicity, magnetic helicity describes the twist and fold of the magnetic field lines. It is a topological property of the field that generally lacks a unique definition. For example, a group of closed, linked and non-twisted flux tubes have a helicity that is equal to the total linking number of the group (for unit flux). While this picture is useful for a physical representation of helicity: a twisting and looping of the fluid, it has no real application to our analysis. Magnetic fields tend to be much more complicated than a collection of flux tubes. For a continuous system the total magnetic helicity is typically defined as

$$H^M = \int_V \mathbf{A}_T \cdot \mathbf{B}_T dV \tag{2.15}$$

where $\mathbf{A}_T$ is the magnetic vector potential and has its usual definition. Magnetic helicity is similar in principle to the other helicities but has no physical meaning. The lack of physical meaning is due to its gauge dependence. If we let $\mathbf{A}' = \mathbf{A} + \nabla\chi$ then you can show that the resulting magnetic

helicity would differ by

$$H^{M'} - H^{M} = \int_V \mathbf{B}_T \cdot \nabla\chi dV = \oint_S \chi \mathbf{B}_T \cdot d\mathbf{S} \tag{2.16}$$

In general such a gauge dependence is a problem, but as long as the gauge does not include eddy scale terms then the results will be equivalent. There is also a modified version of the magnetic helicity suggested by Finn and Antonsen (see Biskamp (2003) and reference there in)

$$H^{M}_{alt} = \int_V (\mathbf{A} + \mathbf{A}_0) \cdot (\mathbf{B} - \mathbf{B}_0)\, dV \tag{2.17}$$

where the reference field $\mathbf{B}_0 = \nabla \times \mathbf{A}_0$ is chosen to match the asymptotic properties of the magnetic field in an open boundary. In a closed boundary, the reference field is chosen to have the same normal components as the magnetic field. This definition of the magnetic helicity is invariant to any gauge transformation, regardless of whether the gauge transformation of $\mathbf{A}$ and $\mathbf{A}_0$ are equivalent. In what follows, we will assume the Coulomb gauge $\nabla \cdot \mathbf{A}_T = 0$ as it does suggest a useful physical meaning of the magnetic helicity. Under the Coulomb gauge, the current helicity and magnetic helicity are highly correlated so that the build up of magnetic helicity follows directly from the build up of current helicity. Further, requiring that the vector potential vanishes at infinity leads to the following definition of the vector potential

$$\mathbf{A}_T(\mathbf{r}) \equiv \int \frac{\mathbf{J}_T(\mathbf{r})}{4\pi \left|\mathbf{r} - \mathbf{r}'\right|} d^3\mathbf{r}' \tag{2.18}$$

which illustrates the strong connection between local values of current and magnetic helicities.

In studying its conservation we wish to derive the evolution of the magnetic helicity, so we begin by deriving the evolution of the vector potential. The evolution of the total vector potential $\mathbf{A}_T$ is obtained by 'uncurling' the Induction equation (2.5) giving

$$\partial_t \mathbf{A}_T = -\mathbf{E} - \nabla\Phi_T = \mathbf{U}_T \times \mathbf{B}_T - \eta \mathbf{J}_T - \nabla\Phi_T \tag{2.19}$$

there the electric field comes from the generalized Ohm's law: $\mathbf{E} = -\mathbf{U}_T \times \mathbf{B}_T + \eta \mathbf{J}_T$. From the

Coulomb gauge it can be shown that the electric potential has the form:

$$\nabla^2 \Phi_T = \nabla \cdot (\mathbf{U}_T \times \mathbf{B}_T) \tag{2.20}$$

As in Vishniac & Cho (2001) we will show the importance that magnetic helicity has on the magnetic field dynamics. Beginning with the evolution of the magnetic helicity density $H^m = \mathbf{A}_T \cdot \mathbf{B}_T$ we find that

$$\begin{aligned} \partial_t H^m &= \partial_t \mathbf{A}_T \cdot \mathbf{B}_T + \mathbf{A}_T \cdot \partial_t \mathbf{B}_T \\ &= -2\eta \mathbf{J}_T \cdot \mathbf{B}_T - \nabla \cdot [\mathbf{B}_T \Phi_T + \mathbf{A}_T \times (\mathbf{U}_T \times \mathbf{B}_T) - \eta (\mathbf{A}_T \times \mathbf{J}_T)] \end{aligned} \tag{2.21}$$

We define the terms within square brackets as the flux of magnetic helicity - J_H, then eq. 2.21 takes the form of a continuity equation for the magnetic helicity density:

$$\partial_t H^m + \nabla \cdot J_H = -2\eta \mathbf{J}_T \cdot \mathbf{B}_T \tag{2.22}$$

where $J_H = \mathbf{B}_T \Phi_T + \mathbf{A}_T \times (\mathbf{U}_T \times \mathbf{B}_T) - \eta (\mathbf{A}_T \times \mathbf{J}_T)$. In a perfectly conducting fluid, $\eta \equiv 0$ magnetic helicity is perfectly conserved, while for finite resistivity $\eta \neq 0$ the volume integral for magnetic helicity evolves as

$$\frac{dH^M}{dt} = \int_V \frac{dH^m}{dt} dV = -2\eta \int_V \mathbf{J}_T \cdot \mathbf{B}_T dV \tag{2.23}$$

for a constant volume. As we will show, the conservation equation 2.22 can be used to constrain the dynamics of the large scale helicity, in a way differing from the kinematic dynamo. Note that the gauge is not required in calculating the equation 2.22, but does assume incompressibility; $\nabla \cdot \mathbf{U}_T = 0$. However the choice of gauge does effect the calculation of magnetic helicity density and the helicity flux term. As the conservation of magnetic helicity is an important property of MHD, we will find that the conservation equation 2.22 places a strong constraint on large scale dynamo action.

As its conservation is important, the robustness of such a conservation should be explored. Like kinetic helicity, it is perfectly conserved for zero resistivity (viscosity). However unlike kinetic helicity, in the presence of infinitesimal dissipation the evolution of the total magnetic helicity is not drastically changed. This is because of the natural inverse cascade that magnetic helicity undergoes which results

in the majority of the magnetic helicity power building up at the largest scales. This can be seen in a simple dimensional argument that leads to: $\mathbf{A} \cdot \mathbf{B} \sim kB/k^2 \cdot B \sim EL$. More helicity tends to be at large scales and is less susceptible to resistivity, which acts most efficiently at small scales.

A more thorough analysis was carried through by Berger (1984), who showed through a Schwarz inequality constraint that the maximal magnetic helicity growth rate was proportional to the square root of resistivity: $dH^m/dt \sim \eta^{1/2}$ and so $dH^m/dt \to 0$ as $\eta \to 0$.

The inverse cascade of magnetic helicity is suggestive of how a small scale dynamo might act as a seed to a large scale dynamo. In such a system, any magnetic helicity created in the small scale would tend to relax to large scale, bringing magnetic energy with it.

So we will follow the work of Vishniac & Cho (2001) in constraining the electromotive force using the requirements of magnetic helicity conservation. To begin, we average eq. 2.22 over eddy scales and assume that $\langle \mathbf{A}_T \cdot \mathbf{B}_T \rangle = \mathbf{A} \cdot \mathbf{B}$. This assumption requires efficient magnetic helicity transfer between scales, and that the eddy scales are smaller than the typical field scale by a factor of at least b^2/B^2. So we have

$$\partial_t \left(\mathbf{A} \cdot \mathbf{B} \right) + \nabla \cdot \langle J_H \rangle \quad = \quad -2\eta \left\langle \mathbf{J}_T \cdot \mathbf{B}_T \right\rangle \tag{2.24}$$

where, for simplicity we rewrite the magnetic helicity flux as

$$J_H = \mathbf{A}_T \times \left(\mathbf{U}_T \times \mathbf{B}_T + \nabla \Phi_T - \eta \mathbf{J}_T \right)$$

so

$$\langle J_H \rangle \quad = \quad \mathbf{A} \times \left(\mathcal{E} + \nabla \Phi - \eta \mathbf{J} \right) + \left\langle \mathbf{a} \times \left(\mathbf{e}_{mf} + \nabla \phi - \eta \mathbf{j} \right) \right\rangle \tag{2.25}$$

where capital and small letters have their usual meaning, and $e_{mf} = \mathbf{U}_T \times \mathbf{B}_T - \mathcal{E}$ is the small scale electromotive force. Additionally, we can calculate the explicit time dependence of $\mathbf{A} \cdot \mathbf{B}$ from the definition of the large scale fields (eq. 2.6, where again we ignore the large scale interactions). Rewriting eq. 2.6 and uncurling it to reveal the evolution of the large scale magnetic potential, we

get

$$\begin{aligned} \partial_t \mathbf{B} &= \nabla \times \mathcal{E} - \eta \nabla \times \mathbf{J} \\ \partial_t \mathbf{A} &= \mathcal{E} - \nabla \Phi - \eta \mathbf{J} \end{aligned} \tag{2.26}$$

where a common vector identity is used to rewrite the dissipation term. And so:

$$\partial_t \left(\mathbf{A} \cdot \mathbf{B} \right) = -\nabla \cdot \left[\mathbf{A} \times \left(\mathcal{E} + \nabla \Phi - \eta \mathbf{J} \right) \right] + 2\mathbf{B} \cdot \mathcal{E} - 2\eta \mathbf{J} \cdot \mathbf{B} \tag{2.27}$$

Combining eqs. 2.24, 2.25 and 2.27 we find that

$$2\mathbf{B} \cdot \mathcal{E} = -\nabla \cdot \langle \mathbf{a} \times \left(\mathbf{e}_{mf} + \nabla \phi - \eta \mathbf{j} \right) \rangle \tag{2.28}$$

While eq. 2.28 is not a full derivation of the electromotive force, it does represent a strong constraint on $\mathcal{E}$. Such a constraint takes on the form

$$\mathcal{E} = \mathcal{E}_\perp - \frac{\mathbf{B}}{2B^2} \nabla \cdot J_h \tag{2.29}$$

The form of $\mathcal{E} \cdot \mathbf{B}$ was first proposed by Bhattacharjee & Hameiri (1986) who constrained the form of J_h by assuming an equilibrium between the dissipation of magnetic energy at small scales and injection at large scales. Such a constraint is not made here, as in typical astrophysical systems, energy flow at large scale is small compared to the energy flow due to turbulent cascade, and an equilibrium between dissipation and the cascade is not required to conserve energy. The second term in 2.29 will be known as the VC-term for the remainder of the work here.

So we find that large scale magnetic fields could be driven by the generation and transport of magnetic helicity at eddy scales. In such a prescription, small fluctuations along the magnetic field caused by turbulent motion create a net magnetic helicity that flows along the magnetic field lines. The perturbation inverse cascades to large scales and is assumed to be efficiently added to the large scale field.

An important feature of such a prescription is the inverse cascade of the small scale helicity. To that end we assume that rather than only being able to track the large scale component of the magnetic helicity, we may track the component of the large scale magnetic helicity that arises due to

the large scale fields, $H \equiv \mathbf{A}\cdot\mathbf{B}$, and the component that is due to the small scale cascade, $h \equiv \langle \mathbf{a} \cdot \mathbf{b} \rangle$. From the equation of motion of the fluctuating magnetic field (eq. 2.7), assuming the FOSA ($\mathbf{G} \equiv \mathbf{0}$) and making the distinction between large scale components and small scale components in eq. 2.24 leads to the evolutions of both contributions

$$\partial_t h = -\nabla \cdot J_h - 2\mathbf{B} \cdot \langle \mathbf{u} \times \mathbf{b} \rangle_t - 2\eta \langle \mathbf{j} \cdot \mathbf{b} \rangle \tag{2.30}$$

$$\partial_t H = -\nabla \cdot (\mathbf{A} \times (\mathcal{E} + \nabla\Phi - \eta\mathbf{J})) + 2\mathbf{B} \cdot \langle \mathbf{u} \times \mathbf{b} \rangle_t - 2\eta \mathbf{B} \cdot \mathbf{J} \tag{2.31}$$

The subscript t denotes the transfer between scales rather than a transfer between positions. The justification of combining H and h together in eq. 2.24 was worked through in the appendix of Vishniac & Cho (2001). They showed that the small scale eddies will add their magnetic helicity to the large scale structure at a rate that approaches the eddy turnover rate as the magnetic field approaches equipartition. They concluded that the distinction between H and h becomes unimportant to the dynamics of the system long before h is saturated by dissipation and magnetic back-reaction.

A logical question arises: how does such a magnetic helicity flux effect the small scale dynamo? And, while forcing magnetic helicity conservation, will a large scale dynamo emerge from the saturated small scale fields?

2.8 Existence of Dynamo Action

In the coming chapters we will be interested in simulating a persistent magnetic dynamo, so some discussion of the required parameter space for the existence of dynamo action should be discussed. One such parameter that is important to the persistent of magnetic energy is the Prandtl number, $Pr = \nu/\eta$, representing the relative strengths of the viscosity and resistivity. It has been shown (see Schekochihin et al. (2004) and Subramanian (1997)) that there is a critical Prandtl number ($Pr_c \in [25, 50]$, depending on your choice of Reynolds number) that above which the magnetic energy will tend to grow and persist and below which the energy will tend to decay away. Naturally, the important parameter in the Prandtl number to a persistent magnetic energy is the resistivity. Subramanian (1997) showed that the critical magnetic Reynolds number, $Rm = UL/\eta$, for persistent magnetic energy has a value of $Rm_c \approx 60$, below which the magnetic energy will not persist. Because dissipation is most efficient as small scales, its likely that this dependence is more closely related to

the growth of the small scale dynamo than the large scale dynamo (Schekochihin et al., 2004).

A second important parameter to the growth and persistence of the dynamo action is the strength of the shearing rate. It is well known (Richardson & Proctor (2010), Vishniac & Brandenburg (1997), Yousef et al. (2008), Singh & Jingade (2013)) that the growth rate of the large scale dynamo in a shearing system is proportional to the shearing rate. The interaction between the shear and the turbulent motion is also well studied, and often parameterized by the dynamo number (Brandenburg et al. (2008), Singh & Jingade (2013)). This dynamo number is derived from the kinematic approximation and depends on the α parameter and shearing rate. Because we are less interested in the effects from the kinematic approximation, we will use the Rossby number, $Ro = k_f u_{rms}/S$, representing the ratio of the eddy turnover rate ($k_f u_{rms}$) to the shearing rate (S) as our means of parameterizing the ratio of turbulent and shearing motion. The use of the Rossby number as a way of parameterizing dynamo action has been done before, typically for stellar dynamos. In those studies, it is usually found that the dynamo activity scales with the inverse square of the Rossby number (Noyes et al., 1984), while it has been argued (Montesions et al., 2001) that such a relation is over simplified and complicated by differential rotation. Regardless, Montesions et al. (2001) agreed that large scale dynamo action will be hindered in stars that posses high Rossby numbers.

Chapter 3

Numerical Method

To test the above prescription, we run direct numerical simulations (DNS) of the MHD equations in a square shearing box of size $L = 2\pi$. Such a setup represents a local study of the disk, as global studies are computationally expensive. By inspection, one can see that a steady state solution of eqs. 2.4 and 2.5 is zero magnetic field, and a linear shear that is unchanging in time. The rotation is assumed to be a constant value in a single direction, for simplicity. To that end, we apply a Reynolds decomposition, where the total field is split between the constant (average) component, and the evolving (fluctuating) components

$$\mathbf{U}_T = \mathbf{U} + \mathbf{u}$$

$$\mathbf{\Omega}_T = \mathbf{\Omega} + \omega$$

$$\mathbf{B}_T = \mathbf{B} + \mathbf{b}$$

$$\mathbf{J}_T = \mathbf{J} + \mathbf{j}$$

where $\mathbf{U} = Sy\hat{x}$ is the shear, its vorticity: $\mathbf{\Omega} = \nabla \times \mathbf{U} = -S\hat{z}$. There is no background magnetic field or current ($\mathbf{B} = \mathbf{J} = 0$) imposed on the boxy. The system is assumed to rotate around the z-axis, with $\mathbf{\Omega}_{cor} = \Omega_{cor}\hat{z}$. Under such a prescription we have constructed the system to be stable to the magnetorotational instability, a known process that is active in astrophysical disks but a complication that is not required for our analysis.

In the above description we have changed the definitions of capital and lower case letters. Here

the capital letters denote background fields that are unchanged in time and the lower case letters denote the fluctuating field that is evolved by the code. This fluctuating field contains all scales and is further split into large and small scale components for the analysis. The equations 2.4 and 2.5 are then modified, leaving the equations of motion for the code:

$$(\partial_t + Sy\partial_x)\,\mathbf{u} + \omega \times \mathbf{u} = -\nabla p' + (2\Omega - S)\,u_y\hat{x} - 2\Omega u_x\hat{y} + \mathbf{j} \times \mathbf{b} + \nu\nabla^2\mathbf{u} + \mathbf{f} \tag{3.1}$$

$$(\partial_t + Sy\partial_x)\,\mathbf{b} = \nabla \times (\mathbf{u} \times \mathbf{b}) + Sb_y\hat{x} + \eta\nabla^2\mathbf{b} \tag{3.2}$$

along with $\nabla \cdot \mathbf{b} = \nabla \cdot \mathbf{v} = 0$. For simplicity, the subscript on the Coriolis term is dropped. The equations 3.1 and 3.2 are solved using a pseudo-spectral method; the linear terms and derivatives are computed in Fourier space, while the nonlinear terms are computed in position space. The data is transformed between position and Fourier space using a modified Fast Fourier Transform (FFT) to be discussed below. To step forward in time, the derivatives and dissipation are handled using a leap-frog method and the integration factor method respectively. The box is initially void of any energy in the fluctuating components. However, there is a quick build up of kinetic energy from the forcing function ($\mathbf{f}$) and the magnetic energy is seeded by numerical inaccuracy in the calculation of the nonlinear terms.

3.1 Boundary Conditions

In the standard shearing box approximation (with shear $\mathbf{U} = Sy\hat{x}$), the boundary conditions are periodic in the x and z directions, and shear periodic in the y direction. In such a system, a particle that leaves the box across the y boundary returns on the opposite y boundary with a shifted position and velocity relative to the shear in the box. Periodic boundary conditions restrict the possible spacing of Fourier space vectors to integers, allowing for FFT algorithms to be used when transforming from one space to another. This fact allows for simplified numerical codes, as FFTs are both computationally inexpensive and readily available for use. The Fourier space vectors (referred to here as k-vectors) can be defined as follows. Here we define the continuous Fourier transform of any function $f(\mathbf{r})$ is

$$\tilde{f}(\mathbf{k}) \quad = \quad \int f(\mathbf{r}) e^{i\mathbf{k}\cdot\mathbf{r}} d^3\mathbf{r} \tag{3.3}$$

so that alternatively the original function may be written as

$$f(\mathbf{r}) = \frac{1}{2\pi^3}\int \tilde{f}(\mathbf{k})e^{-i\mathbf{k}\cdot\mathbf{r}}d^3\mathbf{k} \tag{3.4}$$

which follows from the Dirac delta function identity. Under periodic boundary conditions (for now in all three dimensions) the function must satisfy

$$f(\mathbf{r}) = f(\mathbf{r}+L\mathbf{x}) = f(\mathbf{r}+L\mathbf{y}) = f(\mathbf{r}+L\mathbf{z})$$

Which forces, from eq. 3.4 that $e^{-i\mathbf{k}\cdot\mathbf{r}} = e^{-i\mathbf{k}\cdot(\mathbf{r}+L\mathbf{r})} \rightarrow e^{-iLk_x} = 1$ and similarly for k_y and k_z. This implies that for periodic systems the k-vectors must have the form

$$\mathbf{k} = \frac{2\pi}{L}\left(n_x\hat{x} + n_y\hat{y} + n_z\hat{z}\right) \tag{3.5}$$

for n_x, n_y and n_z integers. In a numerical setting, the integrals in eq. 3.3 and 3.4 are replaced by a discrete sum over $N+1$ Fourier components (ranging over $[-N/2, N/2]$, including zero) where $N = 2^n$ (integer n) for standard FFTs. We will define $\mathcal{F}\{\cdot\}$ as the Fourier transform operator, which returns the Fourier transform of the term inside the curly brackets. So that the numerical Fourier transform takes the form of

$$\begin{aligned}\mathcal{F}\{f(\mathbf{r})\} = \sum_{k_x,k_y,k_z}\tilde{f}(\mathbf{k})e^{-i\mathbf{k}\cdot\mathbf{r}} \rightarrow \quad & k_x \in [-N/2, N/2] \\ & k_y \in [-N/2, N/2] \\ & k_z \in [-N/2, N/2]\end{aligned} \tag{3.6}$$

where the vector $\mathbf{k}$ and its components are defined by eq. 3.5. So we can see by inspection that:

$$\begin{aligned}\mathcal{F}\{\partial_t f\} &= \partial_t\mathcal{F}\{f\} \\ \mathcal{F}\{\partial_j f\} &= ik_j\mathcal{F}\{f\} \rightarrow j \in [x, y, z]\end{aligned} \tag{3.7}$$

With these rules in place, we apply the Fourier operator to eqs. 3.1 and 3.2. After some simplification we find:

$$(\partial_t + iSyk_x)\,\tilde{\mathbf{u}} + \mathcal{F}\{\omega \times \mathbf{u}\} = -i\mathbf{k}\tilde{p} + (2\Omega - S)\,\tilde{u}_y\hat{x} - 2\Omega\tilde{u}_x\hat{y} + \mathcal{F}\{\mathbf{j} \times \mathbf{b}\} - \nu k^2\tilde{\mathbf{u}} + \tilde{\mathbf{f}} \tag{3.8}$$

$$(\partial_t + iSyk_x)\,\tilde{\mathbf{b}} = i\mathbf{k} \times \mathcal{F}\{(\mathbf{u} \times \mathbf{b})\} + S\tilde{b}_y\hat{x} - \eta k^2\tilde{\mathbf{b}} \tag{3.9}$$

It becomes clear the benefit of a pseudo-spectral method, as the spacial derivatives are replaced by simple multiplication in Fourier space. The multiplications within the Fourier operator are calculated in position space then Fourier transformed back to Fourier space. Calculations in Fourier space also benefit from only having to make calculations on half of the available space, then using the reality condition to infer the values on the other half of Fourier space. The reality condition requires any function in position space $\phi(\mathbf{r}, t)$ is purely real. This conditions requires that in Fourier space: $\tilde{\phi}(\mathbf{k}, t) = \tilde{\phi}^*(-\mathbf{k}, t)$, where the asterisks denotes a complex conjugate. In practice, one makes calculations on the space of $k_x \in [0 : N/2 + 1]$, $k_y \in [-N/2 : N/2]$ and $k_z \in [-N/2 : N/2]$ then mirrors the result into conjugate space for the remainder of Fourier space prior to Fourier transforming to position space.

3.2 Aliasing Errors

An important issue in calculating discrete Fourier transforms numerically is aliasing errors. The effect of the error can be seen in the following example. Consider two values in 1-D position space:

$$a(x) = \sum_{k}^{N} \tilde{a}_k e^{-ikx} \quad \text{and} \quad b(x) = \sum_{k'}^{N} \tilde{b}_{k'} e^{-ik'x} \tag{3.10}$$

where $|k|, |k'| \in [0, N]$. The values are represented above by their discrete numerical Fourier transforms, with Fourier modes a_k and $b_{k'}$. If we multiply a and b in position space, we find that the resulting Fourier transform *should* have $|k| \in [0, 2N]$

$$a \cdot b = \sum_{k,k'}^{N} (\tilde{a} \cdot \tilde{b})_{k,k'} e^{-i(k+k')x} \equiv \sum_{k''}^{2N} (\tilde{a} \cdot \tilde{b})_{k''} e^{-ik''x} \tag{3.11}$$

where $|k''| \in [0, N] \oplus [0, N] = [0, 2N]$. However FFTs are limited, in that their maximum allowed wavenumber is N and all other modes must be dropped. The loss of terms $(\tilde{\mathbf{a}} \cdot \tilde{\mathbf{b}})_{k''}$ with wavenumbers

$|k''| \in [N+1, 2N]$ is a way of circumventing the aliasing errors present in the calculation of the Fourier transform. With such an error, modes of wavenumbers $|k''| \in [N+1, 2N]$ are aliased to $|k''| - N$ during the calculation of the transform to Fourier space from position space. The above conclusion can be extended to triple products, as the resulting function would have wavenumber ranging from $[0, 3N]$, in which case 2/3 of the modes are dropped. The aliasing error occurs in processing the position to Fourier space transform, and is most evident in calculating the triple products in eqs. 2.27, 2.28 and 2.30.

To illustrate where such an error may have an effect, consider the vector calculus identity: $\nabla \cdot ((\mathbf{a} \cdot \mathbf{b})\,\mathbf{c}) = \mathbf{c} \cdot \nabla\,(\mathbf{a} \cdot \mathbf{b}) + (\mathbf{a} \cdot \mathbf{b})\,\nabla \cdot \mathbf{c}$. If X is the left side and Y is the right side of the identity, clearly $X = Y\ \forall \mathbf{a}, \mathbf{b}, \mathbf{c}$, however numerically such an equality is not found. In calculating X the triple product in position space is first computed, next the result is Fourier transformed to k-space, cutting the highest 2/3 of the available wavenumbers. Finally, the computation is finished by taking the divergences. On the other hand, to calculate Y the double product $\mathbf{a} \cdot \mathbf{b}$ is first calculated in position space. Next the Fourier transform is preformed and the highest 1/2 wavenumbers are lost - no longer affecting the multiplication with $\mathbf{c}$. The gradient is then computed and $\nabla\,(\mathbf{a} \cdot \mathbf{b})$ is returned to position space to compute the product $\mathbf{c} \cdot \nabla\,(\mathbf{a} \cdot \mathbf{b})$. If we wish to compare X and Y in real space, then we are done and X can be returned to position space without losing any information. To compare the two values in Fourier space we would have to transform the above result, losing the highest 1/2 wavenumbers again. The end result is that since the number of Fourier transforms are different, the Fourier transforms were taken at different steps in the calculation we find that numerically $X \neq Y$.

If most of the power in the fields is at the largest scales (low-k) then aliasing errors do not largely effect the results of the calculation. However, since we are interested in triple products that include the small scale components of the fields these issues become important.

To combat such an issue, we choose to limit (cut) the wavenumbers available for the calculation of such products. To do so, for a quantity $\tilde{a}_k$ where $|k| \in [0, N]$ destined to be used in a triple product, all Fourier components are set to zero if $|k| > N/3$ so that the resulting function is non-zero on $|k| \in [0, N/3]$; this is known as anti-aliasing and is a typical strategy in spectral codes. This ensures that in the process of calculating triple products no information is lost, and the numerical answer should closely match the theoretical one. Doing such a cut also places a strong constraint on the setup of the code, as we require the majority of the power to be concentrated within $[0, N/3]$.

To that end, we choose a forcing function that inputs energy at a wavenumber within those limits. It should be noted that such a requirement is not required for the calculation of the main code, as it requires only double products. However, forcing within $[0, N/3]$ allows for the resolution of both the large scale dynamics important to dynamo theory, as well as the small scale cascade within the inertial range.

3.3 Shear Periodic Boundary Condition

In the shear periodic system, it can be shown (Hawley et al., 1995) that along the y boundary any function must satisfy: $f(\mathbf{r}) = f(\mathbf{r} + L\hat{y} + SLt\hat{x})$. Applying the same work as before you find a new definition for the k-vector

$$\mathbf{k}' = \mathbf{k} - Sk_x t\hat{y} \tag{3.12}$$

where $\mathbf{k} = k_x\hat{x} + k_y\hat{y} + k_z\hat{z}$ is the same vector as in eq. 3.5. The results of eq. 3.12 is a problem for standard FFT algorithms, as they require constant k-vectors that have integer spacing. Below, two methods of dealing with the issue of the shearing boundary condition are considered. The first method, first used by Rogallo (1981) changes coordinates into one that shears with the mean shear, effectively returning the y boundary to periodic. The second, introduced by Brucker et al. (2007) allows use of FFTs by modifying one step of the transform to account for the shear periodic boundary.

3.3.1 Rogallo (1981)

The issue of shear periodic boundary conditions was first resolved by Rogallo (1981) who changed the position coordinate system to one that moved with the large scale shear. This solution removes the shear periodic condition on the y-boundary and returns the system to standard periodic boundary conditions. Under such a system the k-vector space returns to that of eq. 3.5 and standard FFTs may be used. Such a coordinate change takes the form of:

$$\begin{aligned} \mathbf{r}' &= \mathbf{r} - Sty\hat{x} \\ t' &= t \end{aligned} \tag{3.13}$$

and so the partial derivatives transform as

$$\begin{aligned} \partial_t &= \partial_{t'} - Sy\partial_{x'} \\ \nabla &= \nabla' - St\hat{y}\partial_{x'} \end{aligned} \tag{3.14}$$

Under such a transformation, the fluid derivative due to the shear: $(D/Dt)_S = \partial_t + Sy\partial_x$ is replaced by the partial derivative of the new time variable $\partial_{t'}$ and all gradients are replaced by the definition in eq. 3.14. The Rogallo algorithm benefits in its simplicity as it removes the extra nonlinear term in eq. 3.2 and allows for the conversion between position and Fourier space with any standard FFT algorithm. Under such a transformation eqs. 3.8 and 3.9 becomes

$$\partial_{t'}\tilde{\mathbf{u}} + \mathcal{F}\{\omega \times \mathbf{u}\} = -i\mathbf{k}'\tilde{p} + (2\Omega - S)\,\tilde{u}_y\hat{x} - 2\Omega\tilde{u}_x\hat{y} + \mathcal{F}\{\mathbf{j} \times \mathbf{b}\} - \nu k'^2\tilde{\mathbf{u}} + \tilde{\mathbf{f}} \tag{3.15}$$

$$\partial_{t'}\tilde{\mathbf{b}} = i\mathbf{k}' \times \mathcal{F}\{(\mathbf{u} \times \mathbf{b})\} + S\tilde{b}_y\hat{x} - \eta k'^2\tilde{\mathbf{b}} \tag{3.16}$$

where $\mathbf{k}'$ is the modified wavevector, and has the definition from eq. 3.12.

The trade off of such a simple numerical method is in its physical representation. Such a shearing coordinate system will become heavily distorted with respect to the laboratory frame, skewing the dynamics of the system. Additionally, different modes of the turbulent field are either stretched or compressed, depending on their direction of travel. As a result, some scales will be compressed to the point where they are no longer resolved by the code, and hence their information is completely lost. Meanwhile, other modes will be stretched to the point where their scale perpendicular to the shear will shrink to the dissipation scale, artificially amplifying dissipation. To fix this, Rogallo suggested a 'remeshing' step to occur when the 'shearing time' (St) is a half integer ($St = 1/2,\ 3/2,\ 5/2, \ldots$). For the first case, the remesh is given by $\mathbf{r}' \rightsquigarrow \mathbf{r}' + y\hat{x}$ and visualized in figure 3.1. It is iterated for every half integer of the shearing time, so that the mesh is never more sheared than $\pm y/2$. Through the remesh, both energy and dissipation are lost because some Fourier modes are discarded due to anti-aliasing when the new coordinate system is set. In general, more dissipation is lost than energy, as the highest wavenumbers (most responsible for dissipation) are more affected by the remesh than low wavenumbers. To communicate the change in coordinate system to the fields, the magnetic and kinetic power are reoriented in Fourier space. To do so, starting in Fourier space one preforms a 1-D Fourier transform to position space in the y-direction. A phase shift of $k_x y$ is then applied to

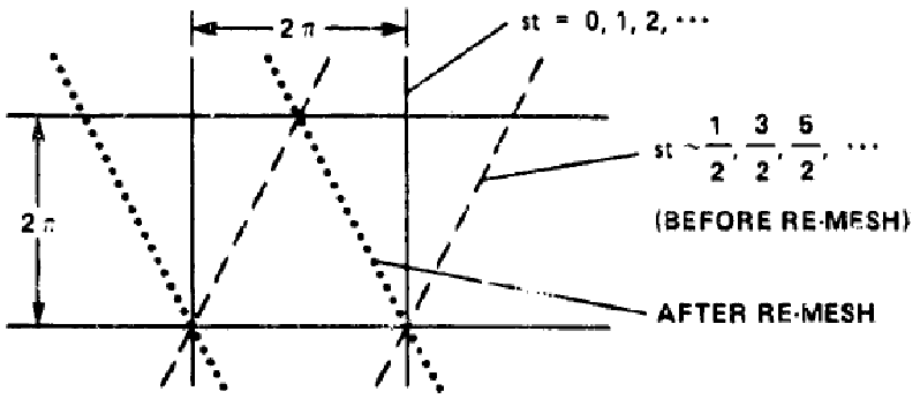

Figure 3.1: Visualization of the remesh step (Rogallo, 1981).

the fields and resulting field is then Fourier transformed back to Fourier space and the remesh is complete. If power is shifted to a wavenumber that was initally zero because of anti-aliasing, the power is discarded when the field is returned to Fourier space. Such a phase change ensures that the magnetic and kinetic energy is mostly conserved throughout the remesh.

An issue in the context of magnetic helicity conservation was found during the remesh. While globally the remesh conserves magnetic helicity in the system, it does not conserve the local structure of the magnetic helicity making the calculation of the time derivative $\partial_t H$ untrustworthy. The effect of the remesh can best be described as a redistribution of helicity in the direction of the remesh (x). Such a redistribution is easily seen when the average (over y and z) magnetic helicity is plotted as a function of x (see figure 3.2).

Fortunately, the choice of how frequent one remeshes is arbitrary, and when one remeshes more often the overall effect of the remesh is reduced (less energy and dissipation lost per remesh). In an attempt to improve fig. 3.2 we increase the remesh rate by a factor of 16. Rather than remeshing at the point $t = S^{-1}(n + 1/2)$ we choose to remesh at $t = S^{-1}(n + 1/2)/16$ and remesh the coordinate system by $y\hat{x}/16$ rather than $y\hat{x}$. This ensures that the resulting coordinate system is never more sheared than $\pm y/32$. Under such a prescription the resulting picture improves (fig. 3.3) but is still insufficient to remove the effect of the remesh completely.

In calculating time derivatives in shearing box codes, one must take into account the distortion of the coordinate system. As a result, time derivatives are often calculated between times of orthogonal

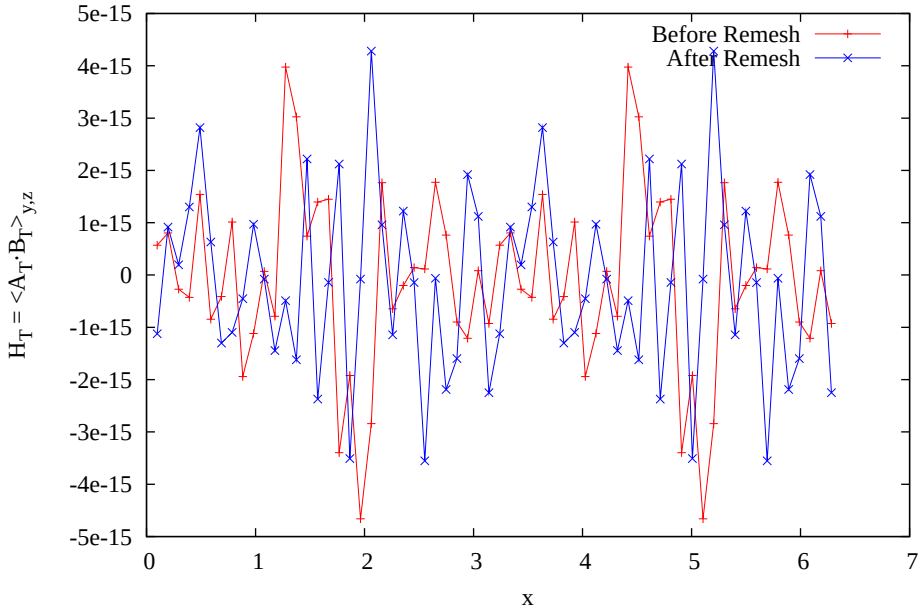

Figure 3.2: The total magnetic helicity averaged over y and z from a Rogallo-based run. The remesh causes a complete redistribution of the magnet helicity in the x component. While in y (see figure A.1) and z the average does not change significantly.

coordinates ($St = n$ in fig. 3.1). This method suffers from the redistribution of magnetic helicity during the remesh that occurs between successive orthogonal coordinate systems. The result of figs. 3.2 and 3.3 does suggest that indefinitely increasing the remesh rate might ultimately fix the issue of the redistribution, however running a remesh step for every time step becomes computationally expensive.

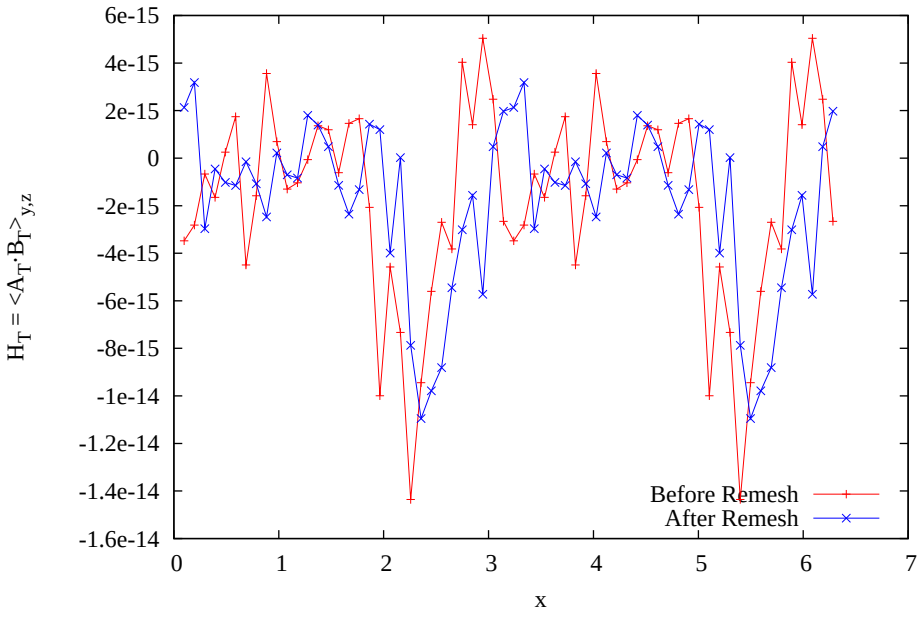

Figure 3.3: The total magnetic helicity averaged over y and z from a Rogallo-based run with higher remesh rate (×16). The increased rate does better in matching the average magnetic helicity as a function of x, but still requires improvement.

3.3.2 Brucker et al. (2007)

An algorithm that approaches the idea of 'remesh every timestep' was worked out and designed by Brucker et al. (2007) to be computationally inexpensive. In their algorithm, they directly calculate the numerical Fourier transform (eq. 3.6) with the shearing definition of the wavevector from eq. 3.12:

$$f(\mathbf{r}) = \sum_{k_x,k_y,k_z}^{N} \tilde{f}(\mathbf{k}) e^{-i(\mathbf{k}\cdot\mathbf{r} - Stk_x y)} \tag{3.17}$$

To do so efficiently requires the three dimensional FFT to be split into: N two dimensional FFTs in x and z, a phase shift to account for the shear, and N^2 one dimensional FFTs in y to finalize the transform to position space. The first step takes $O\left(N \times N^2 \ln N\right)$ operations for the 2-D FFT phase, and finally $O\left(N^2 \times N \ln N\right)$ operations to complete the 1-D FFT and phase shift. An immediate benefit over Rogallo in that the coordinate system remains constant and orthogonal over all time, no longer requiring the remesh. Immediately our situation improves, without a remesh we need not

worry about any drastic steps that redistributes magnetic helicity in the box.

With the Fourier transform defined in eq. 3.17, we again use the modified wavevector: $\mathbf{k}' = \mathbf{k} - Stk_x\hat{y}$ so that the Fourier transform of derivatives becomes:

$$\mathcal{F}\{\partial_t f\} = (\partial_{t'} - iSyk_x)\,\mathcal{F}\{f\} \tag{3.18}$$

$$\mathcal{F}\{\partial_i f\} = ik_i'\mathcal{F}\{f\} \rightarrow i \in [x, y, z] \tag{3.19}$$

Under this new definition of the Fourier transforms, the equations 3.8 and 3.9 again become eqs. 3.15 and 3.16. So conveniently, the equations of motion do not change from the Rogallo algorithm; only the method of dealing with the shearing boundary condition is different. The validity of such an algorithm was covered in Brucker et al. (2007), who compared the dynamics of their code with a similar run of the Rogallo algorithm and found that the evolution of common fluid properties followed Rogallo exactly. The validity of the current implementation of the algorithm is covered later, in section 3.6.1.

3.4 External Forcing Function

To reach an equilibrium we constantly inject energy into the velocity field through a random forcing function $\tilde{\mathbf{f}}(\mathbf{k}_f, t)$ (in eq. 3.9) where $\mathbf{k}_f$ is known as the forcing wavevector and denotes the scale that receives the energy. In practice we select a single scale (single wavenumber k_f) to force, and select a set of wavevectors who satisfy the requirement that $|\mathbf{k}_f| \in [k_f - 0.5, k_f + 0.5]$. Such a requirement ensures that in a one-dimensional spectra, the energy from these forcing components will all be binned in the same k-bin. The vectors selected create a nearly complete sphere in k-space, whose radius is approximately k_f. This allows for isotropic, homogeneous turbulence with an inertial range between k_f and the largest wave number resolved by the code. From the requirement of incompressibility we require that $\nabla \cdot \mathbf{f} = 0$, or: $\mathbf{k}_f' \cdot \tilde{\mathbf{f}} = 0$ in the shearing system. The form of the forcing function is:

$$\tilde{\mathbf{f}}_j(\mathbf{k}_{f,j}, t) = Ae^{i(\phi_1+\phi_2)/2}\left(\mathbf{s}_1 \cos\frac{\phi_2 - \phi_1}{2} + \mathbf{s}_2 \sin\frac{\phi_2 - \phi_1}{2}\right) \tag{3.20}$$

so that the j^{th} forcing mode injects power directly into the velocity mode $\tilde{\mathbf{v}}(\mathbf{k}_{f,j}, t)$. The amplitude A is a slowly varying (less than 1% per timestep) random function, ϕ_1 and ϕ_2 are two varying phases

(less than few degrees per timestep) and unit vectors $\mathbf{s}_1$ and $\mathbf{s}_2$ are perpendicular to both $\mathbf{k}'_f$ and each other. $\mathbf{s}_1$ is chosen to lie only in the xz-plane, and as a result is constant in time. On the other hand, because of the shear periodic system and the time dependence of $\mathbf{k}'_f = \mathbf{k}_f - Stk_{x,f}\hat{y}$, $\mathbf{s}_2$ is time dependent to maintain $\mathbf{k}'_f \cdot \mathbf{s}_2 = 0$. The two vectors $\mathbf{s}_1$ and $\mathbf{s}_2$ remain perpendicular in the shearing frame at all times, as a result the function should be linearly polarized in the shearing periodic system. In the space orthogonal to $\mathbf{k}_f$ helicity is injected into the velocity field by the randomly fluctuating function. The total kinetic helicity injected is determined by the phase difference between $\mathbf{s}_1$ and $\mathbf{s}_2$, and so the amount of helicity injected is given by the randomly fluctuating phases ϕ_1 and ϕ_2. Due to the randomness of its injection, no significant amounts of kinetic helicity will build; so the temporal average of the kinetic helicity will be zero.

3.4.1 Mirror-Symmetry

By inspection of eqs. 3.1 and 3.2 one can see that a sign reversal of the rotation and shear

$$S \to -S \qquad \Omega_{cor} \to -\Omega_{cor}$$

is equivalent to the mirror transformation $y \to -y$ (so also $\partial_y \to -\partial_y$ and $u_y \to -u_y$). Due to the isotropic, homogeneous nature of the turbulence, we expect the code to be statistically symmetric under such a transformation. For this symmetry to hold, we require that $f_y \to -f_{-y}$ under the sign reversal. Because of the reversal of the sign of ∂_y (and so also k_y), the dynamics of the velocity modes $\mathbf{v}_k(k_x, k_y, k_z, t)$ and $\mathbf{v}_k(k_x, -k_y, k_z, t)$ are interchanged. An example of this can be seen in the dissipation term:

$$k^2 = k_x^2 + (k_y - Stk_x)^2 + k_z^2 = k_x^2 + (-k_y + Stk_x)^2 + k_z^2 \qquad \forall\ t$$

so we require that the force also contains the property that the dynamics of two velocity modes of opposite sign of k_y are interchanged when the sign of S is reversed.

We can use the fact that the time dependence of any given forcing mode $\tilde{\mathbf{f}}_j$ is well defined and repeatable, due to the nature of numerically generated random numbers to meet the above requirements. Consider two forcing modes, $\tilde{\mathbf{f}}_j$ and $\tilde{\mathbf{f}}_l$ which inject power into velocity modes $\tilde{\mathbf{v}}(k_x, k_y, k_z, t)$ and $\tilde{\mathbf{v}}(k_x, -k_y, k_z, t)$ respectively. Under a sign reversal, the injection target of the j^{th} and l^{th} modes

are redefined so that $\tilde{\mathbf{f}}_j$ now injects power to $\tilde{\mathbf{v}}(k_x, -k_y, k_z, t)$ and $\tilde{\mathbf{f}}_l$ injects power to $\tilde{\mathbf{v}}(k_x, k_y, k_z, t)$. Because the time dependence of $\tilde{\mathbf{f}}_j$ is set only by the random number generator, such a definition for the target of $\tilde{\mathbf{f}}_j$ ensures that the above requirement is met.

3.4.2 Forcing Modulation

Under this prescription, the resulting turbulence would result in a small scale magnetic helicity flux that is divergence free. Such a result is not ideal since we require a non-zero divergence in the helicity flux to drive the dynamo. To drive the turbulence in a way that creates a non-zero magnetic helicity flux we modulate the forcing function with a function that leads to either a single peak or a double peak in the turbulence in the z-direction. The double peak is caused by a modulation with the function $\sin(z)$ and the single peak results from the modulation with the function $(2/\sqrt{3})\sin^2(z/2)$. Both functions are normalized to the have the same total amplitude when integrated over the z-axis.

3.5 Hyperdiffusion

Hyperdiffusion, also known as hyperviscosity (in the Navier-Stokes equation) or hyperresistivity (in the Induction equation), is a numerical method for suppressing instabilities or obtaining turbulence of high Reynolds number. In such a system, one can often better resolve the inertial range as the dissipation scale is artificially lengthen to be larger than the smallest resolved scale. The second lowest order ($h = 4$) of hyperdiffusion was implemented in an effort to suppress a numerical instability present in the code, while at the same time allowing for the turbulent transport to dominate the dynamics at the eddy scale. The form of the hyperdiffusion term

$$-\nu_h \left(\nabla^2\right)^h \mathbf{u} \quad \text{or} \quad -\eta_h \left(\nabla^2\right)^h \mathbf{b} \tag{3.21}$$

is adopted from Cho & Vishniac (2000a) and is used to damp fluctuations that occur on the grid scale. In the code, the hyperdiffusion terms are handled in the same manner as the physical diffusion terms. Showing up as an integration factor when the simulation is stepped forward. The strength of the hyperdiffusion terms ($\nu_h = \eta_h$) are defined in the same way as in Cho & Vishniac (2000a) and takes the form $\nu_h (N/2)^{2h} \Delta t \approx 0.5$.

3.6 Code Validation

The code, modified by the author was originally written by Jungyeon Cho and used in the work Cho & Vishniac (2000a) and Cho & Vishniac (2000b). It was then modified by Dmitry Shapovalov and used in the work Shapovalov & Vishniac (2011). The original code inputted shear by using a constant component of the forcing function at large scales and selecting the amplitude of such a component to maintain a constant shear. The current work inputs shear using the Reynolds decomposition that resulted in eqs. 3.1 and 3.2 and evolves the fields $\mathbf{u}$ and $\mathbf{b}$ using the algorithm from Brucker et al. (2007) to handle the shearing periodic boundary condition.

3.6.1 Laminar Dynamo

As a test of its mathematical consistency, we will simulate the evolution of the magnetic field in the presence of a shearing laminar flow using the code, and compare the results to an analytical model. We will make the kinematic approximation and assume that there is no other velocity field other than the shearing field, so $\mathbf{u} = 0\ \forall t$. In the code, this is equivalent to 'turning off' the Navier-Stokes equation - setting $\mathbf{u} = 0$ after every timestep. In this test, hyperdiffusion is not used as the system is numerically stable. Analytically, this simplifies the evolution equations (eqs. 3.15 and 3.16) to

$$\begin{aligned} \partial_t \tilde{\mathbf{u}} = \mathbf{0} \quad &\rightarrow \quad \tilde{\mathbf{u}}(t) = \mathbf{u}_0 = \mathbf{0} \forall t \\ &\downarrow \\ \partial_t \tilde{\mathbf{b}} \quad &= \quad S\tilde{b}_y \hat{x} - \eta k'^2 \tilde{\mathbf{b}} \end{aligned} \tag{3.22}$$

where, for simplicity we drop the prime on t'. The benefit being that this linear equation may be solved analytically. Because of its linearity, we do not expect energy to be transferred between scales, nor do we expect energy to be passed between directions, other than by the shear term ($S\tilde{\mathbf{b}}_y \hat{x}$). So we assume that $\tilde{b}_z = 0\ \forall t$ as any initial value would quickly diffuse away, leaving a pair of coupled equations to solve.

$$\partial_t \tilde{b}_x = S\tilde{b}_y - \eta k'^2 \tilde{b}_x \tag{3.23}$$

$$\partial_t \tilde{b}_y = -\eta k'^2 \tilde{b}_y \tag{3.24}$$

The seed field is choose as $\tilde{\mathbf{b}}_0(k_x, k_y \equiv 0, k_z \equiv 0) = b_0\hat{y}$ so that at all times $k'^2 = \left(1 + S^2t^2\right)k_x^2$. Through seperation of variables, one finds from eq. 3.24 that

$$\tilde{b}_y = b_0 e^{-\eta k'^2 t + 2\eta S^2 k_x^2 t^3/3} \tag{3.25}$$

Combining eq. 3.25 and eq. 3.23 allows for the solution of $\tilde{b}_x(t)$. The resulting equation takes the form

$$\left(\partial_t + \eta k'^2\right)\tilde{b}_x = S b_0 e^{-\eta k'^2 t + 2\eta S^2 k_x^2 t^3/3} \tag{3.26}$$

which can be solved using the integration factor method. It follows from eq. 3.26:

$$\begin{aligned} \partial_t\left(\tilde{b}_x e^{\int_0^t \eta k'^2 dt}\right) &= S b_0 e^{-\eta k'^2 t + 2\eta S^2 k_x^2 t^3/3} e^{\int_0^t \eta k'^2 dt} \\ \partial_t\left(\tilde{b}_x e^{\eta k'^2 t - 2\eta S^2 k_x^2 t^3/3}\right) &= S b_0 \\ \tilde{b}_x &= S b_0 t e^{-\eta k'^2 t + 2\eta S^2 k_x^2 t^3/3} \end{aligned} \tag{3.27}$$

The resulting evolution of the magnetic energy is

$$\tilde{b}^2 = |\tilde{b}_x|^2 + |\tilde{b}_y|^2 = b_0^2\left(1 + S^2t^2\right)e^{-2\eta k'^2 t + 4\eta S^2 k_x^2 t^3/3} \tag{3.28}$$

The output of the code is compared to the results of eq. 3.28, shown in the figure below.

The result of the analytic work agrees with the statement earlier that under the effect of such a dynamo the magnetic field grows linearly with time in the direction of the shear. The source of the dynamo comes directly from the shearing term, which reorients the magnetic field from a field primarily in the y-direction to a magnetic field primarily in the x-direction. Ultimately the magnetic energy evolution is dominated by the dissipation term and is completely diffused away as the magnetic field decays to zero. The numerical and analytical solutions are not a perfect match in figure 3.4, which is due to the numerical resistivity that is present in the code. This last fact is easily seen if we consider an amplified resistivity $\eta_{amp} = \eta_{phy} + \eta_{num}(t)$ where the time dependence of the numerical resistivity η_{num} is due to its build up at each time step. In eq. 3.28 we replace η with η_{amp} and fit the function to the data, letting $\eta_{num}(t) = \eta_{num,0} + \eta_{num,1}t + \eta_{num,2}t^2$. In principle, we can continue to add higher powers of time, however in doing so the fit does not improve, and the

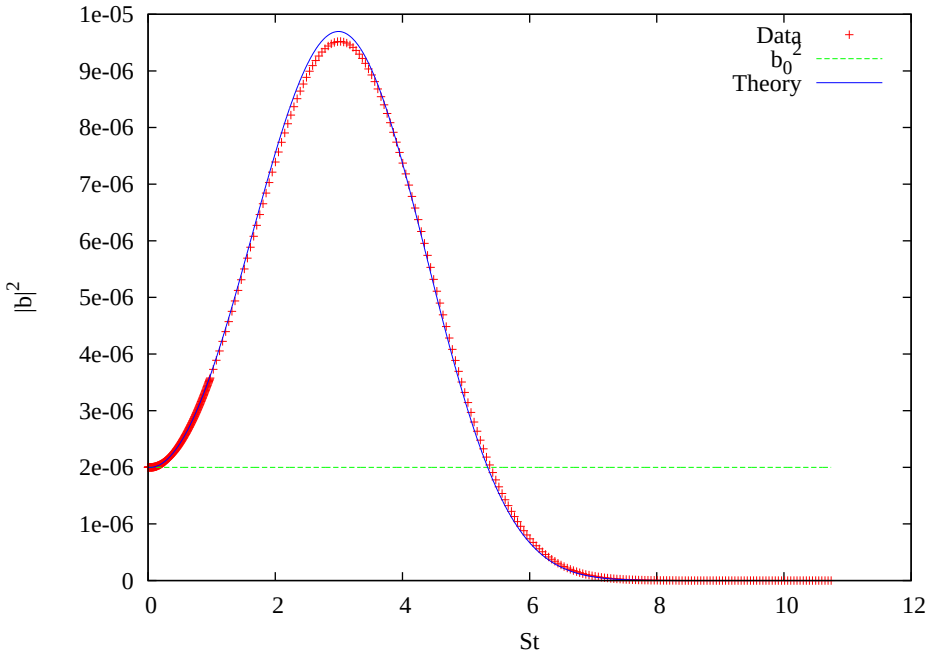

Figure 3.4: Output from the code compared to the analytical results worked out for the Laminar dynamo. The code does well in matching the analytic results over all time, the worse of which is seen at $St \sim 3$ when the magnetic field is the strongest. The observed difference is due to numerical resistivity in the code.

terms $\eta_{num,n} \sim 0$ for $n > 2$ with uncertainties on the same order as the terms themselves. The result of such a fit is shown in figure 3.5, which found that the fit parameters did not depend strongly on physical resistivity. The leading term of the numerical resistivity was the constant term $\eta_{num,0}$ with a value of 27% the physical resisitivity.

We can see by this exercise that the implementation of the Reynolds decomposition to explicitly add the shear and the Brucker algorithm to deal with the resulting shearing periodic boundary conditions seems to be numerically consistent with the analytical results of a simple shearing, laminar dynamo. The inconsistency between the two results can be attributed to the build up of numerical resistivity in the code which has a leading, time-independent term of 27% the size of the physical resistivity.

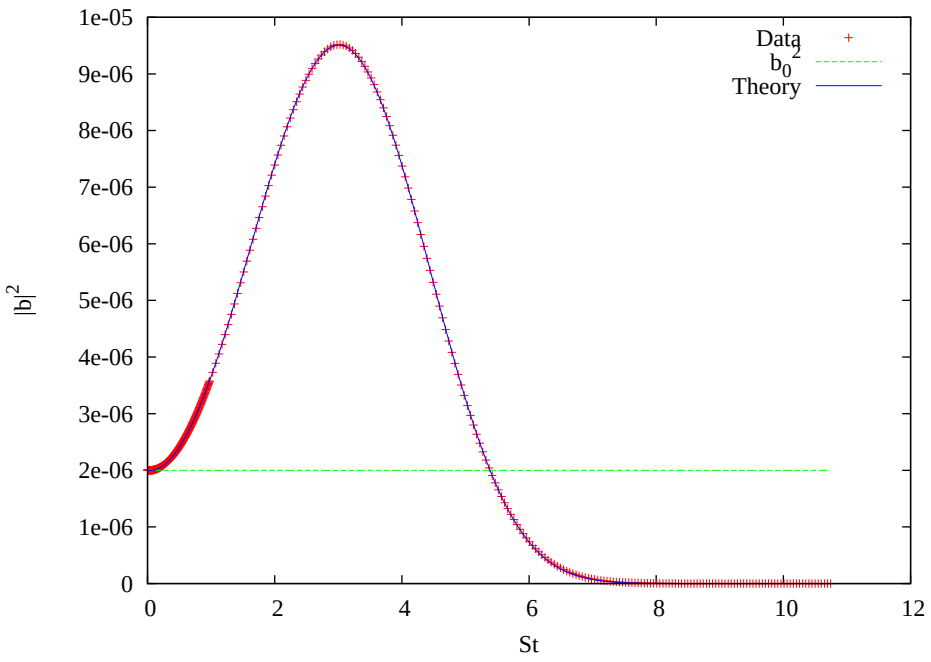

Figure 3.5: Result of assuming a time dependence for numerical resistivity of $\eta_{num} = \eta_{num,0} + \eta_{num,1}t + \eta_{num,2}t^2$. The result of the fit show that $\eta_{num,0} \sim 27\%$, $\eta_{num,1} \sim -1.5\%$ and $\eta_{num,2} \sim 0.03\%$ (% of physical resistivity). The fit parameters did not depend strongly on physical resistivity, and the trend of decreasing values of $\eta_{num,n}$ continued for all n.

3.6.2 Data Visualization

As a first probe into the structure of the turbulent box, visualizations of the kinetic and magnetic energy are presented here. The data was selected from the High Rossby number case (see Results chapter below) and represents a run when the eddy turnover rate is on about two orders of magnitudes higher than the shearing rate. The two data sets are outputted from a very early point (20th timestep - $St \sim 0.00046$) and at a point later on ($St \sim 1$). Figure 3.6 illustrates the large deficit between the initial energies in the kinetic and magnetic field. The velocity field, seeded by the forcing function, very quickly grows up to nearly the same level as its equilibrium strength. Meanwhile the magnetic field is seeded by numerical inaccuracy and begins at a very weak level. It does however grow within a shearing time up to a strength that is comparable to the velocity field. Additionally, the figure illustrates an interesting feature in the growth of magnetic energy. While the structure of the magnetic energy is related to the structure of the kinetic energy, the peaks in the two energies are not well correlated. The highest peaks in the two energy are not related, and some regions of strong

kinetic energy do not show up at the same levels in the magnetic energy. Similarly, at later times the peaks in the magnetic energy are on opposite sides of the box as peaks in the kinetic energy. Finally, the lack of an apparent effect from the background shear on the fields at $St \sim 1$ should be noted. This seems to suggest what is expected from a high Rossby number system, where the turbulent transport is much stronger than any effect from the background shear. It also appears that there is no significant contribution from large scale (ordered) structure to the energy density of both fields possibly due to the weak effect from the shear.

As a point of interest, the magnetic energy is also compared to the power in the vorticity. As mentioned before in the kinematic limit the temporal evolution of the magnetic field and the vorticity are the same. Interestingly, the two plots show an anti-correlation between the build up of magnetic energy and the build up of power in the vorticity.

So as expected we are seeing a highly structured system that becomes diffuse, and only weakly structured when the system is in equilibrium between the forcing and the diffusion. We also find that the magnetic field is only weakly correlated to the velocity field. This is not surprising since at the early times the magnetic energy is dominated by scales much smaller than the eddy scale, where the majority of the kinetic energy is stored.

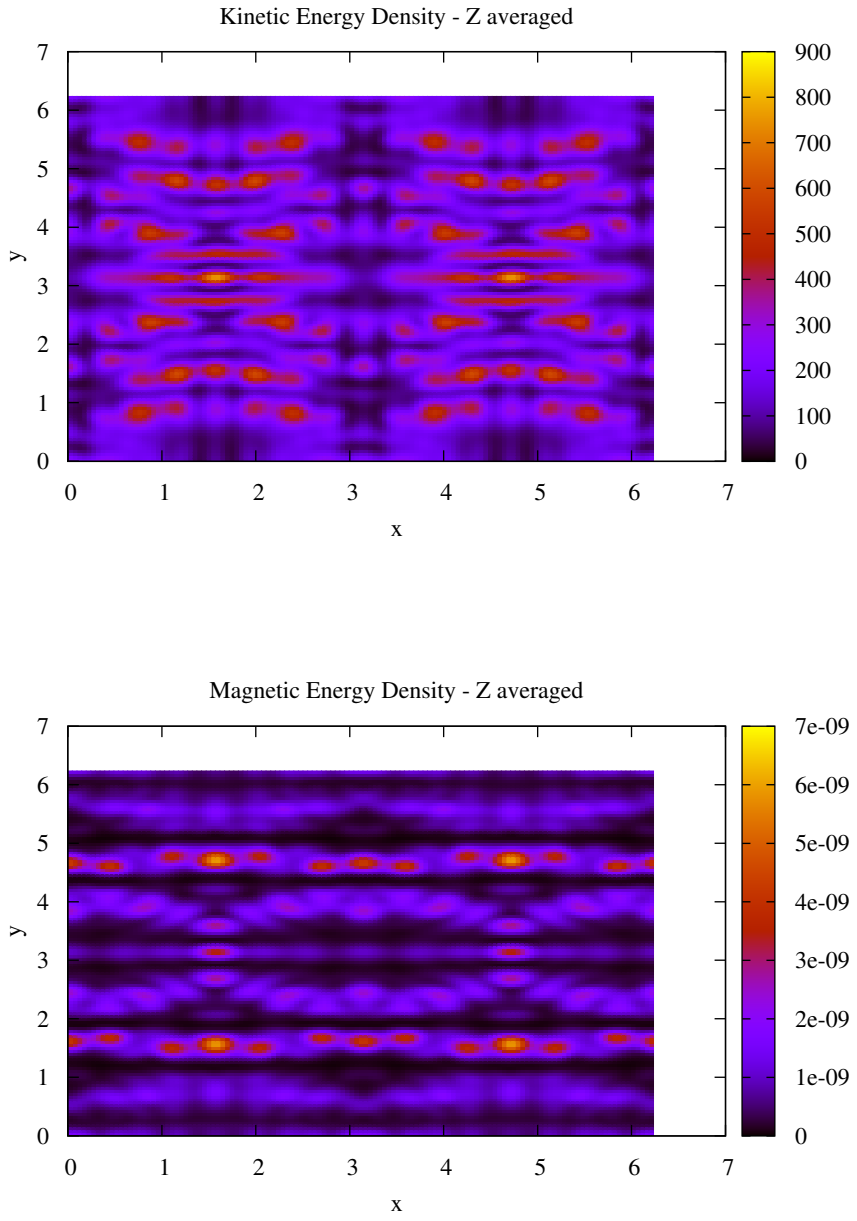

Figure 3.6: Kinetic and magnetic energy density at $St \sim 0.00046$ averaged over the z axis. At early times, the system has not reach equilibrium between the flux of energy from the forcing function and the dissipation. As a result the fluid follows the form of the forcing function very closely.

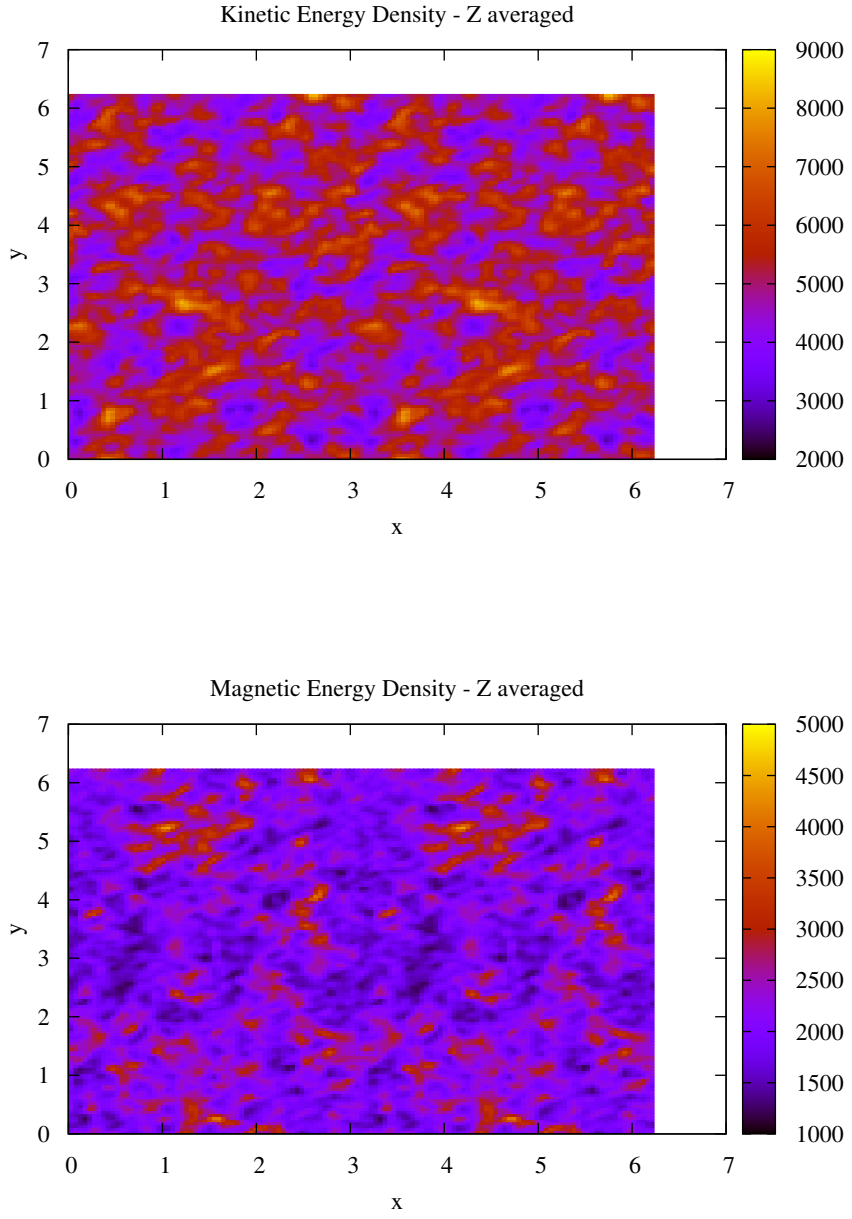

Figure 3.7: Kinetic and magnetic energy density at $St \sim 1$ averaged over the z axis. Long after the code has reached equilibrium between the forcing and dissipation (and at this time the conversion to magnetic energy) the strong features from before have been diffused away.

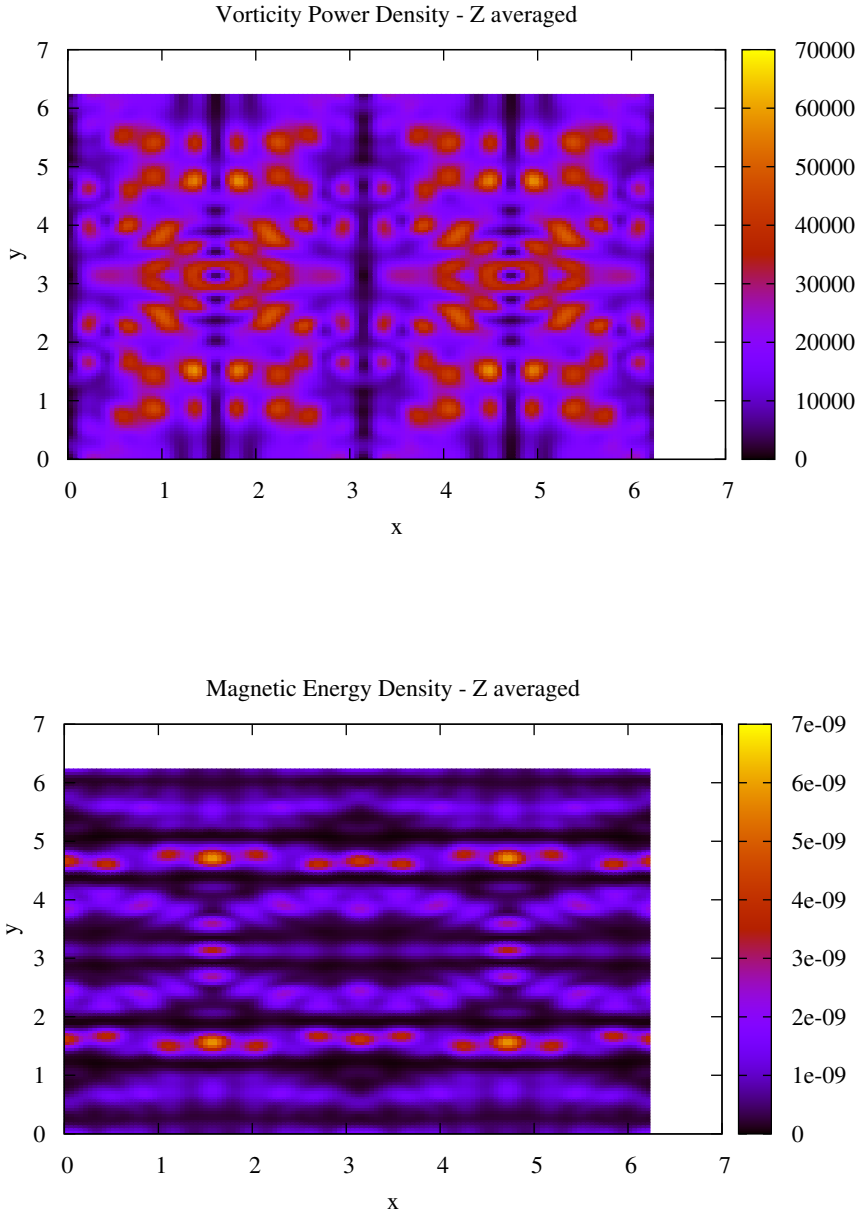

Figure 3.8: Comparing magnetic energy with the z-averaged power in vorticity ($|\omega|^2 = |\nabla \times \mathbf{v}|^2$) at $St \sim 0.00046$. The peaks in magnetic energy are anti-correlated with the peaks in vorticity power. Because of the similarities in their evolution equations, this seems somewhat counter intuitive.

3.6.3 Cascade Equilibrium

Worked out in the turbulence section (section 2.2), in a standard turbulent system an equilibrium is expected between the input of energy and the dissipation. At this point, the energy spectrum of the turbulence was found to conform to what is known as a Kolmogorov spectrum. As an important feature in turbulence, we expect that the code will produce a similar energy spectrum when the magnetic field is weak and has little effect on the dynamics of fluid. Such a phase will be referred to as the kinematic phase and is seen in figure 3.9 as the velocity field reaching an equilibrium phase prior to a shearing time of $St \simeq 10^{-1.25}$. As the strength of the magnetic field grows, the equilibrium

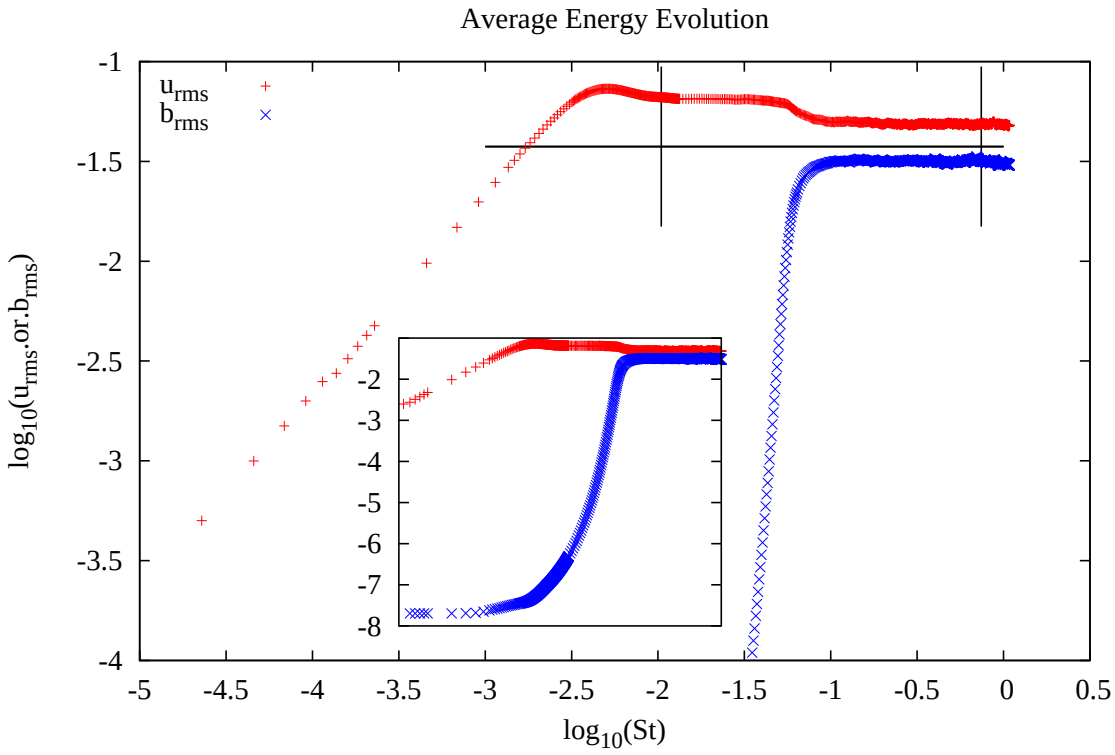

Figure 3.9: Evolution of the root mean square velocity and magnetic field. The inset shows more clearly the evolution of the magnetic field at the earliest times in the simulation. Magnetic energy is seeded initially by numerical accuracy during the calculation of nonlinear terms, but quickly grows to an average energy of $\sim 10^{-16}$ within the first 10 timesteps. The first equilibrium between the forcing function and dissipation is achieved at a shearing time of $St \simeq 10^{-2}$ and is lost at $St \simeq 10^{-1.25}$ when the magnetic field becomes important to the dynamics of the plasma. The horizontal black line denotes the point where above which the plasma is dominated by turbulent eddies, and below which the plasma is dominated by shear. The left and right vertical lines denote the selected times of figures 3.10 and 3.11 respectively.

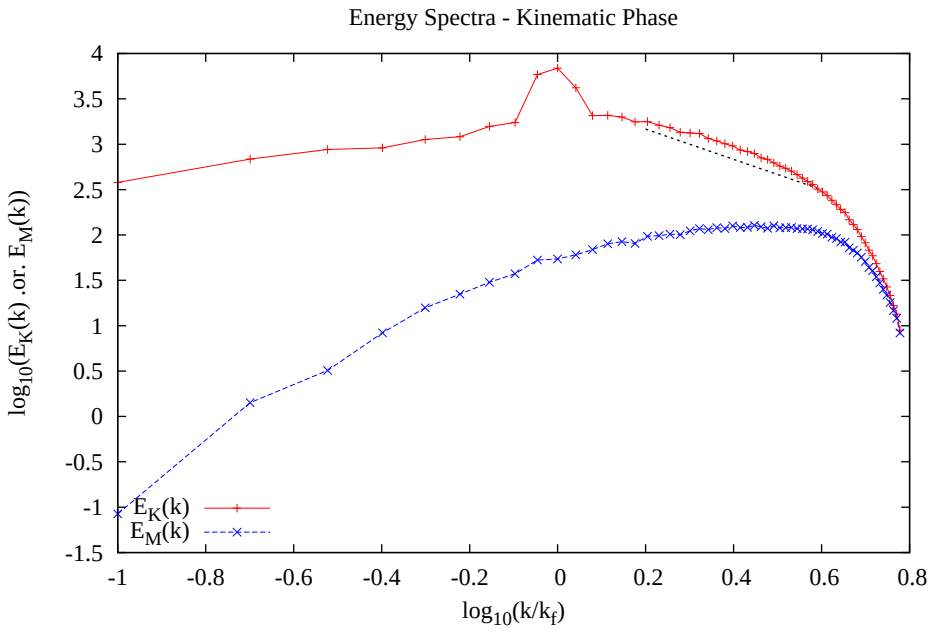

Figure 3.10: Energy Spectra during the early equilibrium phase ($St \sim 0.01$). The slope of a Kolomogorov spectrum is denoted by the blue line. In this phase the kinetic energy is dominated by the forcing function, injecting energy at wavenumbers centered on $k = k_f$ and the dissipation (both physical and hyper). The magnetic energy spectra, dominated by the transfer of energy from the velocity field and dissipation, is in the process of growing.

is broken and the magnetic field saps energy at a rate that, when combined with the dissipation rate exceeds the energy flux from the forcing function. We find that the energy in the velocity field is further decreased until a second equilibrium, between the dissipation rate, conversion (to magnetic energy) rate and input flux from the forcing is reached. This second phase will be called the small scale dynamo phase, as it contains some of the properties (like rapid growth to equipartition at scales up to the eddy scale) that are expected of a small scale dynamo. During the early equilibrium, the kinetic energy spectra ($E_K(k)$) deviates slightly from a true Kolomogorov spectrum in the inertial range between the forcing wavenumber ($k = k_f$) and the dissipation scale (k_d) where the spectrum turns over (see figure 3.10. The reason for the deviation most likely comes from the magnetic field acting like a small (but important) energy sink to the velocity field, breaking the assumption of kinetic energy conservation that is made in deriving the Kolomogorov spectrum. The dissipation scale is determined by the point where the dissipation rate exceeds the eddy turnover rate, so the spectra is dominated most by the physical and hyper dissipation in the code, rather than the turbulent cascade.

At the smallest scales (of the same order as the grid size) equipartition between the magnetic and velocity field is reached very quickly. During the small scale dynamo phase, the kinetic energy takes

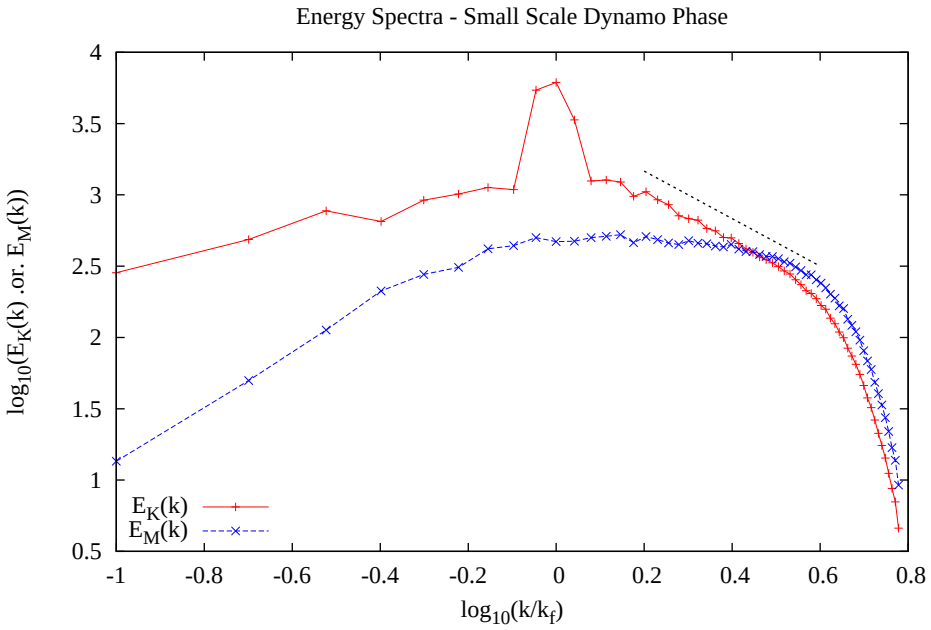

Figure 3.11: Energy Spectra during the second equilibrium phase ($St \sim 0.8$) . The line denoting the Kolmogorov spectrum has not moved with respect to figure 3.10 showing overall drop in kinetic energy and increase of magnetic energy. In the small scale dynamo phase, equipartition is reached very quickly between the smallest scales of the velocity and magnetic fields.

on a slope that is slightly steeper than a typical Kolomogorov spectrum (denoted by the black line). A good approximation of the equipartition scale of such a dynamo action is give by the wavenumber where $E_M(k_e) = E_K(k_e)$. By inspection, this scale is between $2.5 - 2.8k_f$ during the small scale dynamo phase, growing from approximately the grid scale in the kinematic phase (see figure 3.10).

So it is clear that we are simulating a turbulent, shearing box that quickly reaches an equilibrium between the influx of energy from the forcing function, the transformation of kinetic energy to magnetic energy by a small scale dynamo and the dissipation present in the code. The much slower growth of the large scale dynamo will be covered in the following chapter, as it is the main focus of this work.

Chapter 4

Results

The results of numerically integrating the equations 3.15 and 3.16 using the Brucker et al. (2007) algorithm to deal with the shearing boundary conditions and the forcing function described above are discussed here. Energy is inputted into the velocity field by the forcing at a wavenumber of $k_f = 10$ and acts as the initial condition to the velocity field (no initial field is set). The magnetic field is initially seeded by inaccuracy in the calculation of the nonlinear terms in the code at a magnitude of approximately 10^{-16} (accuracy of double precision numbers). These numerical inaccuracy quickly grows and act like a weak, random seed field.

The results will be presented from four runs of the simulation. Three of the runs will vary the Rossby number ($Ro = k_f u_{rms}/S$) which relates the relative strength of the shearing rate to the eddy turnover rate. And the fourth run will vary the magnetic Prandtl number ($Pr = \nu/\eta$, in what follows 'magnetic' will often be dropped when referring to the magnetic Prandtl number) which denotes the relative strength of dissipation in the velocity and magnetic field. In section 4.1 we will begin with a system that has a high Rossby number, up to about 100. No appreciable large scale dynamo is detected in this system and it is dominated by a saturated small scale dynamo that eventually decays. In section 4.2 the system contains a lower Rossby number ($Ro \sim 2$) and contains evidence of large scale dynamo action; but does not result in a strong large scale magnetic field. It seems that the strength of the resulting large scale magnetic field depends on the available energy built up by the small scale dynamo, which in this case does not build up appreciable amounts of energy. In section 4.3 we present Goldilocks' choice of Rossby number: large enough to build up a sufficient pool of energy on the small scale and small enough to ensure that the shearing plays its role in the large

scale dynamo process. We will find that a common factor in these simulations is the eventual decay of magnetic energy, which suggests that the dissipation rate is too large compared to the conversion rate from the velocity field to maintain a persistent magnetic field. So as a fourth test (in section 4.4), we increase the Prandtl number (reducing the resistivity) from unity in the first three cases to about 40 in the fourth case to see if a persistent magnetic field could be created.

In all cases, we will present the correlation between the electromotive force and the terms important to dynamo action. The first term will be the term derived from consideration of the conservation of magnetic helicity (known as the VC-term), the second will be the term derived from the standard kinematic approximation of mean field dynamo theory (known as the kinematic term) and the third term is the term responsible for the back-reaction that suppresses a kinematic dynamo (the back-reaction term).

Note that in all cases the simulation is run on a $64 \times 64 \times 64$ box. A higher resolution ($128 \times 128 \times 128$) run was partially completed for the high Rossby number run and is included in the appendix. The main conclusion from the higher resolution run is that the resolution does not affect the following results. Although higher resolution runs are planned for the future to further solidify this point, as well as search for possible resolution effects.

4.1 High Rossby Number Case

The first presented system was attained by forcing the turbulence with such a strong function that the average eddy turnover rate is about 100 times the shearing rate. As shown in figures 4.1 and 4.2 the high Rossby number case quickly reaches an equilibrium between the small scale velocity and magnetic field, driven by a small scale dynamo. This is where the evolution stops, and no significant large scale magnetic field builds before the small scale dynamo is overcome by the dissipation, and the magnetic field decays. Such a system illustrates the importance of the shear to the dynamo process. With such a high Rossby number it appears that the shear does not have a significant impact on the dynamics to play a part in the dynamo process.

Figure 4.3 shows the correlation between the three important dynamo terms and the electromotive force. At early times the electromotive force is dominated by the VC-term since the kinematic and back-reaction terms are both too small too be considered important. As the system reaches its first equilibrium, the kinematic term jumps just above the ideal case (denoted by the black line -

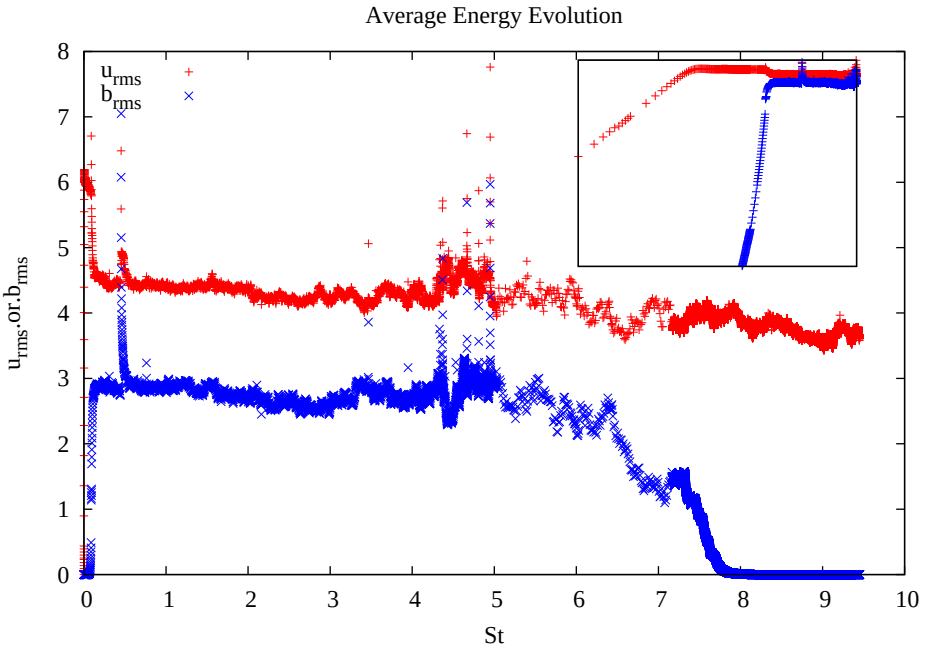

Figure 4.1: The evolution of the root mean squared velocity and magnetic field for the high Rossby number case. The system reaches an equilibrium prior to a shearing time of one and remains there for a few shearing times prior to the dynamo saturating and eventually decaying. The large spikes in energy represent points when the code went unstable, but quickly corrected itself by reducing the timestep of integration. This timestep is set by the CFL condition with a parameter of $C = 0.2$ in this case. When the the parameter is cut in half, the peaks can be eliminated and no noticeable effect is had on the resulting energy spectra (see appendix). The insert is the log scale of the two axis, to emphasize the initial build up of energy.

corresponds to a perfect 1 : 1 correspondence). After the fluid has reached equilibrium with the dissipation, the electromotive force along with the dynamo terms grows up to the right and settles in the top right corner of the plot. During the build up of the small scale dynamo, it seems apparent that the VC-term is still the most influential on the electromotive force since the kinematic term lies above the ideal line - implying an over-estimation of the total growth rate of magnetic energy. The back-reaction term is too small to explain the discrepancy between the kinematic term and the electromotive force. So it appears that the VC-term is a better approximation for the electromotive force than the kinematic term for all of the simulation.

There is some discrepancy between the VC-term and the electromotive seen at the highest values in figure 4.3. This isn't too surprising since the VC-term represents only the parallel component of the electromotive force, and not the full emf. To test its validity, we compare the VC-term to the magnitude of the parallel (to the magnetic field) component of the electromotive force. The

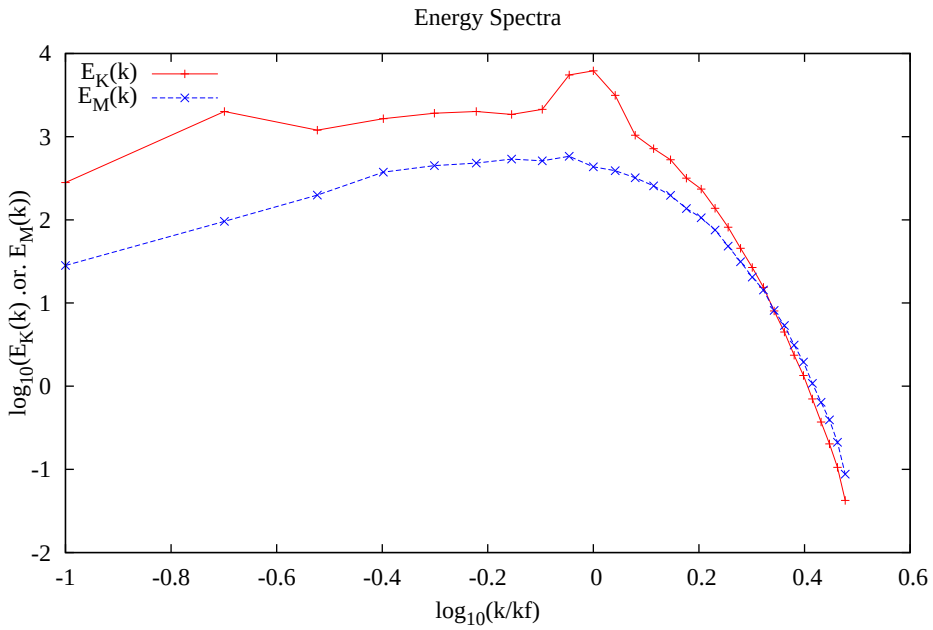

Figure 4.2: Energy spectra for velocity and magnetic energy during the small scale dynamo equilibrium phase.

VC-term estimates the evolution of the parallel emf well, at least after the initial random seeding by numerical inaccuracy and subsequent fast growth. The match between the parallel component and the VC-term is not perfect, and overall the VC-term tends to overestimate the parallel electromotive force for most of the simulation. The reason for this is not entirely clear, but is most likely is due to the finite dissipation in the code.

Because the inverse cascade of magnetic helicity is an important process in the magnetic helicity conserving dynamo, estimating the contribution to the large scale magnetic helicity from small scale components are an important probe of the system. In figure 4.5 the average magnitude of the temporal derivative and the helicity flux are compared to the average magnitude of the term responsible for transporting magnetic helicity across scales. At early times the two terms appear to be different, suggesting that the inverse cascade takes time to fully activate. Once in full swing, it appears that the inverse cascade in the code acts in a way that we expect and a strong correlation is seen between the two terms.

As a first result, we are seeing a system that builds up a pool of magnetic energy at small scales that reaches equipartition with the velocity field very quickly. This small scale dynamo is as far as the system seems to evolve, and we see no evidence for a large scale dynamo prior to the system

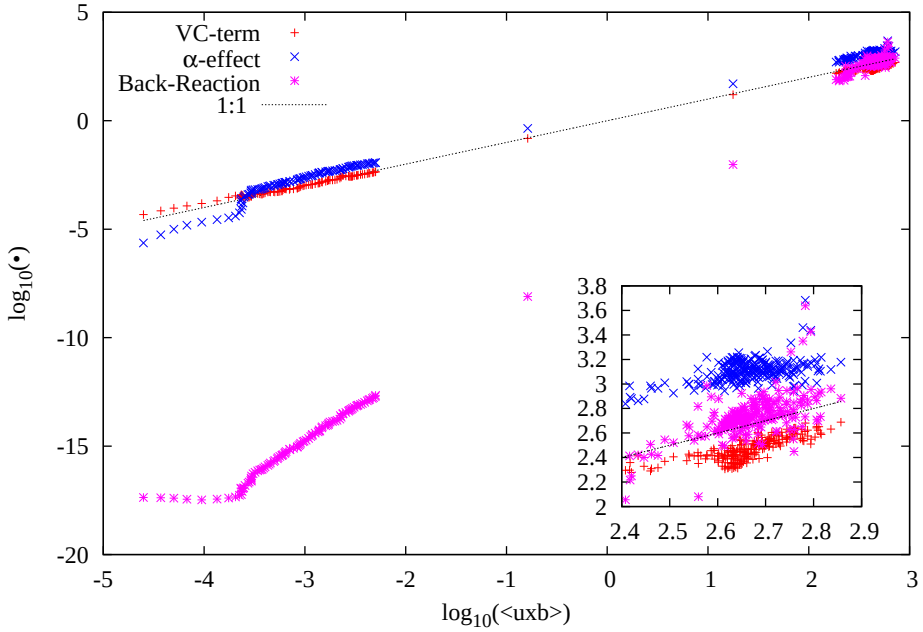

Figure 4.3: Comparison of the average magnitudes of important dynamo terms. Here we compare the electromotive force with terms derived by the kinematic approximation of mean field dynamo theory (α-effect, $\tau_{eddy}h^k/3$) and the VC-term ($\nabla \cdot \mathbf{J}_h\mathbf{B}/2B^2$). The black line denotes an ideal case when the term is exactly equal to the electromotive force. At very early times (far left of the plot) the kinematic term underestimates the electromotive force, while the VC-term lies just above the ideal case. Its likely that at this time the VC-term is dominating the initial growth of the magnetic field. When the kinetic energy reaches its first equilibrium phase the kinematic term gets closer to the ideal case and remains just above the electromotive force for the remainder of the simulation. It is apparent that the VC-term is a better approximation for the electromotive force throughout the simulation. The kinematic term tends to overestimates the electromotive force, and the back-reaction term ($\tau_{eddy}h^{cur}/3$) is too small to explain the discrepancy. At late times (right side of plot and inset) the back-reaction term has grown to be nearly the same magnitude as the kinematic term, as expected from before.

decaying away. This system illustrates the need for a non-trivial effect from the shear in building a large scale dynamo. Such a result agrees with similar results from work in stellar dynamos (Noyes et al., 1984) which suggest that higher Rossby numbers hinder the growth of large scale magnetic fields.

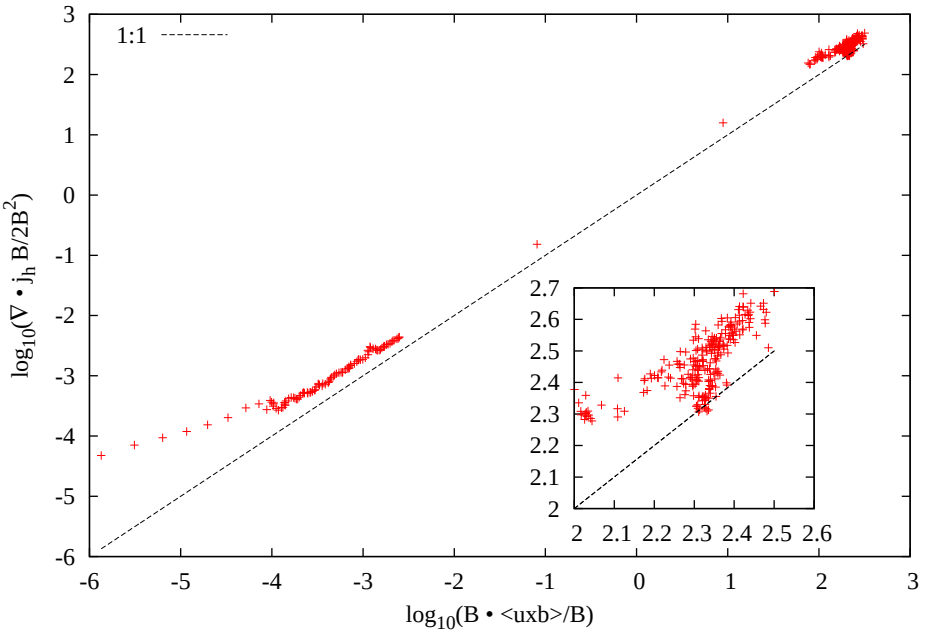

Figure 4.4: The parallel component of the electromotive force compared to the VC-term. The VC-term shows a very strong linear correlation to the electromotive force after a short time, while it does tend to stay above the line of perfect correspondence. This suggests an over estimation of the parallel electromotive force by the VC-term. The reason for this might be due to the dissipation of present in the code, that reduces the actual value of the electromotive force.

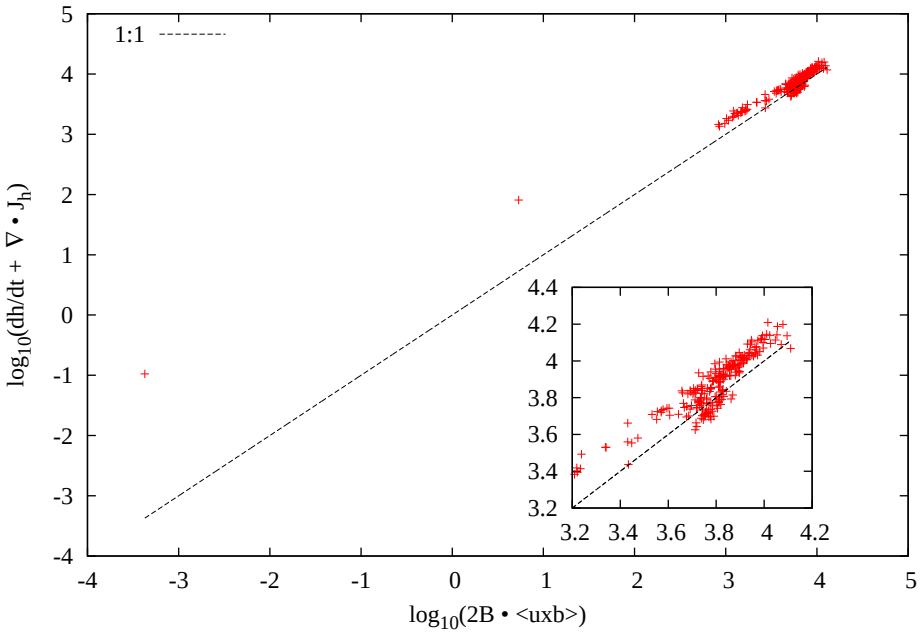

Figure 4.5: Temporal evolution of the large scale component of the small scale magnetic helicity. At early times (left side of plot) the two terms tend to disagree, suggesting a lag between the start of the simulation and efficient inverse cascade of the magnetic helicity. We find that the magnetic helicity under goes an inverse cascade in the way that we expect, with only a small discrepancy caused by non-zero resistivity in the code.

4.2 Low Rossby Number Case

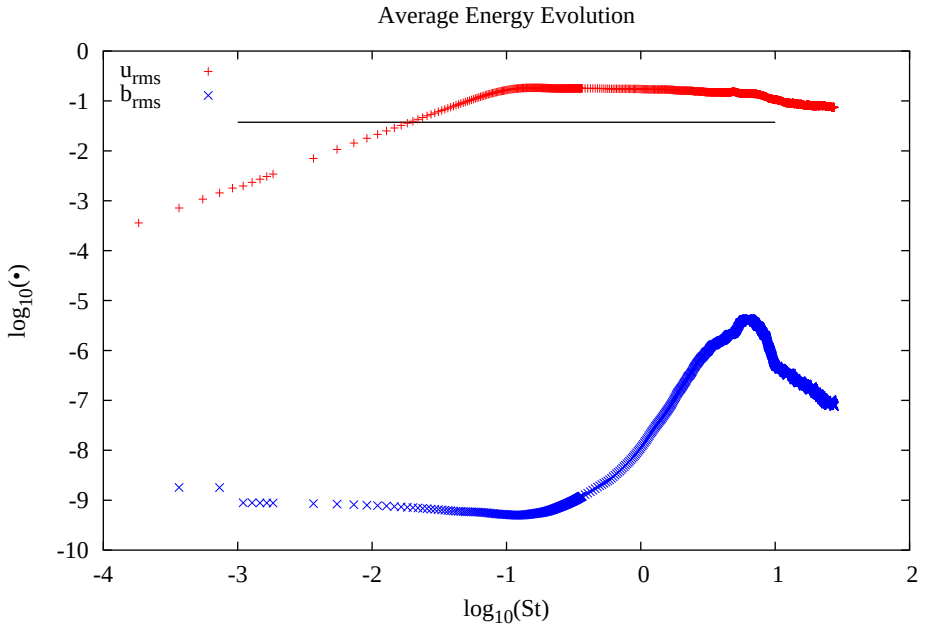

Figure 4.6: Average energy evolution of the velocity and magnetic fields for the lower Rossby number case. The black line denotes the energy for a Rossby number of one. Here we see the dynamo begin while the small scale magnetic field is still small. As a result the resulting large scale magnetic field begins very weak, compared to the velocity field. As before, the horizontal black line denotes the point where above which the eddy turnover rate is larger than the shearing rate.

As a second test, the amplitude of the forcing function is dropped so that the resulting Rossby number ends up at about two. In this system the energy in the magnetic field does not build up to a significant level prior to the advent of the dynamo. The large scale dynamo can be observed in figure 4.7 by a build up of energy at the largest scales. At shearing times prior to $St \sim 10$, the magnetic spectra peaks just below the forcing scale and decreases to larger scales. As the simulation progresses past a shearing time of 10 (in this case) the spectra levels off at the largest scales energy begins to build up at $k = 1$, growing with respect to the energy around the eddy scale. Overall, the total energy in the magnetic field decays during the formation of the large scale dynamo. This suggests that the conversion rate between the velocity and magnetic fields, and the subsequent dynamo growth rate is lower than the total dissipation in the code. This property has been seen before in linear shearing dynamo simulations for systems that have Prandtl numbers ($Pr = \nu/\eta$) of order unity (see Singh & Jingade (2013)).

Figures 4.8 - 4.10 plot the same dynamo terms as in section 4.1. In general, the evolution of the

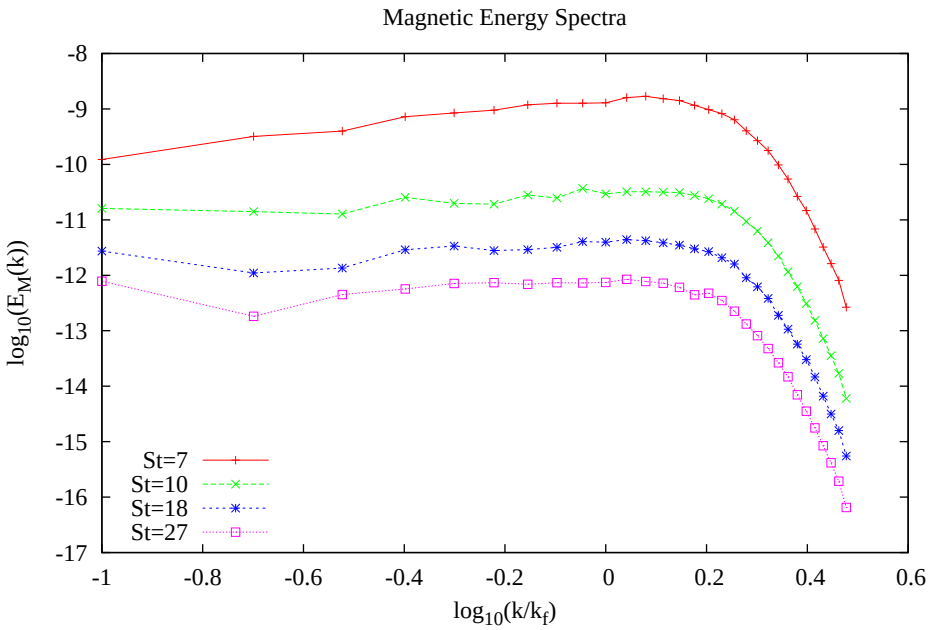

Figure 4.7: Evolution of the magnetic energy spectra as the dynamo action begins to take effect. The dynamo action can be seen by a flattening out of the energy spectra as the shearing time passes ten (the forcing wavenumber in the code).

terms start in the lower right corner of the plot and evolves up to the top left. After a short time the curve evolves back down, often covering the same space of the plot in the decaying phase as in the growth phase. We find very similar properties to the correlation plots in the above section: the kinematic term tends to over estimate the growth rate from the electromotive force throughout the simulation. This discrepancy can not be explained by the back-reaction term, as it is too small to ever come into play in the dynamics. Meanwhile, the VC-term remains strongly correlated throughout the simulation and estimates the size of the electromotive force very well.

In this case, the evolution of the dynamo terms with respect to the evolution of the electromotive force remains similar to the case of high Rossby number. One difference is seen in comparing the VC-term with the parallel emf which shows a stronger deviation in the small Rossby number case compared to the large Rossby number case. Additionally, we find that the resulting strength of the driven magnetic field depends on the pool of small scale energy that is initially built up by the small scale dynamo. By the time that the large scale dynamo action begins, which is around a shearing time equal to the wavenumber of the forcing function the system transforms what ever energy is stored in the small scale field into a large scale field. The result is likely more of a property of the

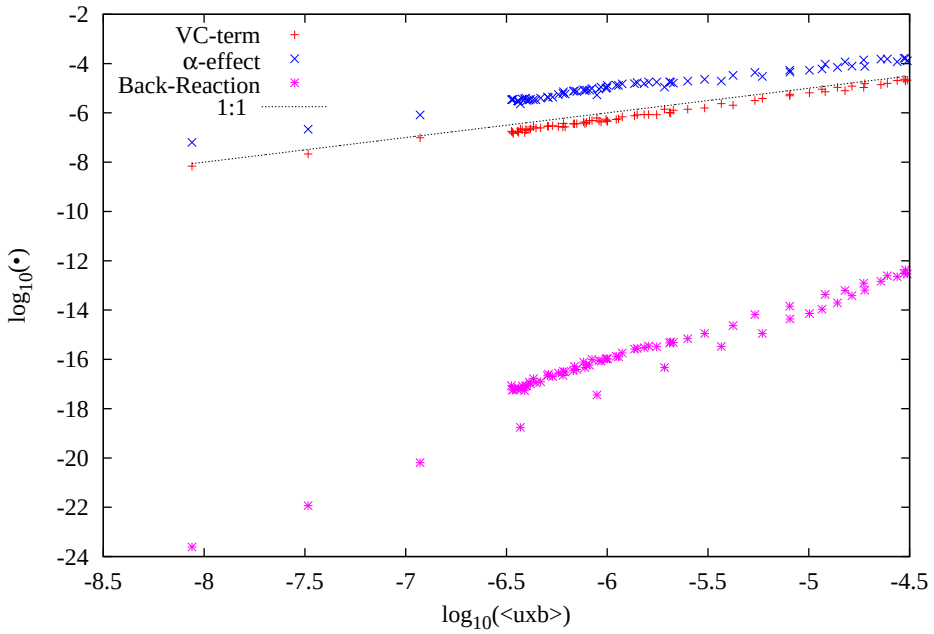

Figure 4.8: Correlation of the important dynamo terms to the electromotive force. The kinematic term ($\tau_{eddy} h^k/3$) over estimates the size of the electromotive force over the whole simulation. Meanwhile, the size of the electromotive force seems to be well estimated by the VC-term ($\nabla \cdot \mathbf{J}_h \mathbf{B}/2B^2$) over the whole simulations. Again, the back-reaction term ($\tau_{eddy} h^{cur}/3$) never reaches a high enough magnitude to explain the discrepancy between the electromotive force and the kinematic term.

code than a physical result, related to how efficiently energy is injected into the system. The forcing function injects energy at each timestep, so when the shearing rate is strong compared to the eddy turnover rate ($Ro \sim 1$) the energy injection rate with respect to the shearing rate is lower. So less energy is inject into the system, and transferred to the magnetic field by the time the large scale dynamo begins to work. While numerical in nature, it does suggest a strong connection between the large scale and small scale dynamos. Finally, it appears that the small scale dynamo saturates well below equipartition (with the small scale kinetic field) as the large scale dynamo begins to transfer energy. Such a results is related to the back-reaction that has been discussed before.

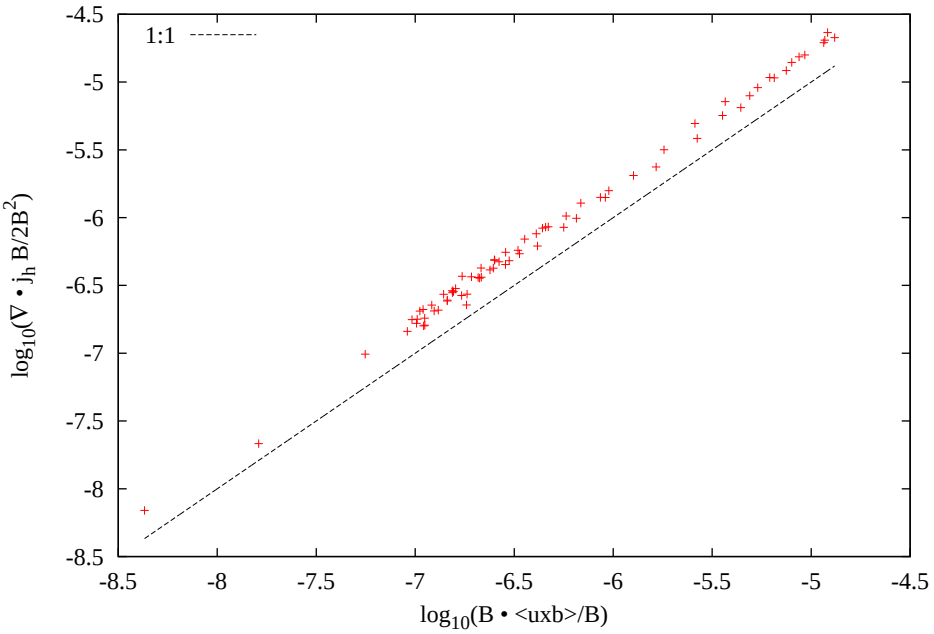

Figure 4.9: The correlation of the VC-term with the parallel (with the magnetic field) component of the electromotive force. Interestingly, the VC-term seems to be a worse estimation of the parallel emf than in figure 4.4 when the turbulence was much more important to the dynamics than the shear.

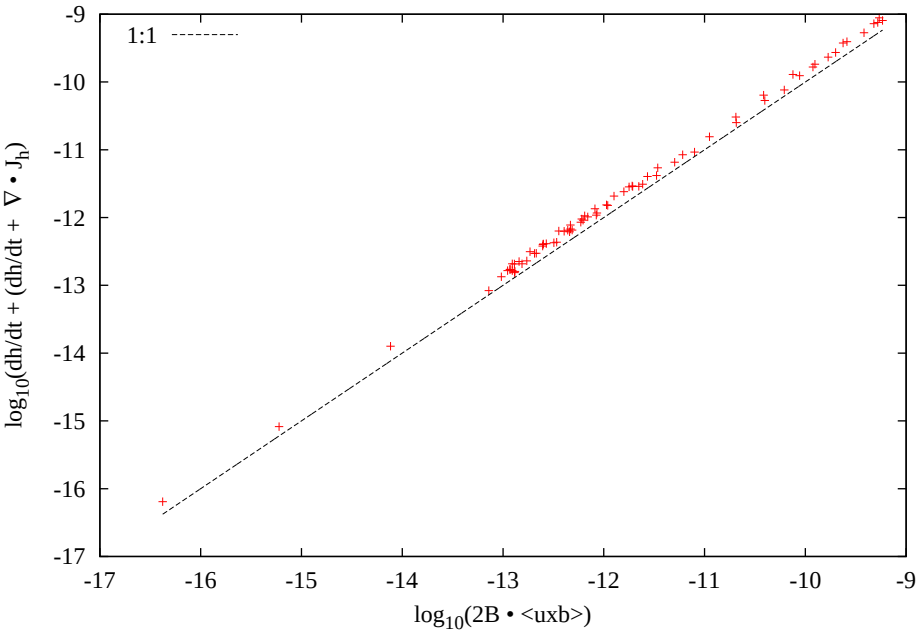

Figure 4.10: Temporal evolution of the large scale component of magnetic helicity from small scale fluctuations. The evolution is as expected, and suggests a minimal effect from dissipative forces to the evolution of the small scale component of large scale helicity.

4.3 Goldilocks Case

As a final study of the effect of the Rossby number, the 'Goldilocks' case is presented here. In this case, the Rossby number ends up between five and ten, so the effect of the shear is slightly weaker than in the last case. In this system the small scale dynamo is able to run to equipartition prior to the switching on of the large scale dynamo. As a result the large scale dynamo has much more energy to draw from, giving a large scale magnetic field with an appreciable energy - at least initially. Like the other systems, the Prandtl number is unity and the magnetic energy begins to decay not long after the beginning of the large scale dynamo phase.

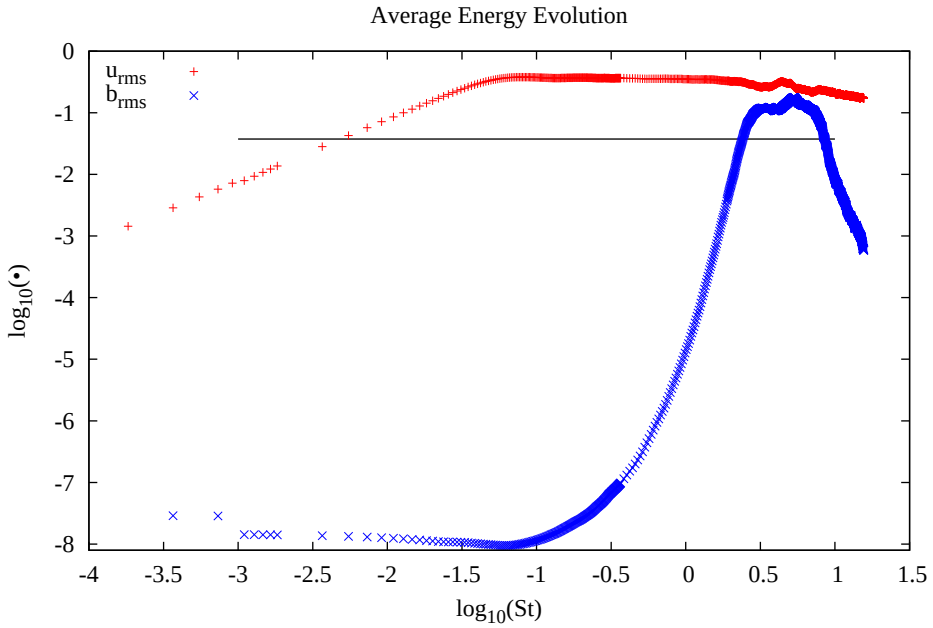

Figure 4.11: Evolution of the average energy in the Goldilocks case. With a Rossby number between five and ten, the shear is strong enough to cause the initiation of a large scale dynamo, while weak enough that the system can build a saturated small scale dynamo prior to the emergence of the large scale dynamo. The flux of energy to the magnetic field is not large enough to maintain the field against dissipation, so the system will tend to lose its magnetic energy as time goes on. As before, the horizontal black line denotes the point where above which the eddy turnover rate is larger than the shearing rate.

Like in the weak Rossby case, the magnetic dynamo begins to appear just before the shearing time reaches the forcing wavenumber. The effect of the dynamo growth is easily seen in figure 4.12 between the curves for the spectra at shearing times $St = 2$ and $St = 10$. The system has about the same total magnetic energy at those points, but more energy is stored at the largest scales than in

the small scale. As before, we find that the VC-term is well correlated to the full electromotive force, and the kinematic term consistently over estimates the growth rate of the large scale magnetic field. Additionally we can see that at the highest values of the back-reaction term, it does not get large enough to explain the discrepancy between the estimates of the kinematic term and the electromotive force.

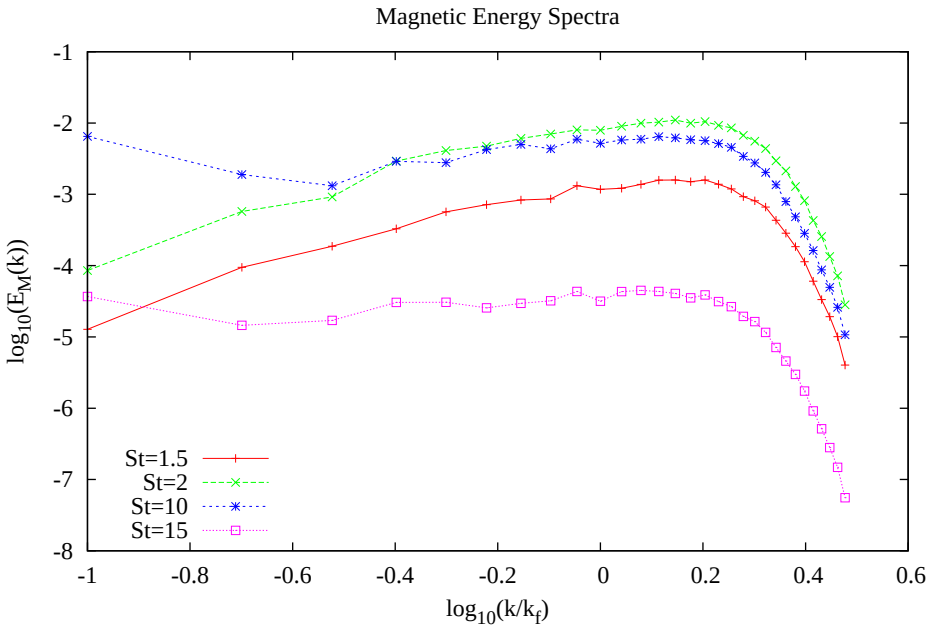

Figure 4.12: Evolution of the magnetic field spectra for the Goldilocks case. The effect of the large scale dynamo is clear, and evident when comparing the spectra from $St = 2$ and $St = 10$. Those shearing times represent points on either side of the energy peak in figure 4.11 where the system has roughly the same total amount of magnetic energy.

So in this Goldilocks case, the relative strength of the shear to the turbulent motion is such that we get a strong initial large scale magnetic field after the build up and saturation of the small scale dynamo. Similarly to the last two cases, the system does not persist and eventually decays to zero. This decay is due to the finite resistivity over-powering the rate at which the energy is transferred to the magnetic field from the velocity field on the eddy scales, and then from the small scale magnetic field up to the large scale through the inverse cascade of magnetic helicity.

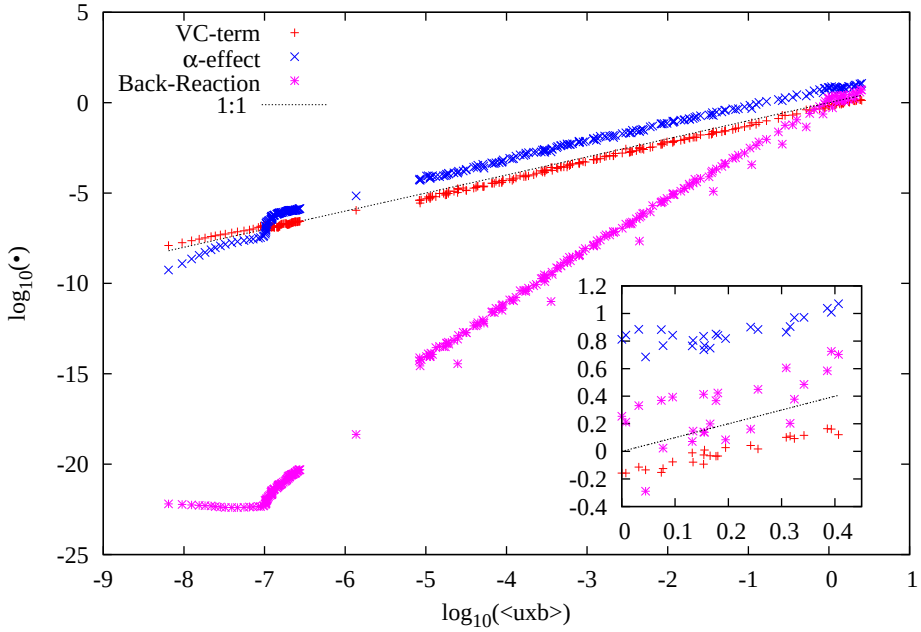

Figure 4.13: Correlation of dynamo terms to the electromotive force. Again we are seeing a consistent over estimation of the electromotive force by the kinematic term ($\tau_{eddy} h^k/3$), even when the back-reaction term ($\tau_{eddy} h^{cur}/3$) has grown. The VC-term ($\nabla \cdot \mathbf{J}_h \mathbf{B}/2B^2$) does well to estimate the evolution of the electromotive force, throughout the simulation. The evolution of the system begins as always in the bottom left corner and grows up and to the right. After the system reaches its maximum magnetic energy and begins to decay, the curve evolves back down towards the left corner.

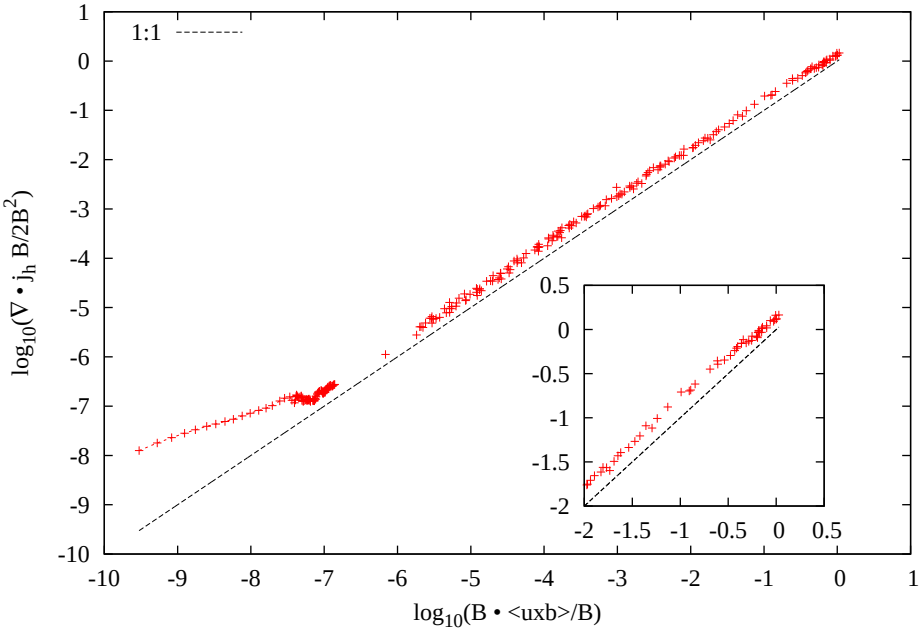

Figure 4.14: Correlation of VC-term and parallel emf. Again, the VC-term seems to overestimate the parallel emf which suggests another source term that is parallel to the large scale magnetic field.

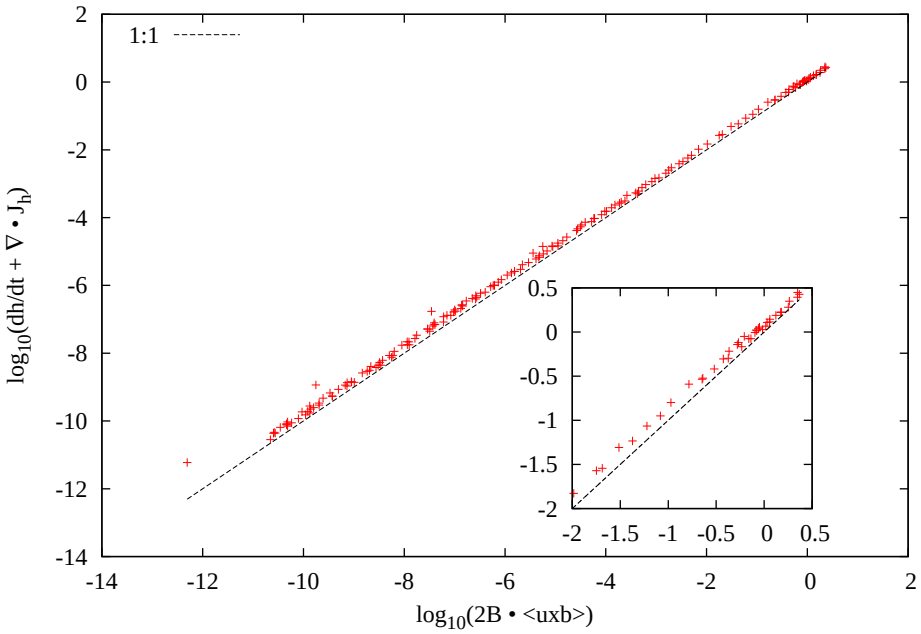

Figure 4.15: Evolution of the large scale component of the small scale helicity. Some impact from dissipation is apparent, since the time evolution does tend to sit slightly higher than the transfer term. Such a result is suggestive of the source for this decaying system.

The weak energy transfer from the velocity field to the magnetic field can be illustrated by plotting the functions representing the transfer of energy between the velocity and magnetic field. These transfer functions are defined by dotting either the velocity field into the Induction equation, or the magnetic field into the Navier-Stokes equation. An example of the form of one of these transfer functions is the dot product of the velocity field into the Lorentz force, which denotes the transfer of energy from the magnetic field to the velocity field. The functions denoting the transfer of energy between the velocity and magnetic field, $T_{v|vk}, T_{v|bk}$ and $T_{b|vk}$ are shown in figure 4.16. The subscripts of these function $(X|Y)$ are read: 'from Y to X', and denotes the transfer of energy to either the velocity or magnetic field from any particular Fourier component of the velocity or magnetic field. Their definition is derived from dotting the target field into the source field, the

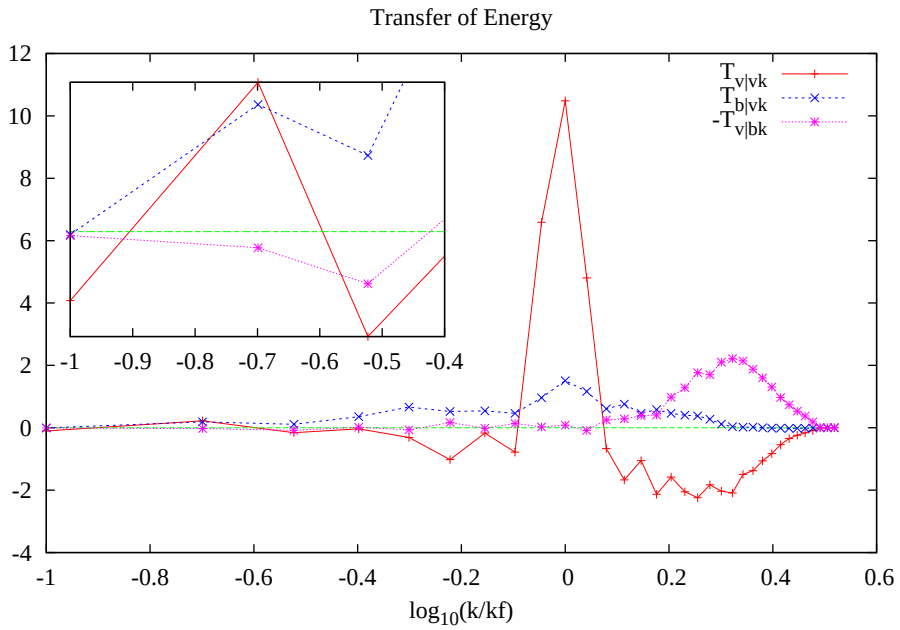

Figure 4.16: Transfer of energy between the velocity and magnetic field, the notation $X|Y$ means 'to X from Y'. The green line denotes zero flux. The insert focuses on the transfer of energy at the largest scales. The rate of energy transferred to the velocity field from the forcing is about five times the rate transferred to the magnetic field. The transfer to the large scale of the magnetic field is only weakly done by the velocity field - so it is expected that any energy carried to the largest scale is done so by the dynamo process.

definitions are as follows (Cho & Vishniac, 2000a):

$$
\begin{aligned}
T_{v|vk}(k) &= \sum_{k-0.5<|p|<k+0.5} -v^*(p)\cdot\mathcal{F}\{(\nabla\times\mathbf{v})\times\mathbf{v}\}(p) \\
T_{b|vk}(k) &= \sum_{k-0.5<|p|<k+0.5} +v^*(p)\cdot\mathcal{F}\{(\nabla\times\mathbf{b})\times\mathbf{b}\}(p) \\
T_{v|bk}(k) &= \sum_{k-0.5<|p|<k+0.5} -b^*(p)\cdot\mathcal{F}\{(\mathbf{b}\cdot\nabla)\,\mathbf{v}\}(p)
\end{aligned}
$$

From figure 4.16, we find that the flux from the forcing wavenumber to the velocity field is about five times the rate that energy is transferred to the magnetic field from the velocity field. Considering the significantly lower flux of energy into the magnetic field than into the velocity field, a possible way of obtaining an equilibrium in the magnetic energy will be to reduce the effect of the dissipation in the magnetic field by decreasing the resisitivity.

4.4 High Prandtl Number Case

Less resistivity, while maintaining the same viscosity level implies an increase in the Prandtl number ($Pr = \nu/\eta$) in the code, which is set to 40 in this run. This is achieved by first increasing the viscosity by two orders of magnitude to minimize the effect from numerical resistivity, which we estimated in the laminar dynamo test. The physical resistivity is then set to a fortieth of the viscosity - which should ensure that the Prandtl number is about 40 (assuming minimal numerical effects). Other parameters in this case are set to the same as in the Goldilocks case.

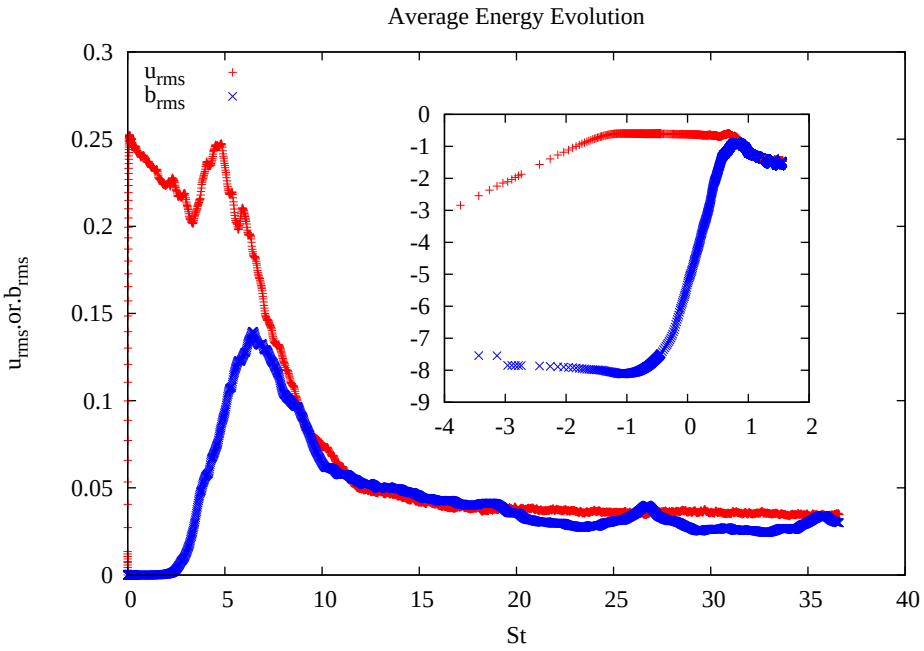

Figure 4.17: Average energy evolution of kinetic and magnetic energy, the inset shows the log of the two axes to emphasize early evolution. The magnetic and velocity fields reach an equilibrium at a shearing time of about 7. Unlike in previous cases the fields seem to reach an equilibrium between the forcing, the conversion to magnetic energy and the dissipation by both fields.

We find that the velocity and magnetic fields grows very similarly to the Goldilocks case, quickly growing magnetic energy at small scales (see figure 4.18) until equipartition is reached. Additionally the velocity field is suppressed by the build up of magnetic energy, however unlike in previous cases the magnetic field does not decay as strongly and the two fields reach an equilibrium.

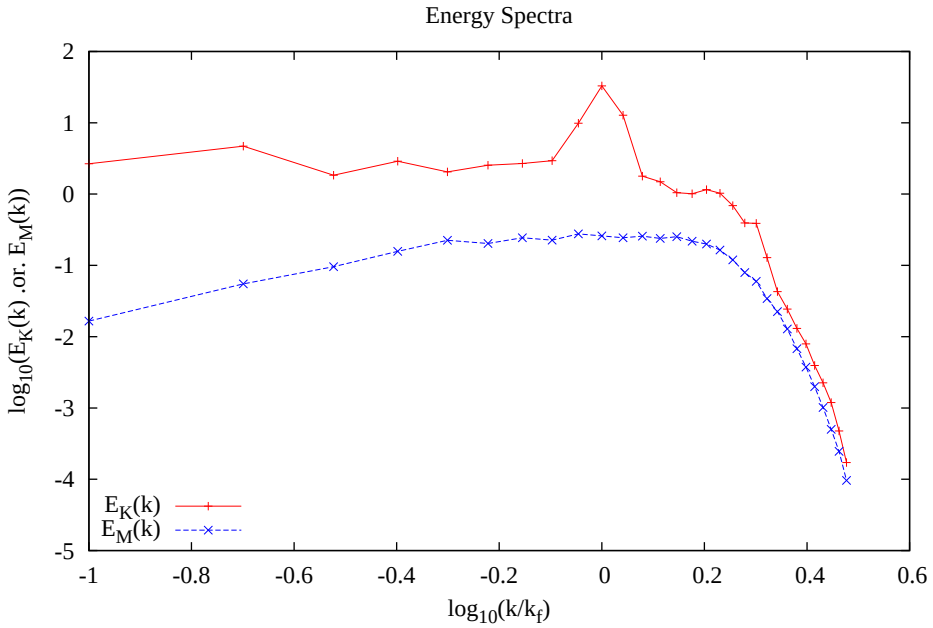

Figure 4.18: Magnetic and kinetic energy spectra at early times. The small scale magnetic and velocity fields reach equipartition quickly and build the required energy pool for the large scale dynamo.

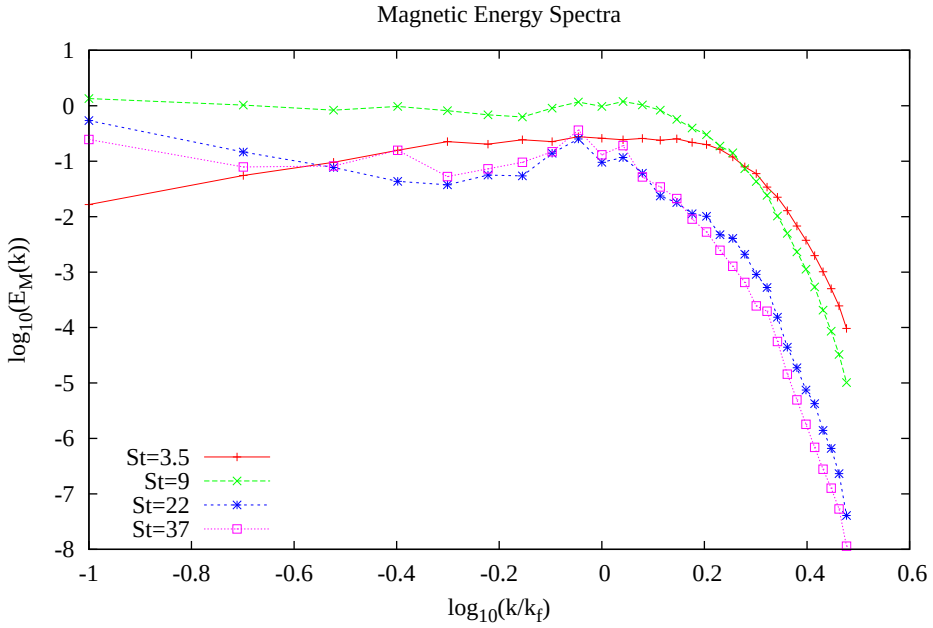

Figure 4.19: Evolution of the magnetic energy spectra for the high Prandtl number case. The build up of magnetic energy at large scales occur at around the same shearing time as in the former cases. However, unlike previous cases the resulting large scale magnetic field persists much longer. We also see evidence of scale separation between the largest scale and the eddy scale.

Looking at the power spectra, we are seeing a similar build up of magnetic energy at large scales as the shearing time approaches 10. However unlike in previous cases, the magnetic energy is not strongly suppressed as time moves forward and the large scale energies persist through many tens of shearing time. Additionally, we are seeing stronger evidence of scale separation between the large scale and small scale energies, which is an important assumption in mean field dynamo theory.

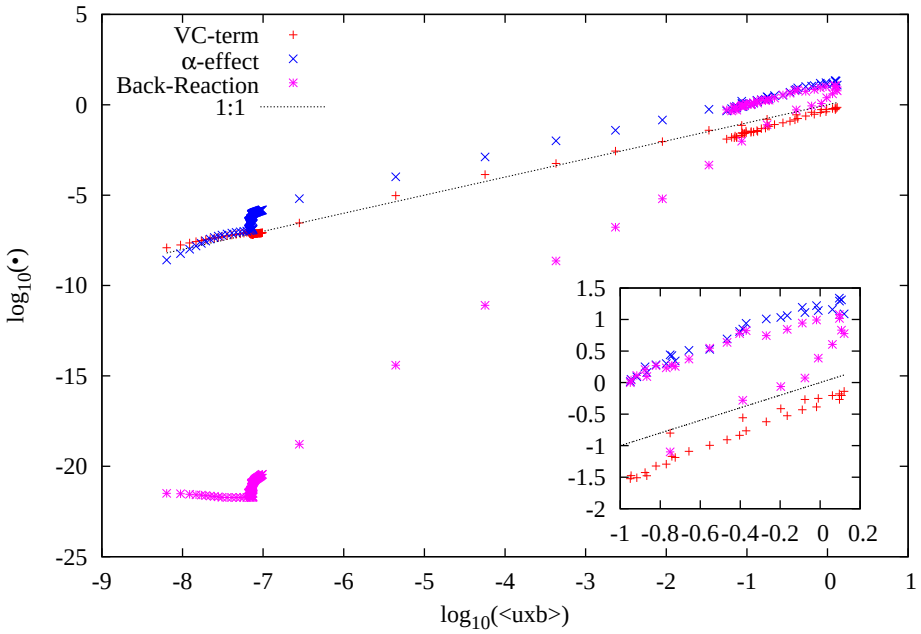

Figure 4.20: Correlation of the electromotive force and the important dynamo terms. The curves evolve from left to right but makes a turn at the top right (see insert) as the two fields reach equilibrium. As always the kinematic term ($\tau_{eddy}h^{k}/3$) overestimates the electromotive force for most of the simulation. Interestingly, the back-reaction ($\tau_{eddy}h^{cur}/3$) term evolves to match the magnitude of the kinematic term almost exactly. This is the first case where such a match is found, and could explain the discrepancy between the two terms from earlier cases, possibly being due to finite numerical resistivity. Such an effect is minimized here because of the increased physical viscosity in the code.

The correlation between the dynamo terms and the electromotive force is shown in figure 4.20. Similarly, we find that that VC-term estimates the size of the full electromotive force well early on in the simulation, then underestimates the emf when the system reaches an equilibrium. Additionally, the kinematic term does well at very early time, but as the small scale dynamo reaches equipartition the kinematic term begins to over-estimate the electromotive force. As before, the back-reaction term is not large enough to explain the deviation between the kinematic term and the emf at early times. However, as the system reaches its second equilibrium the back-reaction term turns up and

reaches a magnitude that is nearly equal to the kinematic term.

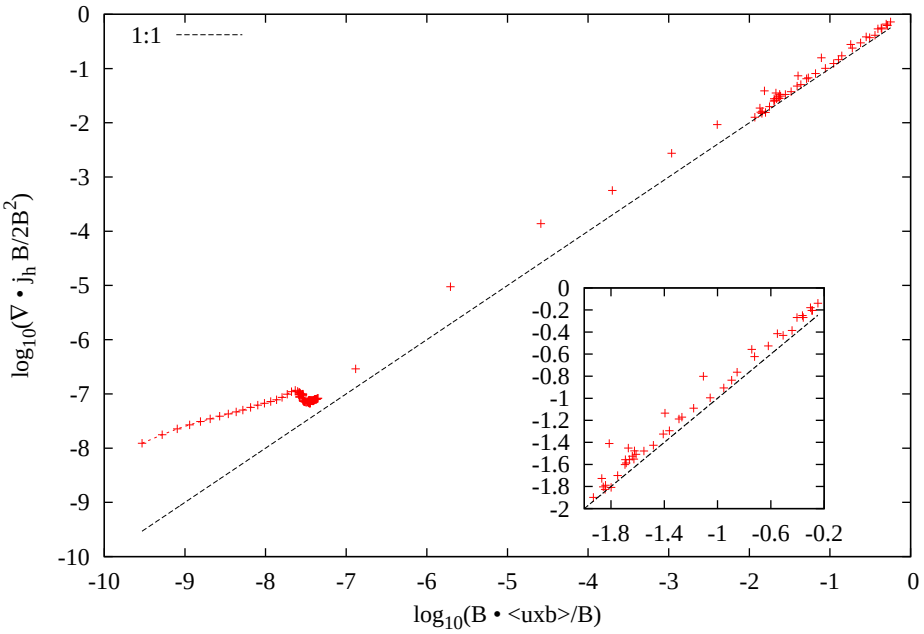

Figure 4.21: VC-term compared to the magnitude of the parallel emf. The VC-term shows a very strong correlation between the parallel emf and the VC-term which suggests that the deviation seen in previous cases is caused by numerical dissipation which is minimized in this case.

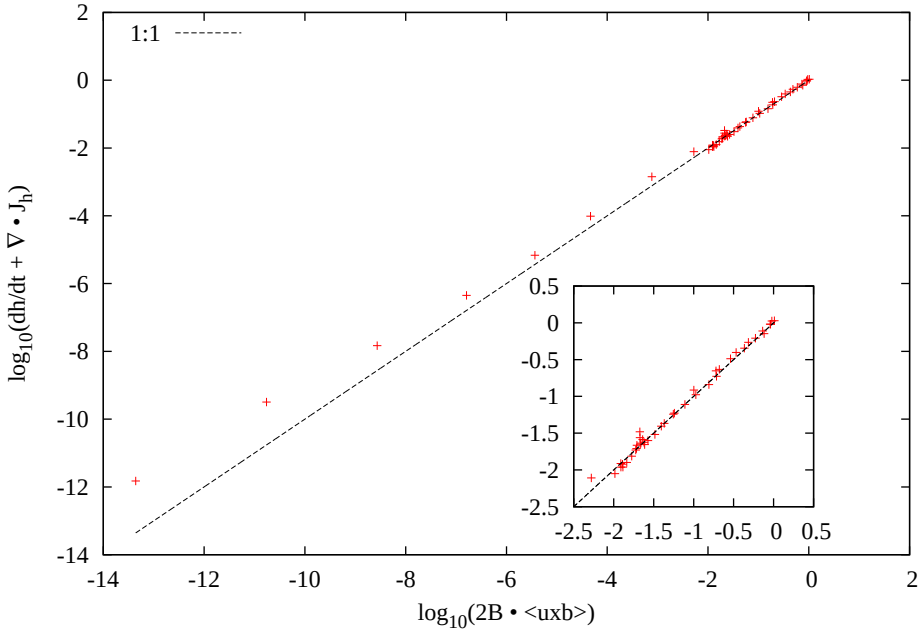

Figure 4.22: Temporal evolution of the large scale contribution by small scale helicity. At early times it appears that the inverse cascade of magnetic helicity does not dominate the evolution of h until the system reaches an equilibrium.

In figure 4.21 we find that the VC-term overestimates the parallel emf at early times, but matches very well when the system reaches equilibrium. The deviations that were observed in earlier plots appear to be suppressed by choosing a higher viscosity and Prandtl number. Suggesting that the deviation seen before was caused by effects from numerical dissipation. The strong correlation between the magnetic helicity transfer term and the temporal evolution of h at late times suggests that the dissipation is unimportant to the inverse cascade of magnetic helicity during the late phases of the simulation.

4.5 Discussion

Here we have presented the results of four runs of a shearing box simulation of magnetic dynamos. While some of the physical parameters are changed between runs, we can see that the correlation between dynamo terms and the electromotive force are unchanged. In general, we are seeing that the VC-term acts a good estimation (differing by between 3% and 50%) of the electromotive force at early times and a good estimation (differing by about 20%) of the parallel component of the electromotive force at late times. Additionally, it was observed that the kinematic term never estimates the electromotive force very well. Over the majority of the simulation, the kinematic term is between 10 and 30 times the size of the electromotive force. At early times the discrepancy has no obvious source, since the back-reaction term begins at 12 orders of magnitude smaller than the kinematic term and no sufficient suppression of the α-term exists. Meanwhile at late times, the back-reaction term grows larger and ends up at an average magnitude of a few times smaller than the kinematic term which which could explain the discrepancy, but does not fully cancel out the proposed effect of the α-term. One possible explanation of the early discrepancy comes from the modified (by the large scale magnetic field) kinematic term that was introduced in section 2.7.3. This test has been tried, but is not sufficiently large to explain the discrepancy of the α-term. Additionally, because the suppression term is proportional to $1/(1+R^2)$ where R is the magnetic field scaled by the equipartition energy and the magnetic Reynolds number. The term is on the order of $1/(1+Rm)$ at equipartition which represents a maximum value of ~ 0.998 for the High Prandtl Number case. This scaling factor is never large enough to explain the discrepancy of the α-term. The implication of this discrepancy is that while the kinematic approximation is often used to explain the emergence of the large scale magnetic dynamo, its resulting electromotive force overestimates the observed

electromotive force in the code.

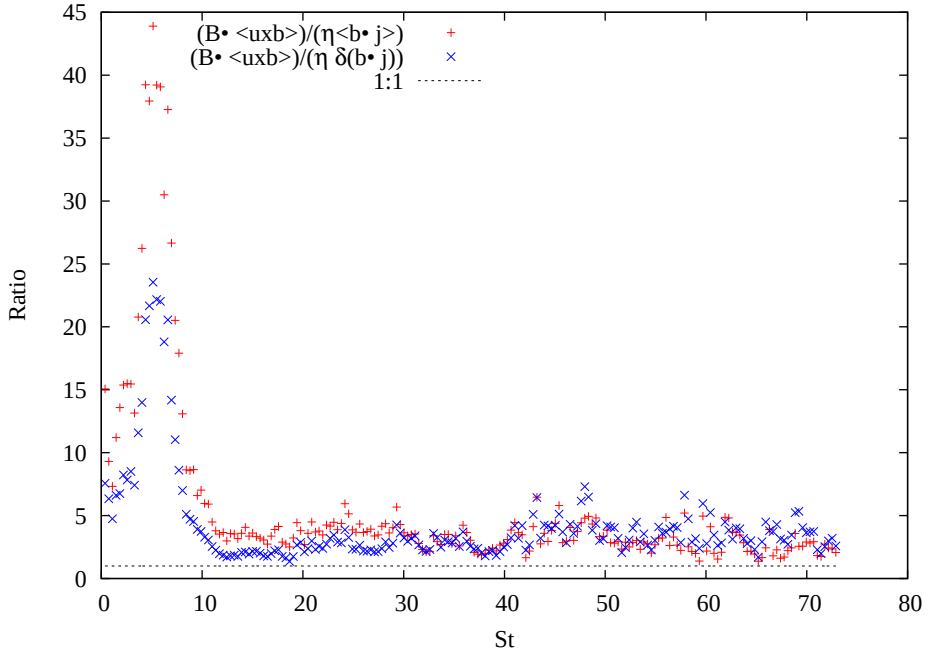

Figure 4.23: Comparison of the transfer term ($2\mathbf{B}\cdot\langle\mathbf{v}\times\mathbf{b}\rangle$) with the dissipation at the large ($2\eta\langle\mathbf{b}\cdot\mathbf{j}\rangle$) and small scales ($2\eta\delta(\mathbf{b}\cdot\mathbf{j})$) for the high Prandtl number case. At early times ($St<10$), before the system is equilibrium the transfer is much stronger than the dissipation. This is not surprising since the magnetic field is week at early time, so the dissipation term (which is proportional to the current helicity) is also small. At later times ($St>10$), when the system has reached an equilibrium, the transfer term remains between two and five times the size of both the dissipation at the large and small scales. The black line denotes the point where the transfer term is equal to the dissipation.

The conservation of magnetic helicity, and its inverse cascade in an important property of the proposed dynamo mechanism. As a check, in figure 4.23 we show that the transfer of magnetic helicity ($2\mathbf{B}\cdot\langle\mathbf{v}\times\mathbf{b}\rangle$) is more important to the dynamics of the magnetic helicity than the dissipation at the large scale ($2\eta\langle\mathbf{b}\cdot\mathbf{j}\rangle$) and small scale ($2\eta\delta\left(\mathbf{b}\cdot\mathbf{j}\right)$). We find that at early times ($St<10$) the transfer is higher than both dissipation terms by a factor of between 5 and 45. Alternatively, at later times ($St>10$) the transfer term is between 2 and 5 times the size of the dissipation. This shows that the cascade of magnetic helicity, which draws helicity from the small scale magnetic field and transports it to the large scale, has a higher effect on the dynamics of the magnetic helicity than the dissipation. Seeing this affirms our previous results in figure 4.22 which showed that the time evolution of the large scale component of the small scale helicity (h) is mostly dominated by the inverse cascade of the magnetic helicity. The difference between the two terms in figure 4.22 at later times, about 25% of the time evolution of h, is on the same order as the size of the large scale dissipation.

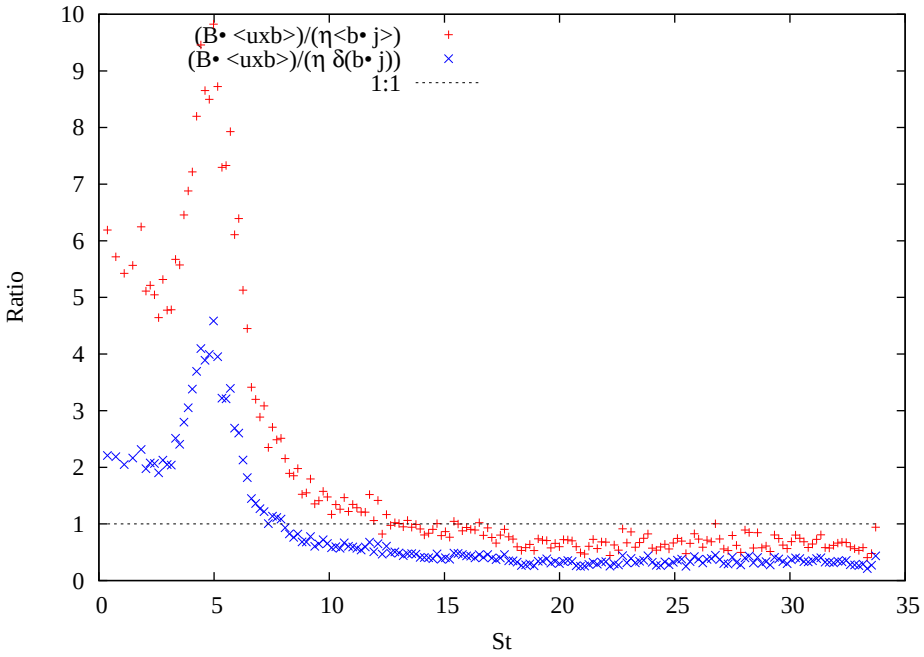

Figure 4.24: Comparison of the transfer term ($2\mathbf{B}\cdot\langle\mathbf{v}\times\mathbf{b}\rangle$) with the dissipation at the large ($2\eta\langle\mathbf{b}\cdot\mathbf{j}\rangle$) and small scales ($2\eta\delta(\mathbf{b}\cdot\mathbf{j})$) for the Goldilocks case. The curves follow a similar trend as in the high Prandtl number case, however the ratio is drastically different. At best, the transfer is about 10 times the dissipation at the large scale, and never more than 5 for the small scales. And at later times ($St > 10$) the dissipation at both scales are always higher than the transfer term. This implies that as magnetic helicity is created at the forcing scale, it will tend to dissipate faster than it can be transferred to large scales. This severely cuts off the energy source for the large scale dynamo, as its pool of small scale magnetic energy to draw from is preferentially dissipated rather than transferred. The black line denotes the point where the transfer term is equal to the dissipation.

Alternatively, as seen in figure 4.24, in the Goldilocks case when a magnetic dynamo is observed but quickly decays, the ratio of the transfer and dissipation terms evolves to an equilibrium position below one. This implies that the magnetic helicity that is produced at the forcing scale will preferentially decay rather than transfer to higher scales. This tendency has the observed effect of an initially growing dynamo, driven by a dominant transfer (at $St < 10$), that eventually decays as the transfer term loses out to dissipation. As seen in figure 4.15, there was a small discrepancy between the temporal evolution of h and the transfer term. Now it appears that the difference could be attributed to the dissipation, which will tend to provide a larger effect to the dynamics of the magnetic helicity than the transfer. To this point, the transfer term did provide a good estimation to the time evolution of h at the time when the electromotive force was the highest (top right corner of figure 4.15). This time is at $St \sim 5$ and corresponds to the point where the transfer term is much more dominant (by a factor of about 10) than the dissipation, as expected.

Meanwhile, we have seen the importance of large Prandtl number to the persistence of magnetic energy. Because the energy flux into the magnetic field is significantly less than the flux of energy into the velocity field, we require less resistivity to allow for an equilibrium to exist. Otherwise, the magnetic field acts as an energy sink and the system decays. Such a result has been seen before in work by Schekochihin et al. (2004), who found an exponential growth of the small scale dynamo for Prandtl numbers above a critical value of $Pr_{crit} \in (25, 50)$. Our choice of Prandtl number falls within their range and affirms the belief that the large scale and small scale dynamos are strongly linked. Such a link appears to be in the form of the small scale magnetic acting as an energy pool for the build up of large scale magnetic fields, which seems to explain the weak large scale dynamo in the small Rossby number case. In that case, the small scale dynamo did not grow an appreciable amount of magnetic energy by the time the large scale dynamo process began, so the large scale dynamo was only able to produce a weak large scale magnetic field. Overall, we find that by maintaining a strong small scale dynamo that persists, we allow for a strong large scale magnetic dynamo to grow and persist over many shearing times. Such a persistence at small scale is helped by lowering the resistivity in the code. It should be noted that the result of requiring a large Prandtl number for the persistence of the magnetic energy may not be fully extended up to very large Reynolds numbers (low viscosity). And it is likely that even Prandtl numbers lower than one could produce a persistent large scale magnetic fields, as long as the magnetic Reynolds number is also very high. Such a property can not be studied with the current implementation of the code, because of our finite numerical viscosity and resistivity places an upper limit on our possible Reynolds numbers.

To fully understand the properties of the system a full parameter search over different Rossby numbers, shearing rate and Prandtl numbers is required. Such a study could search for the critical Rossby number where a small scale dynamo does not produce a large scale dynamo. Additionally, it has been suggested (Singh & Jingade, 2013) that the initial exponential growth rate of the magnetic energy is linearly dependent on the shearing rate. This dependence has not been investigated here. Finally the importance of the Prandtl number to the long term persistence of magnetic energy seems like an important avenue of study, especially given our choice of Prandtl number being close to the critical value in Schekochihin et al. (2004). The result of that work seems to be related to the low conversion rate of kinetic energy to magnetic energy, which requires less dissipation to achieve an equilibrium between the two fields and dissipation.

Chapter 5

Conclusion

Here we have run direct numerical shearing box simulations of MHD turbulent plasmas, forced by a mechanical forcing function. The geometry of the simulation and background shear is meant to represent the local properties of a galactic or accretion disk. The purpose of such a simulation is to understand the underlying physics that results in the large scale magnetic dynamo growth that is observed in such systems. We have shown that the standard kinematic approximation of mean field dynamo theory generally overestimates the observed electromotive force responsible for driving the dynamo by at least one order of magnitude. Such an overestimation has been suggested before, and we find that the back-reaction term does grow sufficiently large at late times to explain it. At earlier times, the discrepancy is less clear and could be caused by the suppression of the α parameter by the build up of large scale magnetic field - though the usual form of the suppression does not suffice in explaining the discrepancy. The modification to mean field dynamo theory that we are interested in comes from the consideration of the conservation of magnetic helicity, which is perfect in ideal MHD and approximate in the limit of vanishing resistivity. It was shown that this conservation of magnetic helicity strongly constrained the possible form of the electromotive force, restricting the parallel (to the large scale magnetic field) electromotive force to the term that was called the VC-term in this work. The VC-term is proportional to the divergence of the large scale component of the small scale magnetic helicity flux and the large scale magnetic field. The physical picture that is suggested by this term is that small scale magnetic helicity is created by twisting motions at the eddy scale by turbulent motions in the fluid. The helicity undergoes an inverse cascade meaning that it will tend to grow in size, rather than break apart into smaller eddies like the velocity field. The inverse cascade

causes the initially small twists in the magnetic field to grow along the field line until they reach the largest scale in the system, where it is assumed that they add their energy to the large scale field very efficiently.

The persistence of such a dynamo is dependent on the size of the magnetic Prandtl number, requiring a larger Prandtl number than unity. The physical reason for such a dependence appears to be due to the inefficiency that energy is transferred to the magnetic field by turbulent motions. By comparison, the energy transferred to the velocity field by the forcing function is about five times as efficient. Such a difference in energy flux requires the resistivity to be lower than the viscosity so that an equilibrium can be reached between the energy into the magnetic field and the energy out. Such a Prandtl number requirement may not be as prevalent in systems of high Reynolds and high magnetic Reynolds numbers because the magnetic resistivity would be naturally lower, and an equilibrium may be more easily reached. A test of the high Reynolds and high magnetic Reynolds numbers may not be tested in the current implementation of the code, as the finite numerical dissipation places an upper limit on Re and Rm.

In this work, we have intentionally omitted some important properties of astrophysical systems, compressibility and self gravity for example, in order to calculate the important underlying physics driving large scale magnetic growth. With this insight, we strive to build a better model for the evolution of the large scale magnetic field in plasmas, so that it may be used in solving other problems in astrophysics.

Appendix A

Supporting Figures

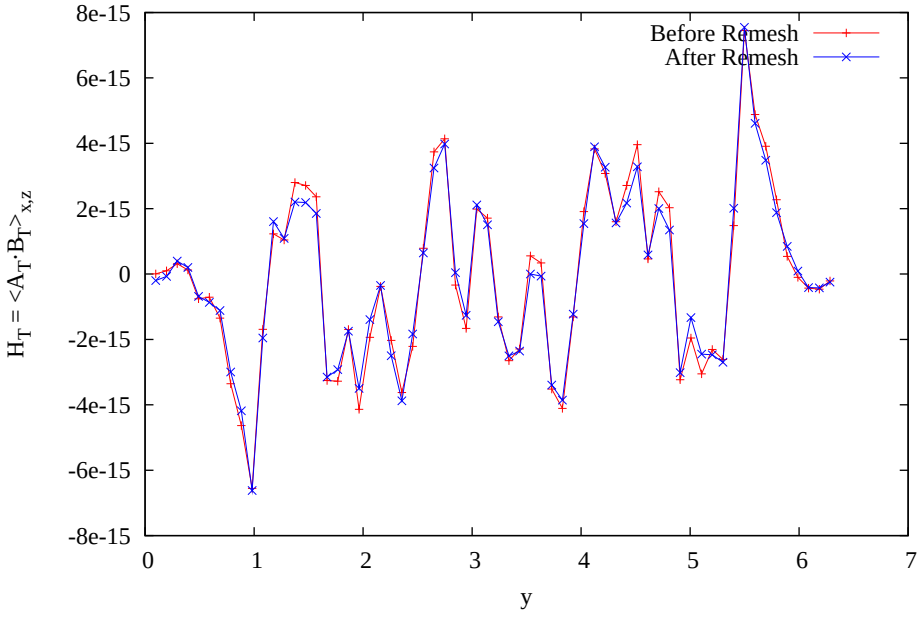

Figure A.1: The total magnetic helicity averaged over x and z, shown as a function of y in a Rogallo-based run. We find that globally, the magnetic helicity is conserved; shown here by the small changes as a function of y. The same result here is seen in z - only small changes primarily due to aliasing errors.

Appendix B

Effect of Instabilities

Shown in figure 4.1 the code has a tendency to become unstable. The instability shows up as a build up of energy at the grid size, but causes the code to quickly diverge. To help control the instability the time step was restricted by the CFL condition, and a hyperdiffusion term was added to the evolution of both the magnetic and velocity fields. The CFL condition (often called the Courant condition) ensures that the during one timestep, no perturbation is allowed to cross an entire grid cell. The typical CFL condition takes the form:

$$dt \leq C\min\left(\frac{\Delta x}{u}, \frac{\Delta y}{v}, \frac{\Delta z}{w}\right) \tag{B.1}$$

for a velocity field $\mathbf{u} = (u, v, w)$ and the constant C is no larger than one. In MHD, one generalizes the CFL condition to include the consideration of the magnetic field. So that eq. B.1 is generalized to:

$$dt \leq C\min\left(\frac{\Delta x}{u}, \frac{\Delta y}{v}, \frac{\Delta z}{w}, \frac{\Delta x}{b_x}, \frac{\Delta y}{b_y}, \frac{\Delta z}{b_z}\right) \tag{B.2}$$

The choice of C is arbitrary, other than the requirement of it being no greater than one. For the high Rossby number run $C = 0.2$, but shows instances of instability that are recovered by a change to the timestep and the hyperdiffusion.

An important question is whether an instability could be responsible for creating any kind of long lasting structure in the turbulence. Intuitively the answer is no - since the instability is at the

lowest scales where the diffusion is the most efficient.

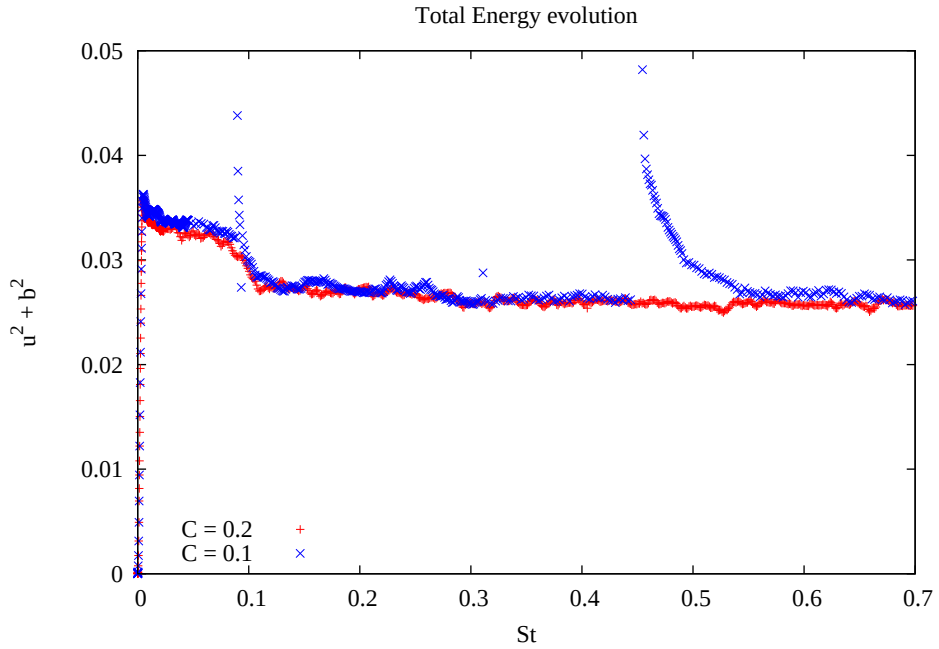

Figure B.1: Total energy evolution for two different choice of the constant C. When the constant is reduced, the overall evolution of the total energy is unchanged, while the instabilities are completely eliminated.

Important to our analysis, we also consider the effect on the distribution of energy in the magnetic energy spectrum. So we take a point after the first instability ($St \sim 0.2$) and output the spectra. The result of which is shown in figures C.2 and C.3.

Neither spectra show a large difference for different a different choice of C. Suggesting that the instabilities do not change any conclusions that are made. Because the instabilities occur on the smallest scales, the hyperdiffusion can quickly stabilize the code as long as the timestep is reduced quickly.

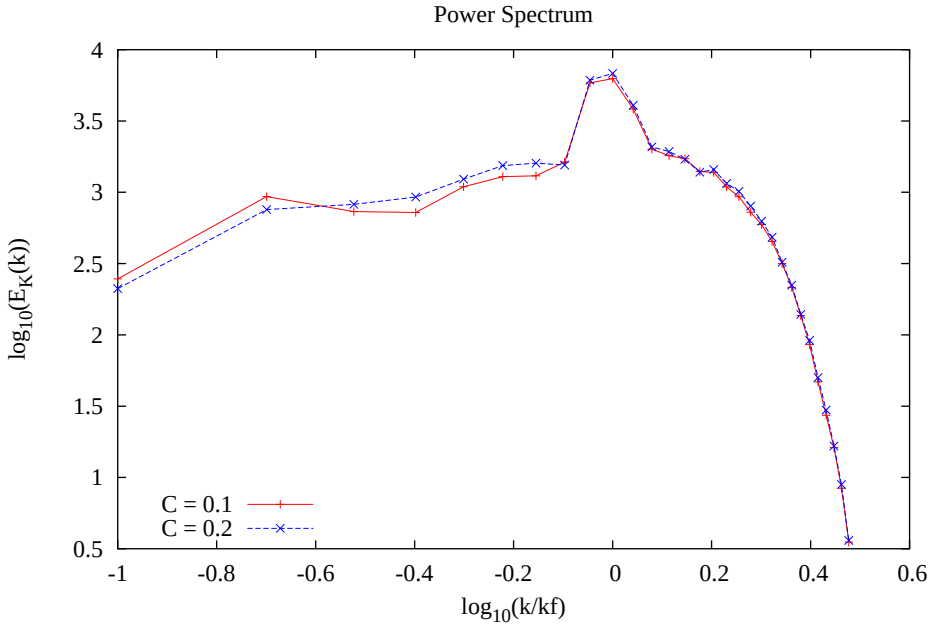

Figure B.2: Velocity spectra for $St = 0.2$ for different choices of C.

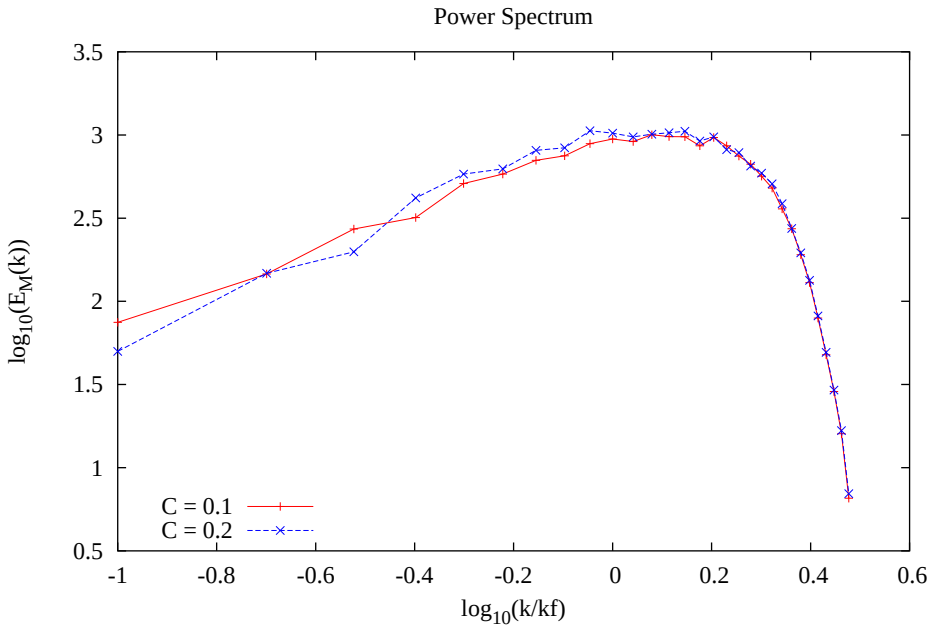

Figure B.3: Magnetic spectra for $St = 0.2$ for different choices of C.

Appendix C

High Resolution Case

A higher resolution ($N = 128^3$) run of the high Rossby number simulation has been partially complete, and its results are presented here. The energy evolution and the energy spectra are presented in the Numerical Methods chapter, so we skip them here. Instead we focus on the results of studying the correlation of important dynamo terms.

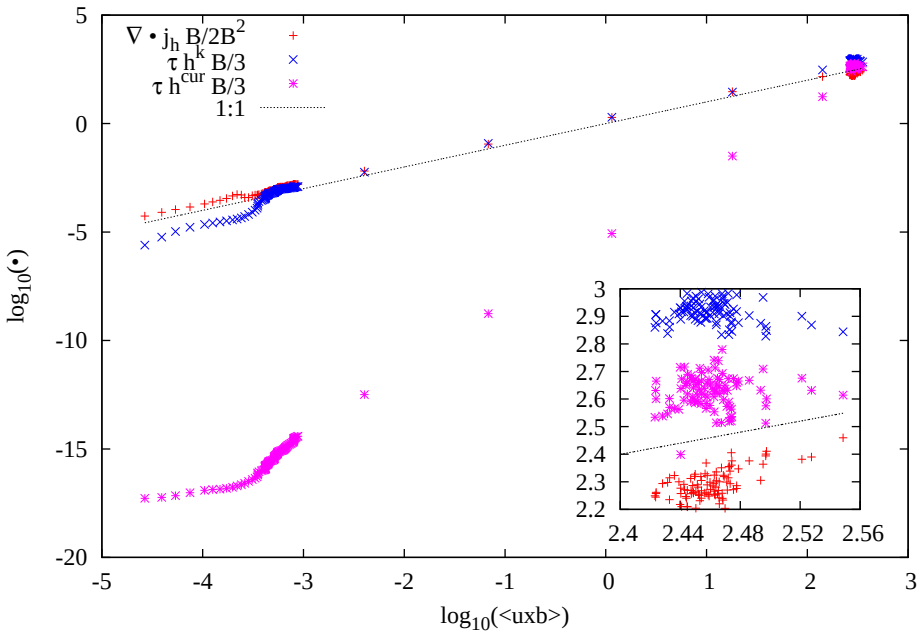

Figure C.1: Correlation of the important dynamo terms to the electromotive force for higher resolution run.

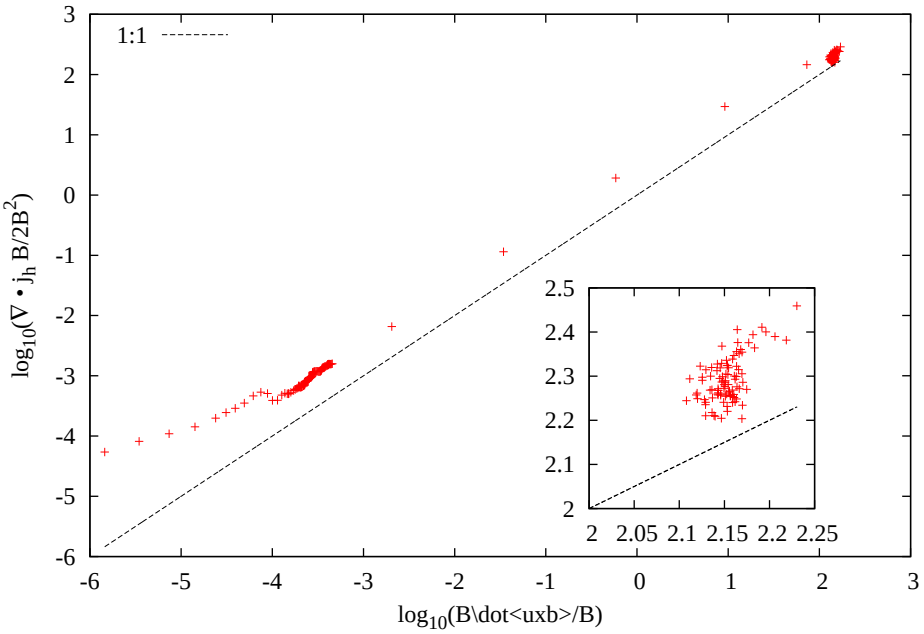

Figure C.2: The correlation of the VC-term with the parallel (with the magnetic field) component of the electromotive force for higher resolution run.

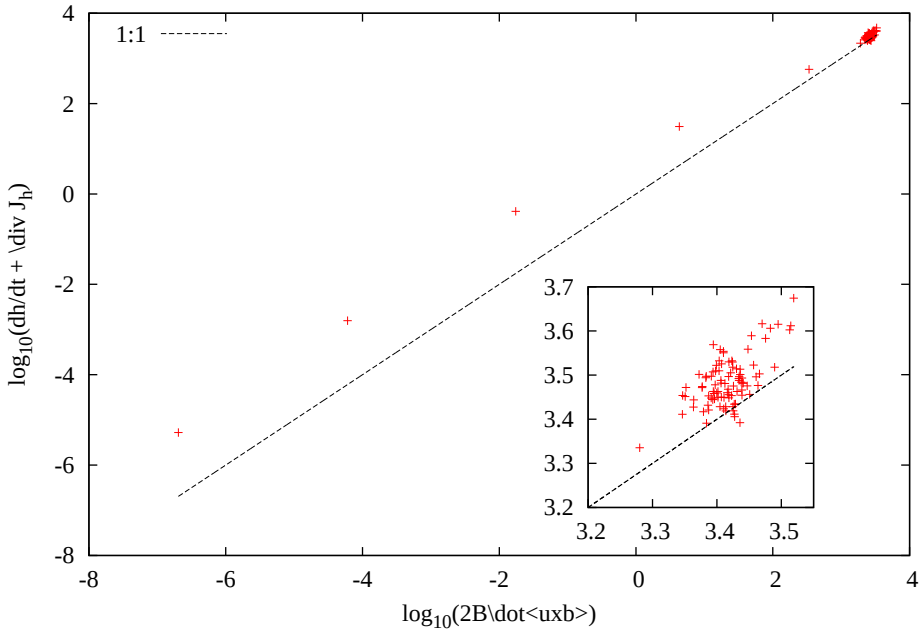

Figure C.3: Correlation of temporal derivative of small scale component to large scale magnetic helicity for higher resolution run.

The correlation plots follow similar structure to the lower resolution cases. At early times, it

appears that the kinematic term and the VC-term appear to be of similar magnitude, while at later times the familiar deviation of the kinematic term is observed. A similar deviation between the VC-term and the parallel emf is also observed while it appears that the curve is approaching the ideal line.

Here we see that the resolution does not show significant difference from the lower resolution case. The dependence of the resolution needs to be studied further, as we expect that the instabilities would be reduced for higher resolution runs.

Bibliography

Beck, R., Brandenburg, A., Moss, D., Shukurov, A. & Sokoloff D., 1996. *Galactic Magnetism: Recent Developments and Perspectives*. Annu. Rev. Astron. Astrophys. **34**: 155-206.

Berkhuijsen, E.M., Horellou, C., Krause, M., Neininger, N., Poezd, A.D., Shukurov, A. & Sokoloff D.D., 1997. *Magnetic fields in the disk and halo of M51.* A& A **318**:700-720

Berger, M.A. 1984 *Rigorous New Limits on Magnetic Helicity Dissipation in the Solar Corona*. Geophys. Astrophys. Fluid Dynamics**30**:79-104.

Bhattacharjee, A. & Hameiri, E. 1986 *Self-Consistent Dynamolike Activity in Turbulent Plasmas*. Phys. Rev. Letters **57**:206-209.

Biermann L, 1953. *Origin and Propagation of Cosmic Rays*. Annu. Rev. Nucl. Sci **2**:335-364.

Biskamp, D., 2003. *Magnetohydrodynamic Turbulence*. Cambridge University Press.

Brandenburg A., Radler K.-H., Rheinhardt M. & Kaplya P.J. 2008 *Magnetic Diffusivity Tensor and Dynamo Effects in Rotating and Shearing Turbulence*. arXiv:0710.4059v2.

Brucker, Kyle A., Isaza, Juan C., Vaithianathan T., Collins Lance R. 2007. *Efficient algorithm for simulating homogeneous turbulent shear flow without remeshing*. J. Comptu. Phys. **225**: 20-32.

Busse, F.H. 1978 *Magnetohydrodynamics of the Earth's Dynamo*. Annu.Rev. Fluid Mech **10**:435-462.

Cattaneo F. & Hughes D.W. 1996. *Nonlinear Saturation of the Turbulent α effect*. Phys.Rev.E. **54**:R4532-R4535.

Cattaneo, F. & Vainshtein, S.I., 1991. *Suppression of Turbulent Transport by a Weak Magnetic Field* . ApJ **376**:L21-L24

Chen, Q., Chen, S. & Eyink, G.L. 2003 *The Joint Cascade of Energy and Helicity in Three-Dimensional Turbulence*. Phys.Fluids **15**:361-374.

Chertkov, M., Falkovich, G., Kolokolov, I. & Vergassola, M. 1999. *Small-Scale Turbulent Dynamo*. Phys.Rev.Let. **83**:4065-4068.

Cho, J. & Vishniac, E.T. 2000a. *The Generation of Magnetic Fields Through Driven Turbulence*. ApJ **538**:217-225.

Cho, J. & Vishniac, E.T. 2000b. *The Anisotropy of Magnetohydrodynamic Alfvén ic Turbulence*. ApJ **538**:217-225.

Chorin A.J. & Marsden J.E., 1992. *A Mathematical Indroduction to Fluid Mechanics*. 3rd Ed. Springer-Verlag New York Inc.

Elmegreen, B.G. & Scalo, J. 2004 *Interstellar Turbulence I: Observations and Processes*. Annu.Rev.Astrophys **42**:211-273.

Fermi E., 1949. *On the Origin of Cosmic Radiation*. Phys. Rev. **75**:1169-1174.

Richardson K.J & Proctor M.R.E. 2012 *Fluctuating $\alpha\Omega$ dynamos by iterated matrices*. Mon. Not. R. Astron. Soc. **422**:1.53-1.56.

Frisch, U., Pouquet, A., Léorat, J. & Mazure A., 1975. *Possibility of an Inverse Cascade of Magnetic Helicity in Magnetohydrodynamic turbulence* . J. Fluid Mech. **68**:769-778.

Gruzinov, A.V. & Diamond P.H., 1994. *Self-Consistent Theory of Mean-Field Electrodynamics*. Phys. Rev. Lett **72**:1651-1653.

Gruzinov, A.V. & Diamond P.H., 1996. *Nonlinear Mean Field Electrodynamics of Turbulent Dynamos*. Phys. Plasmas **3**:1853-1857.

Hawley, John F., Gammie, Charles F. & Balbus, Steven A. 1995 *Local Three-Dimensional Magnetohydrodynamic simulations of Accretion Disks*. ApJ, **440**: 742-763.

Hoyle, F. 1953 *Cosmic Origin of Radiation at Radio Frequencies*. Nature **172**: 296-297.

Hoyle F. 1959 *Radio-Source Problems*. MNRAS **4**:338-359.

Kazantsev A.P. 1968. Sov. Phys. JETP 26, 1031.

Kraichnan R.H. & Nagarajan S., 1967. *Growth of Turbulent Magnetic Fields* . Phys. Fluids **10**:859-870.

Kulsrud, R.M., 1999. *A Critical Review of Galactic Dynamos*. Annu.Rev.Astrophys **37**:37-64.

Kulsrud, R.M. & Anderson, S.W., 1992. *The Spectrum of Random Magnetic Fields in the Mean Field Dynamo Theory of the Galactic Magnetic Field*. ApJ **396**:606-630.

Moffat, H.K. 1978. *Magnetic Field Generation in Electrically Conduction Fluids*. Cambridge, England, Cambridge University Press.

Montesions B., Thomas J.H., Ventura P. & Mazzitelli I. 2001. *A new look at the relationship between activity, dynamo number and Rossby number in late-type stars*. MNRAS **326**: 877-884.

Noyes R.W., Hartmann L.W., Baliunas S.L., Duncan D.K. & Vaughan A. H. 1984. *Rotation, convection, and magnetic activity in lower main-sequence stars*. ApJ **279**: 763.

Parker E.N., 1966. *The Dynamical State of the Interstellar Gas and Field*. ApJ **145**:811.

Parker E.N., 1969. *Origin of the Magnetic Field of the Galaxy*. ApJ **157**:1129-1135.

Parkder E.N., 1969. *Amplification of Weak Magnetic Fields in Turbulent Flow*. Apj **157**:1119-1127.

Parker E.N 1977 *The Origin of Solar Activity*. Annu.Rev. Astron.Astrophys. **15**:45-68.

Parker, E.N. 1979. *Cosmical Magnetic Fields: Their Origin and their Activity*. Oxford, Clarendon Press; New York, Oxford University Press.

Poezd, A., Shukurov, A. & Sokoloff, D.D. 1993 *Nonlinear Dynamo in a Disk Galaxy*. IAUS **157**:349-353.

Pudritz R.E. & Silk J. 1989. *The Origin of Magnetic Fields and Primordial Stars in Protogalaxies* ApJ **342**:650-659.

Rogallo, R.S. 1981, *Numerical experiments in homogeneous turbuelnce*. Technical Report 81315, NASA.

Scalo, J.& Elmegreen, B.G. 2004 *Interstellar Turbulence II: Implications and Effects*. Annu.Rev.Astrophys **42**:275-316.

Schekochihin A.A., Cowley S.C., Taylor S.F, Maron J.L. & McWilliams J.C. 2004 *Simulations of the Small-Scale Turbulent Dynamo*. ApJ **612**: 276.

Shapovalov, D.S. & Vishniac, E.T. 2011. *Simulations of Turbulent Dynamos Driven by the Magnetic Helicity Flux*. ApJ **738**:66-77.

Singh N.K. & Jingade N. 2013. *Numerical Studies of Dynamo Action in a Turbulent Shear Flow*. arXiv:1309.0200v1.

Subramanian K. 1997. *Dynamics of Fluctuating Magnetic Fields in Turbulent Dynamos Incorporating Ambipolar Drifts*. arXiv:astro-ph/9708216v1.

Teitelbaum, T. & Mininni, P.D. 2008 *Effect of Helicity and Rotation of the Free Decay of Turbulent Flows*. arXiv:0811.4373v1.

Vainshtein, S.I. & Cattaneo, F. 1992 *Nonlinear Restrictions on Dynamo Action*. ApJ **393**:165-171.

Vainshtein, S.I. & Zeldovich, Y.B., 1972 *REVIEWS OF TOPICAL PROBLEMS: Origin of Magnetic Fields in Astrophysics (Turbulent "Dynamo" Mechanisms)*. Sov.Phys.Uspekhi **15**:159-172.

Vishniac, E.T. & Brandenburg A. 1997 *An Incoherent α-Ω Dynamo in Accretion Disks*. ApJ **475**:263-274.

Vishniac, E.T. & Cho, J. 2001 *Magnetic Helicity Conservation and Astrophysical Dynamos*. ApJ **550**:752-760.

West, R.J., Nazarenko S., Laval, J.P. & Galtier S. 2003. *Small-Scale turbulent dynamo -a Numerical Investigation*. arXiv:astro-ph/0305396v2.

Yoshizawa, A. 1990 *Selfconsistent Turbulent Dynamo Modelling of Reversed Field Pinches and Planetary Magnetic Fields*. Phys.Fluids B **2**:1589-1600.

Yousef T.A, Heinemann T., Rincon F., Schekochihin A.A., Kleeorin H., Rogachevshii I., Cowley S.C. & McWilliams J.C. 2008 *Numerical experiments on dynamo action in sheared and rotating turbulence*. arXiv:0807.1122.

Zeldovich Ya.B., Ruzmaikin A.A., Sokoloff D.D., 1983 *Magnetic Fields in Astrophysics* . The Fluid Mechanics of Astrophysics and Geophysics Volume 3, Gordon and Breach, Science Publishers, Inc